FINAL REPORT

STUDY TO DEVELOP THE EQUATIONS DESCRIBING THE CHARACTERISTICS OF RATE AND ATTITUDE SENSORS ASSOCIATED WITH SPACECRAFT CONTROL SYSTEMS

BY

THE BENDIX CORPORATION
ECLIPSE-PIONEER DIVISION
TETERBORO, NEW JERSEY

April, 1966

Contract No. NAS 1-4874

Prepared for

NATIONAL AERONAUTICS & SPACE ADMINISTRATION

Prepared by:

Jack Clair
Assistant Senior Staff Scientist

Approved by:

M. Frieder
Assistant Senior Staff Scientist

E. E. Lademann
Chief Engineer
Guidance & Control Laboratory

TABLE OF CONTENTS

ABSTRACT

The intent of this report, in compliance with the tasks as outlined in the Scope of Work under Contract No. NAS1-4874 is to provide computation requirements for the evaluation of four integrated sensor systems in carrying out their respective attitude modes. For each attitude mode, the requirements are itemized in compatibility with accompanying simulation block diagrams and include error models of the sensors utilized. Evaluations are available via computations of the true angular deviations of the spacecraft from its required attitude. Peak values or RMS values of these deviations are the types of figures of merit by which the integrated systems can be evaluated. Data additional to the error models of the sensors (scale factor, dynamic range, format of output, cost, delivery time, power, weight, volume and reliability) are also included in the report.

"ERRATA"

for

FINAL REPORT CONTRACT NO. NAS 1-4874

Issued April, 1966

ITEM I: Figure 1, Section 2

"δ" should be ρ (rho)

ITEM II: Figure 5, Section 2 Output load (11).

"Mij" - should be "mij"

ITEM III: Figure 6, Section 2 Output box "Command Matrix Computer"

"mij" - should be "Mij"

Output of box "Strapdown Gyro Matrix Computer"

"M'ij" - should be "m'ij"

ITEM IV: Page 3-5 Equations (8-a) and (8-b) should be respectively:

$$a_1 = \tan^{-1}\left(\frac{-s_{1y}}{s_{1z}}\right) = \tan^{-1}\left(\frac{\varepsilon_z s_{1xI} - s_{1yI} - \varepsilon_x s_{1zI}}{\varepsilon_y s_{1xI} - \varepsilon_x s_{1yI} + s_{1zI}}\right)$$

$$a_2 = \tan^{-1}\left(\frac{-s_{2y}}{s_{2z}}\right) = \tan^{-1}\left(\frac{\varepsilon_z s_{2xI} - s_{2yI} - \varepsilon_x s_{2zI}}{\varepsilon_y s_{2xI} - \varepsilon_x s_{2yI} + s_{2zI}}\right)$$

ITEM V: Figure 4, Section 3

Output of box (7c)

"ε_x" - should be "ε_z"

ITEM VI: Figure 5, Section 4

(1) Delete "W_z" where it appears

(2) "W" - should be "W_y"

(3) "W_z^y" - should be "W_y"

(4) Insert "W_z" in output of comparator second from bottom, left side of figure.

ITEM VII: Figure 7, Section 4

(1) Output of box (34)

"a'_2" - should be "a_2"

(2) Output of box (41)

"δ_z" - should be "α_z" (alpha)

(3) Output of box (40-1)

"δ_{xit}" - should be "α_{xiT}" (alpha)

(4) Output oi box (40-2)

"δ_{x2t}" - should be "α_{x2T}" (alpha)

ITEM VIII: Figure 8, Section 4

The set comprising Θ_{BI}, left side of page should read:

$$\left.\begin{array}{l}\alpha_{z1}\\ \alpha_{xT1}\\ \alpha_{z2}\\ \alpha_{xT2}\end{array}\right\} \Theta_{BI}$$

ITEM IX: Section 5 page C.6

Second equation; numerator:

"$2O\pi$" - should be "2π"

I. INTRODUCTION

The final repot is a compilation of (1) the computer simulations required to determine the accuracy with which four attitude modes will be carried out by the integrated sensor systems proposed herein for each, and (2) the data received via a sensor survey as stipulated in the statement of work. Error models of all sensors required in the integrated systems have been included in the computational requirements. Error models of gimbal angle and angle rate sensors, not required in the integrated sensor systems, but required as coupling and feedback parameters for the error signal outputs of the integrated systems, are indicated in section VI. The utilization of CMG gimbal angle and angle rate data is understood to follow the arguments of NASA TR, May 1965, (Kurzhals and Grantham) wherein equation (B-10) indicates how six error signals of an assumed integrated sensor system, k_1 through k_6, will be coupled with measured gimbal angle data, to generate gimbal angle rate commands. These command rates,, in turn will be compared with measured gimbal rates to generate error signals for the six velocity servos driving the gimbals of the SIXPAC. Dynamic models of the servos and CMG's will yield the true gimbal angle and gimbal angular rates. Insertion of the error models of the gimbal angle and gimbal angular rate sensors will yield indicated angles and rates. The

indicated angles are then fed into the command rate computer as given by (B-10) of the NASA TR, while the indicated rates are bucked against the command rates to generate the indicated velocity servo error signals.

The integrated sensor systems for the four attitude modes yield components along vehicle axes of the vehicle small angle error vector referred to the command reference frame required for the maneuver. Such error signals, in contrast to Euler angle error signals. as indicated in (B-12) of the NASA TR, are not sensitive to geometric attenuation of gain, in that the CMG torque reference axes are also vehicle fixed axes. Where accuracy has been adequate in simulating rapid maneuvers despite large deviations between the intermediate axes of the Euler angle errors and the torque delivery axes, unduly large electronic gains have been required to overcome the effects of these misalignments. Power savings are another factor in keeping error signal axes as closely aligned as possible with control torque axes.

The recommendation of a gyro strapdown system over a three axis gyro platform or over three single axis gyroplatforms follows from estimates of (1) the accuracies in the expected environment,

(2) the complications in maintaining rotational isolation from the vehicle for some of the maneuvers and (3) cost, weight, and power, generally. For the first item only is there any advantage in favor of platforms, but this was found tobbe too slight and also unnecessary in terms of specified accuracy to overcome its significant disadvantages with regard to the second and third items. As indicated in sections II and IV, a strapdown system can be used with feasible programming requirements of its computer for widely different and demanding maneuvers. It could also be used, with star tracker updating, for the inertial hold mode specified in section III. In fact, it is recommended that such a system be considered as an alternative to the pure star tracker system indicated in section III.

The biggest gaps in the information required to estimate realistically the effects of errors in input data are the errors in spacecraft velocity components and target slant range required as inputs for the system of section II, and the spacecraft geocentric position components required as inputs for the system of section IV. The velocity and position data are feasibly generated by an onboard Kepler orbit extrapolation of data transmitted to the spacecraft from tracking stations, with intermittent updating of the Kepler orbits by these tracking stations as required. The errors in the extrapolated data should be feasibly kept quite small,

but how small is not known. The target slant range data can be determined from an onboard extrapolation based on two accurate sightings of the target combined with spacecraft position data which in effect provides an initial triangulation of the target. Again error models of the inputs for this computation are lacking.

Of the four attitude systems discussed in sections II through V, the system executing roll of the vehicle, with the roll axis held to the geodetic vertical down to $.01^{\circ}$ error (Horizon Spectrometry-IV) is considered to be most marginal. An alternative was suggested in that section which would roll stabilize the vehicle, thus precluding the problems of periodic occultation of stars and periodic reacquisitions, and shifting the horizon sweep function to a gimballed experimental package. Complete simulation of its errors would require, as indicated in section IV, specification of the package dynamics inclusive of its servo.

With regard to the system discussed in Section II, it may be regarded as an automatic vernier control, manual corrections via a high powered sighting scope being made intermittently to correct for variable atmospheric refraction effects and gyro drift. Further investigation, utilizing some of the data required for the fully atuomatic system (discounting initial aiming at the selected target), may reveal significant simplification for a system aided manual control. Reliable manual control error models would be crucial in making decisions

on the effectiveness of such continuous manual controls. The area of investigation here would necessarily include elaborate simulation facilities.

The term "gyrocompassing" constraint is referred to in the system discussed in section II, and refers to its heading or yaw reference capability. This capability depends on integrating the coupled outputs of the three rate gyros, rather than on a coupling between vehicle roll and orbital angular velocity which allows, with additional constraints, a measure of yaw via the roll rate gyro. This latter method of determining yaw is properly referred to as "gyrocompassing" and hence the term is used inappropriately in section II.

Concerning the utilization of star tracker data to establish an inertial frame (or correct a gyro drifting reference frame), the data reduction schemes for III and IV depend on gimbal angle data from two stars (three gimbal angles in III and four in IV). In both cases, tracking of two stars simultaneously with two trackers, or sequentially with one tracker is required. This two-star data scheme is indicated because of the feasibility, in the time allowed for this study, in deriving the error signals based on tracker data and stored constants, An alternative scheme, used for correcting a drifting reference frame is discussed in R-323, MIT Instrumentation Laboratory, February 1961 (Hutchinson). This scheme depends on the azimuth data from three stars. This data is to be stored in the data reduction computer as a single tracker acquires and tracks in sequence the three stars. It has the advantage over

the two-star schemes with regard to the geometric resolution afforded by the three stars being independent of the choice of the reference coordinate frame, although this statement is not made in the cited report. For the purposes of this study, however, this advantage is of no significance since the angular coordinates chosen for the reference stars are not limited, as they would in orbital operation, by the statistics of geometric resolution afforded by two-star or three-star combinations. In addition, the MIT Report makes allowance for astronomical aberration which if ignored leads at most to an error of ± 5 arc seconds for a star line of sight normal to the plane of the orbit. The measured data required in the computer are two components of inertial vehicle velocity as resolved in the drifting reference frame. Velocity components referred to the non-drifting reference frame must be stored. The differences between the measured and stored velocities as well as the differences between the measured and stored azimuth data are linearly weighted to generate the three components of a small angle drift vector. While section III requires an inertial hold mode in support of a telescope experiment of accuracy down to 0.1 arc seconds, it was agreed that no attempt would be made to hold the vehicle attitude to such an order of magnitude. Therefore whether a two-star or three-star data reduction scheme is adopted, the astronomical aberration correction discussed in the MIT Report should be waived. As to the telescope control itself, the fine guidance tracker utilizing the large optics and the experimental star itself, precludes the need

for any non-drifting reference. The telescope, as its orbits, will then automatically sweep out a cone in the period of an orbit as seen in inertial space, and of apex at most 10 arc seconds. The dynamic demand on the control system is obviously negligible. The evaluations attendant on the error models using corrective star trackers must be regarded as optimistic since no allowance has been made for vehicle flexure and mounting misalignment between reference axes for the vehicle mounted star trackers and those for the strapdown gyros. Since estimates of such misalignments are hard to come by without detailed knowledge of the structure separating the star trackers and the strapdown gyros, as well as the mounting accuracies for each of these sensors, no such allowance was made in the error models. It is suggested that some investigation be made realistically estimating this source of error if absolute accuracy, as well as stringently limited variation in the reference frames for the various experiments is required. Along these lines, with regard to Horizon Spectrometry, section IV, the misalignment between the experimental package (suggested as an alternative in sweeping the horizon) and the reference axes of the star trackers must be carefully estimated and compared with the total allowed vertical error of .01 degrees.

On the whole, the results of this study should provide a sound guide to system requirements in carrying out the vehicle attitude modes, and their evaluation by a computer simulation which includes the main sources of error of the required sensors.

II. EARTH MAPPING EXPERIMENT

APPENDICES

C. Target Tracking Equations Under Spacecraft Gyrocompassing

D. Definitions of Some Matrices

E. Basis of Spacecraft Control Error Signals

1. Introduction

According to the NASA-TR (Kurzhals and Grantham) and further discussions at Langley, this experiment consists in keeping the roll axis of the spacecraft normal to the orbital plane, while it is rolled so as to maintain an optical instrument which is fixed to the spacecraft trained on a target. It is further stipulated that the target tracking operation be maintained from emergence on the forward horizon to submergence on the rearward horizon. At 200 nautical miles altitude, the horizon to horizon sighting time is about 15 minutes. For a gyro platform as the spacecraft attitude monitor, the drift rate about each axis would be about .1 degree per hour, leading to an accumulated drift of .025 degrees per axis. The stipulated accuracies per axis are understood to be .001 degrees per second or 3.6 degrees per hour, and .01 degrees We thus predict that a gyro platform as the sensor of spacecraft attitude, is well within the margin for rate accuracy, but will drift during the experiment to about 2.5 times that allowed for angular error. A strapdown gyro system would suffer a drift rate of about .3 degrees per hour per axis, still an order of magnitude less than the rate error allowed, but would drift to about .075 degrees during the experiment or 7.5 times the allowance. Since either the platform or the strapdown system would require optical updating in order to satisfy experimental angular accuracy, it is proposed that the strapdown system be used as the attitude monitor, with an astronaut operated optical updating.

The choice of the strapdown system is based on its being available as a sensor package, wheras the platform gimbal measurements could not be counted on for availability.

If the targets were always in the orbital plane, or, equivalently on the ground track, only the spacecraft roll degree of freedom would be required. In general, there would be targets of interest off the ground track. Hence another degree of freedom is afforded by gimballing the sighting telescope about a spacecraft transverse axis, and is designated as the x-axis as shown in Figure 2. In the general case, then, the problem of maintaining a scope trained on the target is that of determining continuously a roll rate of the spacecraft and an azimuth angle of the telescope gimballed on one degree of freedom relative to the spacecraft.

As shown in this report, the determination of these two parameters from orbital and target data requires the simultaneous determination of the attitude of the spacecraft relative to the inertial reference frame (I) which would enable the craft to be rotated so as to maintain the target on the crosshairs of the telescope. Because of the gyro compassing constraint stipulated (maintaining the roll axis normal to the orbital plane, the required command angular velocity of the spacecraft relative to the I-frame has two components which are zero (x- and y-, as shown in Figure 2), and the roll component to be determined

Ω_{cz}, by the command matrix computer. Since the computer must determine simultaneously the nine command matrix elements defining the commanded attitude of the spacecraft relative to the reference frame (I), these nine attitude parameters, rather than the commanded roll rate, are used as the reference data which is mixed with the integrations of the rate gyro data to generate error signals. The error signals are thus attitude error signals rather than attitude rate error signals. The computations of x-y, y-, and z- axis error signals (as resolved in the spacecraft frame and therefore in the CMG reference frame) are linear combinations of the elements of the computed command attitude matrix and the computed rate gyro attitude matrix. Because of the gyro compassing constraint in the command, three of the nine command elements are constants, and thus only six command elements need be computed. Hence, the overall computation of command parameters, six matrix elements, the command roll rate, and the command azimuth of the sighting scope (totalling eight), requires eight computational constraints. The block diagram of the computer yielding the command parameters is shown in Figure 3 with equation numbers as indicated in Section 2.

This computer is shown in Figure 6 as p art of the overall on-board computer necessary for generating the optically corrected error signals which are to be fed into the control law used for the earth mapping spacecraft control. Its inputs are (1) $(V)_1$, the instantaneous velocity of the spacecraft relative

to the earth as resolved in the nondrifting gyro reference frame, (2) s, the instantantous slant range to the target, (3) nine constants, which are the initial elements of the command attitude matrix relative to the I-frame, (4) the initial command azimuth for targetting the telescope, which if initially commanded when the target emerges in the forward horizon can always be taken as zero and (5) the three constants which are the components of the angular velocity of an earth fixed frame, E, relative to the nondrifting gyro frame, I, as resolved in the I-frame. Comparing Figures 3 and 6, the command roll rate, Ω_{cz} is computed only as an intermediate constraint towards generating its ten outputs. There are nine command matrix elements, three of which are initial elements and hence need not be computed, and the command azimuth for the sighting telescope. This latter parameter is to be used only as an input for the telescope servo.

If the orbital and target data were error free, if there were no gyro drift, and if initial conditions inserted into two differential analyzers (the command matrix and strapdown gyro computer) were also without error, the target should remain there throughout the experiment. Assuming the command input data to be without error, and assuming all initial conditions are error free, the drifts of the gyros will result in drifts of the error signals to the control logic, with a consequent drift on all three axes of the spacecraft away from its commanded attitude. The effect of this drift will, of course, show up as a drift

of the target away from the crosshairs, of the sighting scope, and in practice can be fully corrected down to the negligible error resulting from the human eye's limit of resolution as aided by a high power telescope.

This could be limited to seconds of arc, and for purposes of the required accuracy of this experiment, assumed to be without error. Thus, the optical feedback to the astronaut can fully correct for the drift of the gyros, at least in principle. How the correction should actually be applied is at this time not clear, since it is recognized that the correction consists in both manually adjusting the telescope in azimuth, and applying summed corrections derived from the optical data (i.e. the displacement of the target from boresight) to two error signal axes of the spacecraft.

Although the operation of this experiment would require capability in tracking out-of-orbit plane targets and thus would require an azimuth command of a telescope, nothing is gained in including this in the simulation, since the largest dynamic demand on the spacecraft control is for targets in the plane of the orbit. The simulation indicated in Figures 4 and 5 is then for this case, and no azimuth command computation is required. In addition, some uncertainty at this time as to how to apply the optical data for updating the spacecraft control precludes including optical updating in the discussion on simulation of error effects.

2. REQUIRED COMPUTATIONS

2.1 On-board Command Matrix

$$\Omega_{cz} = \Omega_{EIz} + \Omega_{EIy} \tan A_c + \frac{V_{cx}}{s} \sec A_c \qquad (1)$$

$$A_c = \int_o^t \{\frac{1}{s}[V_{cz} \sec A_c - \dot{s} \tan A_c] - \Omega_{EIx}\} dt' + A_{co} \qquad (2)$$

$$\Omega_{EIx} = M_{11}\Omega_{EIxI} + M_{21}\Omega_{EIyI} + M_{31}\Omega_{EIzI} \qquad (3)$$

$$\Omega_{EIy} = M_{12}\Omega_{EIxI} + M_{22}\Omega_{EIyI} + M_{32}\Omega_{EIzI} \qquad (4)$$

$$\Omega_{EIz} = M_{130}\Omega_{EIxI} + M_{230}\Omega_{EIyI} + M_{330}\Omega_{EIzI} \qquad (5)$$

$$V_{cx} = M_{11}V_{xI} + M_{21}V_{yI} + M_{31}V_{zI} \qquad (6)$$

$$V_{cz} + M_{130}V_{xI} + M_{230}V_{yI} + M_{330}V_{zI} \qquad (7)$$

$$M_{11}(t) = \int_o^t \Omega_{cz}(t') M_{12}(t') dt' + M_{110} \qquad (8\text{-}1)$$

$$M_{12} = -\int_o^t \Omega_{cz} M_{11} dt' + M_{120} \qquad (8\text{-}2)$$

$$M_{21} = \int_o^t \Omega_{cz} M_{22} dt' + M_{210} \qquad (8\text{-}3)$$

$$M_{22} = -\int_o^t \Omega_{cz} M_{21} dt' + M_{220} \qquad (8\text{-}4)$$

$$M_{31} = \int_o^t \Omega_{cz} M_{32} dt' + M_{310} \qquad (8\text{-}5)$$

$$M_{32} = -\int_o^t \Omega_{cz} M_{31} dt' + M_{320} \qquad (8\text{-}6)$$

$$M_{13} = M_{130}$$
$$M_{23} = M_{230}$$
$$M_{33} = M_{330}$$

2.2 On-board Strapdown Gyro Matrix

$$m'_{11}(t) = \int_o^t [- W_y(t') m'_{13}(t') + W_z(t') m'_{12}(t')]dt' + m'_{110}$$

$$m'_{12} = \int_o^t [- W_z m_{11} + W_x m_{13}]dt' + m'_{120}$$

$$m'_{13} = \int_o^t [- W_x m_{12} + W_y m_{11}]dt' + m'_{130}$$

$$m'_{21} = \int_o^t [- W_y m_{23} + W_z m_{22}]dt' + m'_{120}$$

$$m'_{22} = \int_o^t [- W_z m_{21} + W_x m_{23}]dt' + m'_{220} \qquad (9)$$

$$m'_{23} = \int_o^t [- W_x m_{22} + W_y m_{21}]dt' + m'_{230}$$

$$m'_{31} = \int_o^t [- W_y m_{33} + W_z m_{32}]dt' + m'_{310}$$

$$m'_{32} = \int_o^t [- W_z m_{31} + W_x m_{33}]dt' + m'_{320}$$

$$m'_{33} = \int_o^t [- W_x m_{32} + W_y m_{31}]dt' + m'_{330}$$

2.3 On-board Error Signals

$$\epsilon_x' = m'_{12} M_{130} + m'_{22} M_{230} + m'_{32} M_{330}$$

$$\epsilon_y' = m'_{13} M_{11} + m'_{23} M_{21} + m'_{33} M_{31} \qquad (10)$$

$$\epsilon_z' = m'_{11} M_{12} + m'_{21} M_{22} + m'_{31} M_{32}$$

2.4 True Attitude Matrix of Spacecraft Referred to I frame in Terms of Euler Angles

$$\begin{aligned} m_{11} &= \cos\psi \cos\theta \\ m_{12} &= \cos\psi \sin\theta \sin\phi - \sin\psi \cos\phi \\ m_{13} &= \cos\psi \sin\theta \cos\phi + \sin\psi \sin\phi \\ m_{21} &= \sin\psi \cos\theta \\ m_{22} &= \sin\psi \sin\theta \sin\phi + \cos\psi \cos\phi \end{aligned} \qquad (11)$$

$$m_{23} = \sin\psi \sin\theta \cos\phi - \cos\psi \sin\phi$$
$$m_{31} = -\sin\theta$$
$$m_{32} = \cos\theta \sin\phi$$
$$m_{33} = \cos\theta \cos\phi$$

2.5 Centripetal Acceleration of Rate Gyros Resolved in B frame

$$a_x = (\Omega_x \ell_x + \Omega_y \ell_y + \Omega_z \ell_z)\Omega_x - \Omega^2 \ell_x$$
$$a_y = (\Omega_x \ell_x + \Omega_y \ell_y + \Omega_z \ell_z)\Omega_y - \Omega^2 \ell_y \qquad (12)$$
$$a_z = (\Omega_x \ell_x + \Omega_y \ell_y + \Omega_z \ell_z)\Omega_z - \Omega^2 \ell_z$$

2.6 Rate Gyro Error Model (Drift Rate Components Resolved in B Frame

$$\Delta W_x = c_o + c_1 a_x + c_2 a_y + c_z a_x a_y$$
$$\Delta W_y = c_o + c_1 a_y + c_2 a_z + c_z a_y a_z \qquad (13)$$
$$\Delta W_z = c_o + c_1 a_z + c_2 a_x + c_z a_z a_x$$

18. PIRIG (MIT-Bendix)

	Typical	Specification	Units
c_o	5.25×10^{-3}	7.88×10^{-3}	rad/hr
c_1	1.09×10^{-4}	1.64×10^{-4}	rad/hr/ft/sec^2
c_2	1.09×10^{-4}	1.64×10^{-4}	rad/hr/ft/sec^2
c_3	5.5×10^{-6}	8.2×10^{-6}	rad/hr/(ft/sec^2)^2

(c_o here corresponds to .3 degrees/hour and .45 degrees/hour revising evaluation previously given.)

With the above evaluations, drift rate components are in radians per hour for acceleration components in feet per second squared.

2.7 Small Angle Drift Vector of Computed Reference Frame (G) Relative to Non-Drifting Frame (I), Resolved in B Frame.

$$(\delta_G)_B = \begin{matrix}\delta_x \\ \delta_y \\ \delta_z\end{matrix} = \begin{matrix}\int_o^t \Delta W_x(t')\,dt' \\ \int_o^t \Delta W_y(t')\,dt' \\ \int_o^t \Delta W_z(t')\,dt'\end{matrix} \qquad (14)$$

2.8 True Error Signals Resulting from Non-Drifting Gyro Data

$$\epsilon_x = m_{12}M_{130} + m_{22}M230 + m_{32}M_{330}$$

$$\epsilon_y = m_{13}M_{11} + m_{23}M_{21} + m_{33}M_{31} \qquad (15)$$

$$\epsilon_z = m_{11}M_{12} + m_{21}M_{22} + m_{31}M_{32}$$

2.9 Indicated Error Signals

$$\epsilon'_x = \epsilon_x - \delta_x$$

$$\epsilon'_y = \epsilon_y - \delta_y \qquad (16)$$

$$\epsilon'_z = \epsilon_z - \delta_z$$

2.10 Euler Angles Corresponding to Command Attitude Matrix, (M_{B_cI})

ω $\theta_c = -\sin^{-1}(M_{31})$ (17-a)

$\phi_c = \tan^{-1}(M_{32}/M_{33})$ (17-b)

$\psi_c = \tan^{-1}(M_{21}/M_{11})$ (17-c)

2.11 Command Matrix Computation for Target in the Orbital Plane ($A_c = 0$)

$$\Omega_{cz} = \Omega_{EIz} + \frac{V_{cx}}{s} \qquad (18)$$

Referring back to Section 2.1, equation (18) replaces (1) and of equations (2) through (7) only (5) and (6) are required.

2.12 Additional Definitions

Ω_{cz} - computed command rate about roll axis

A_c - computed azimuth angle of sighting telescope

$\Omega_{EIx}, \Omega_{EIy}, \Omega_{EIz}$ - earth angular velocity relative attitude frame

V_{cx}, V_{cz} - components of vehicle velocity relative to earth as resolved on axes of commanded vehicle attitude frame

V_{xI}, V_{yI}, V_{zI} - inputs profiles of vehicle relative to earth as resolved on inertial reference axes

M_{ij} - direction cosines of commanded vehicle altitude frame

3. SUGGESTED VALUES FOR INITIAL CONDITIONS

3.1 Initial Command Attitude Matrix

The target is assumed to lie in the plane of the orbit. For simplicity the X_1 and Y_1 axes of the I-frame are assumed to lie in the plane of the orbit, the Z_1 axis normal to the orbit. The target is sighted at the forward horizon. Additionally by design, the Y_I axis points to the target as it emerges. Then

$$M_{B_C I}^{(0)} = \begin{bmatrix} M_{110} & M_{120} & M_{130} \\ M_{210} & M_{220} & M_{230} \\ M_{310} & M_{320} & M_{330} \end{bmatrix}$$

$$= \begin{bmatrix} 1 & 0 & 0 \\ 0 & 1 & 0 \\ 0 & 0 & 1 \end{bmatrix}$$

(See Appendix D for general method of evaluation).

3.2 Initial Strapdown Gyro Matrix

This matrix after computation is initiated, defines the attitude of the spacecraft relative to a drifting G-frame. At the instant of initiation of computation, the matrix, in practice will suffer no gyro drift since it is measured from star tracker data. Hence the initial condition gyro matrix defines spacecraft attitude relative to the non-drifting reference frame, I.

As a matter of interest in the effectiveness of the control system, it is suggested that initial conditions here depart radically from the commanded initial condition. The simulation should then reveal the dynamic transients in Euler angle errors or the linear craft frame error angles suggested in 2.8 and 2.9.

Suggested values are that initial Euler angles be $\theta_0 = 15°$, $\psi_0 = 15°$.

The values of the initial condition matrix for the strapdown system are then

$$m_{110} = \cos \psi_0 \cos \theta_0$$

$$m_{120} = \cos \psi_0 \sin \theta_0 \sin \phi_0 - \sin \psi_0 \cos \phi_0$$

$$m_{130} = \cos \psi_0 \sin \theta_0 \cos \phi_0 + \sin \psi_0 \sin \phi_0$$

SIMPLIFICATION OF THE GYRO ERROR MODEL AND ITS INTERFACE IN THE SIMULATION

Referring to 2.6 it will be shown here that the acceleration sensitive terms lead to entirely negligible contributions to the drift rate for each gyro under the expected rotation rates of the spacecraft.

If the gyros were placed as much as 4 feet from the roll axis along the craft's x- and y- axes each, the centripetal acceleration components, under maximum roll axis rate, $\hat{\Omega}_{cz}$ = 1.12 degrees/sec.

$= 1.97 \times 10^{-2}$ rad./ secl, are

$$a_x = -\Omega^2 l_x = a_y = -\Omega^2 l_y$$

$$= -(1.97 \times 10^{-2})^2 \times 4 = 1.55 \times 10^{-3} \text{ ft./sec.}^2$$

The typical values cited for the 18. PIRIG gyr o are

$$C_o = 5.25 \times 10^{-3} \text{rad/hr}$$

$$C_1 = 1.09 \times 10^{-4} \frac{\text{rad/hr}}{\text{ft/sec}^2} = C_2$$

$$C_3 = 5.5 \times 10^{-6} \frac{\text{rad/hr}}{(\text{ft/sec}^2)^2}$$

Then for the x-gyro, for example, with drift rate model as follows:

$$\Delta W_x = C_o + C_1 a_x + C_2 a_y + C_3 a_x a_y,$$

$$C_o = 5.25 \times 10^{-3} \text{ rad/hr}$$

$$C_1 a_x = 1.7 \times 10^{-7} \text{ rad/hr} = C_2 a_y$$

$$C_3 a_x a_y = 1.32 \times 10^{-11} \text{ rad/hr}$$

Thus, under maximum acceleration induced by rotation about the roll axis the unbalance drift components are more than 4 orders of magnitude smaller than the acceleration insensitive drift C_o, while the compliance drift is more than 8 orders smaller. Hence the gyro drift rate model can be simplified under the expected environment to

$$\Delta W_x = C_o = 5.25 \times 10^{-3} \text{ rad/hr}$$

$$\Delta W_y = C_o = 5.25 \times 10^{-3} \text{ rad/hr}$$

$$\Delta W_z = C_o = 5.25 \times 10^{-3} \text{ rad/hr}$$

Then the simulation of the interface of the gyro error model can exclude the computation of acceleration inputs to the rate gyros.

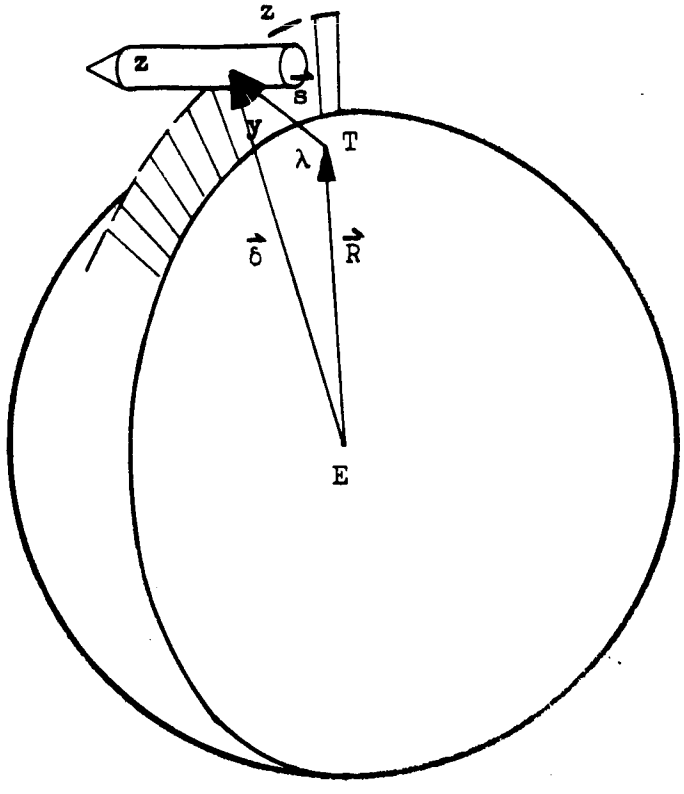

$\bar{s}$ - target to spacecraft vector

$\bar{\delta}$ - spacecraft geocentric vector

$\bar{R}$ - target geocentric vector

GYROCOMPASSED SPACECRAFT AND TARGET

FIGURE 1

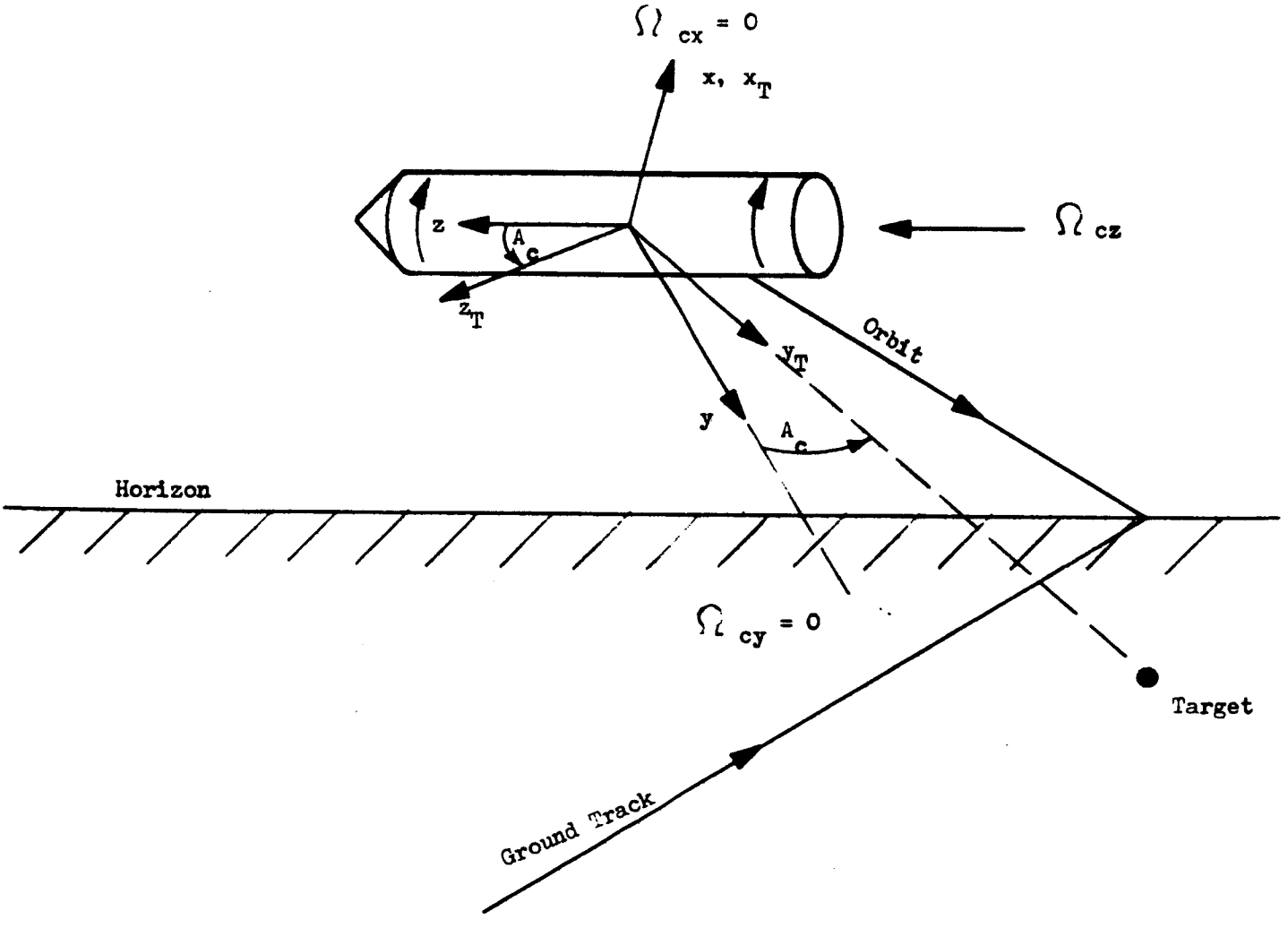

TARGET COORDINATE FRAME

FIGURE 2

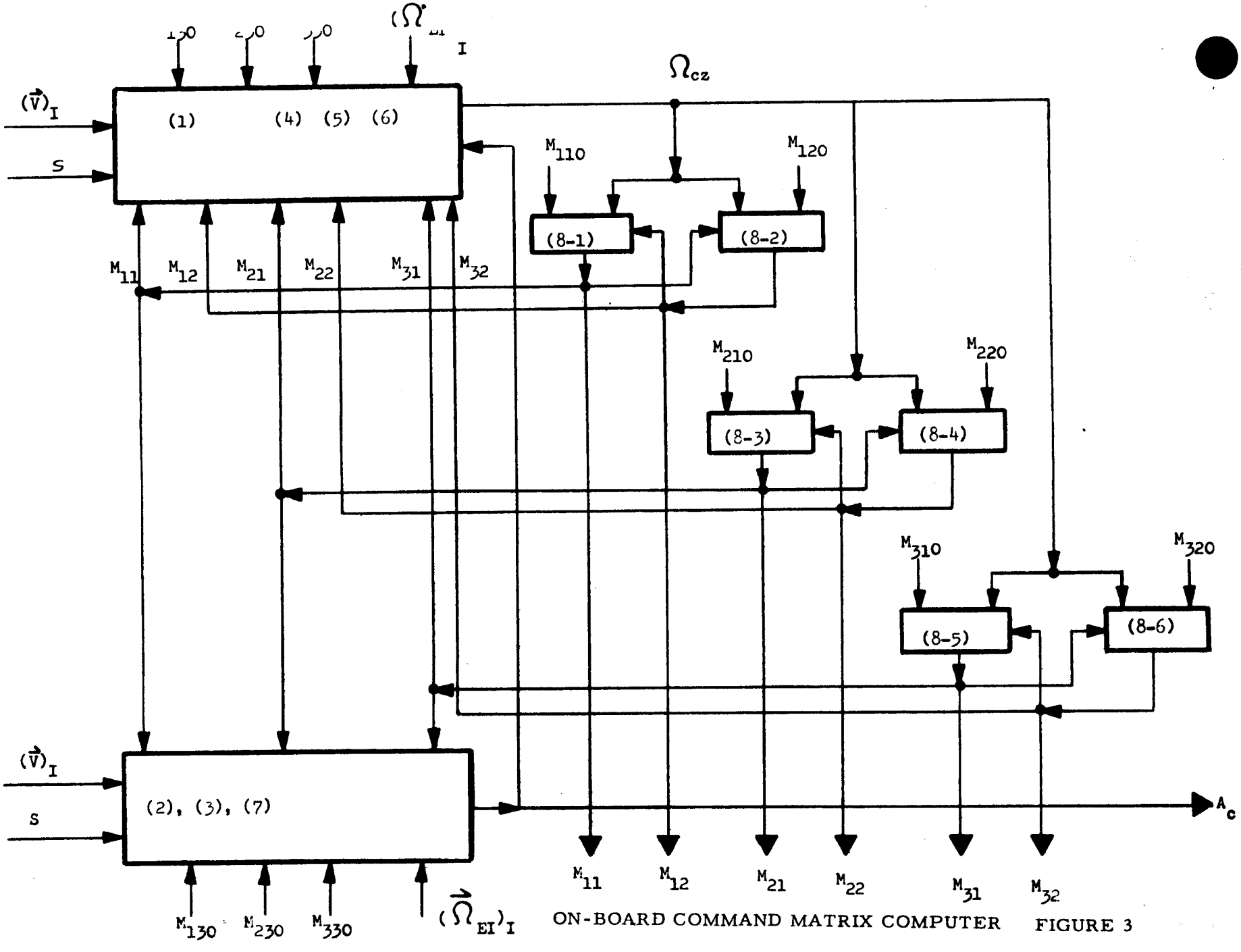

ON-BOARD COMMAND MATRIX COMPUTER FIGURE 3

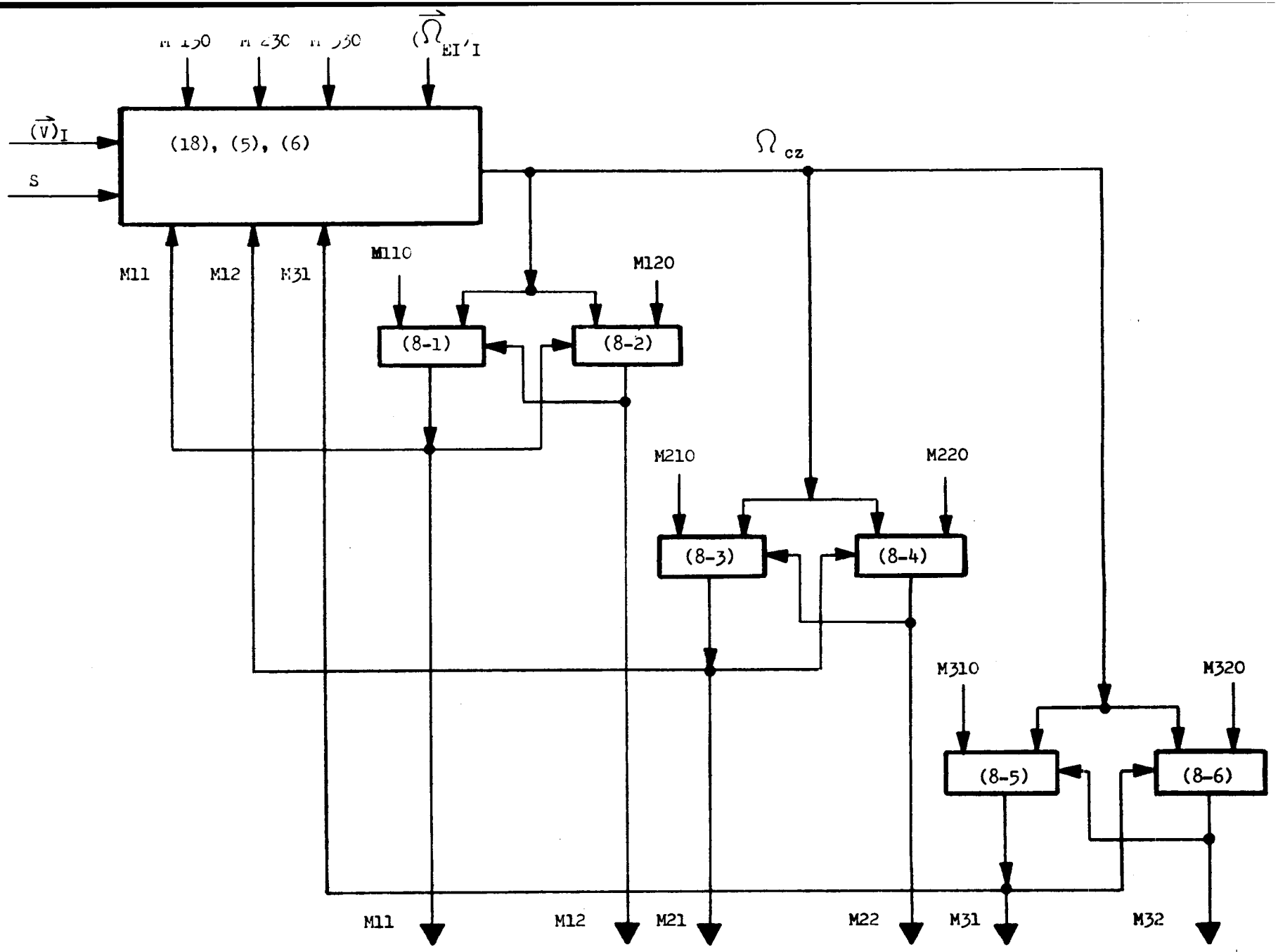

COMMAND MATRIX COMPUTER FOR SIMULATION OF TARGET IN ORBITAL PLANE

FIGURE 4

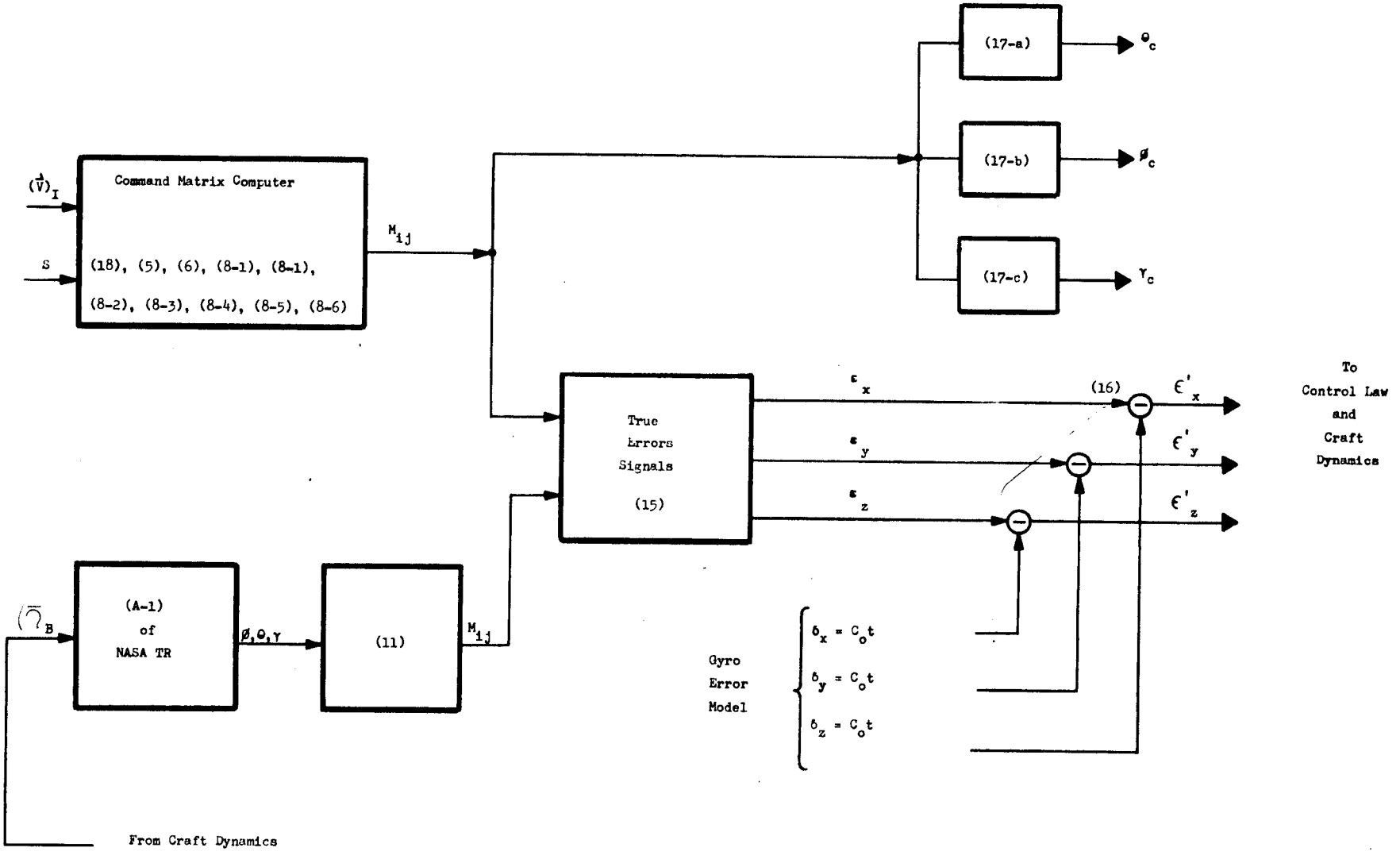

INTERFACE O F STRAPDOWN GYRO ERROR MODEL IN SIMULATION OF EARTH MAPPING EXPERIMENT

FIGURE 5

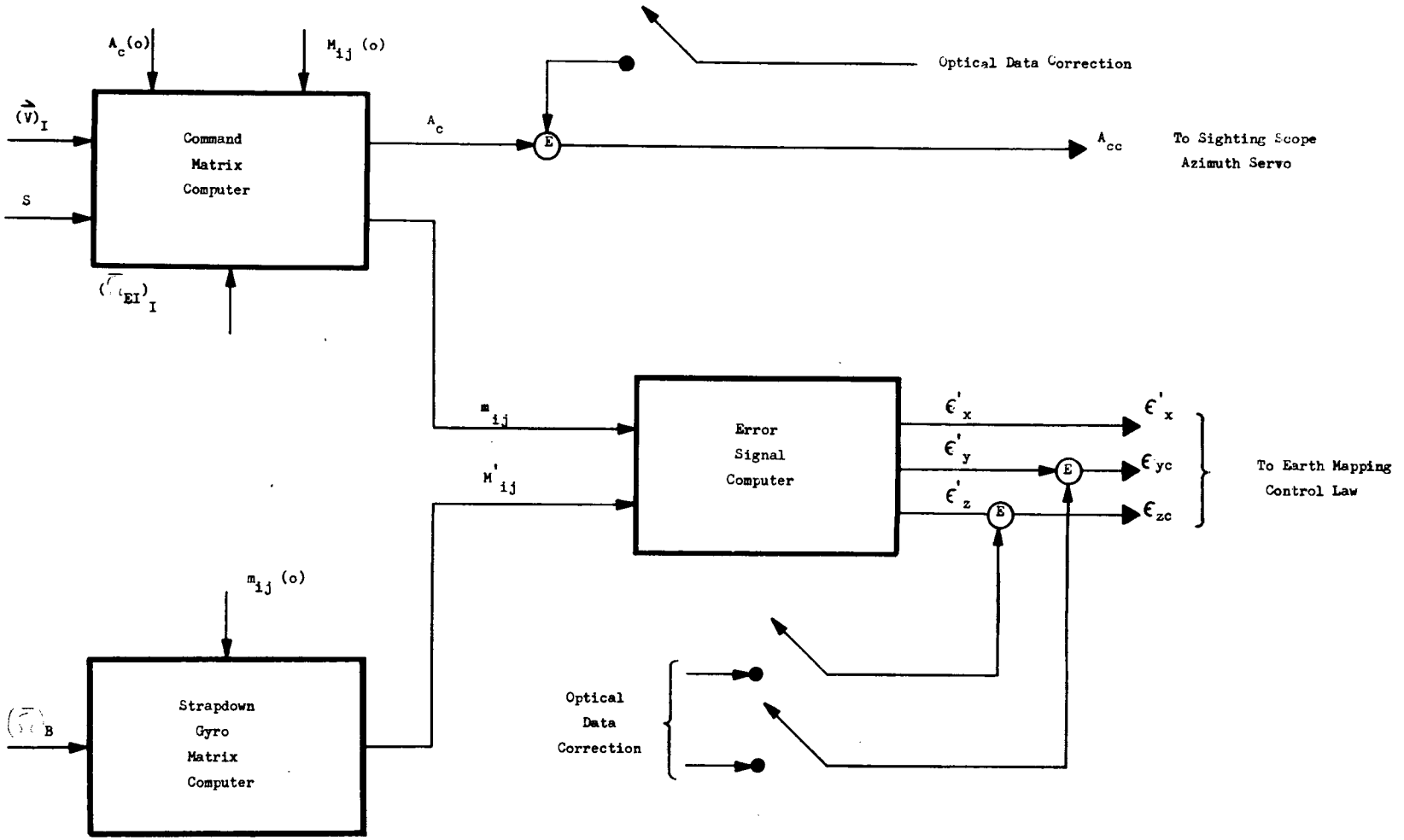

OVERALL ON-BOARD COMPUTER - EARTH MAPPING SPACECRAFT CONTROL

FIGURE 6

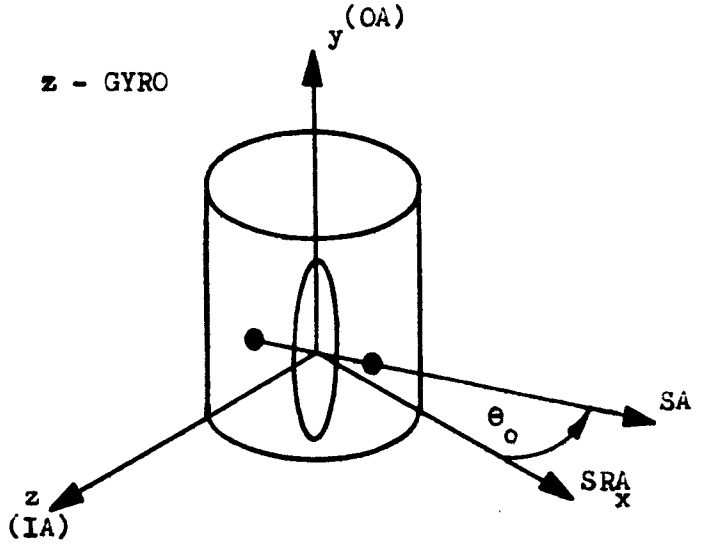

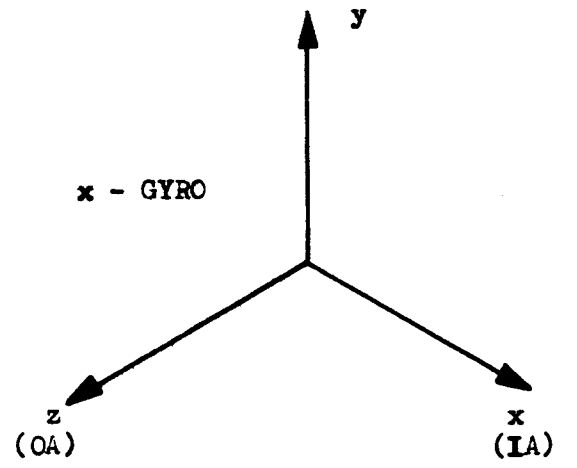

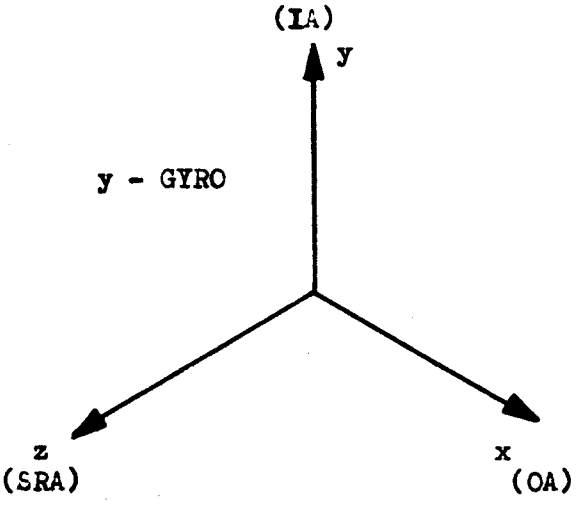

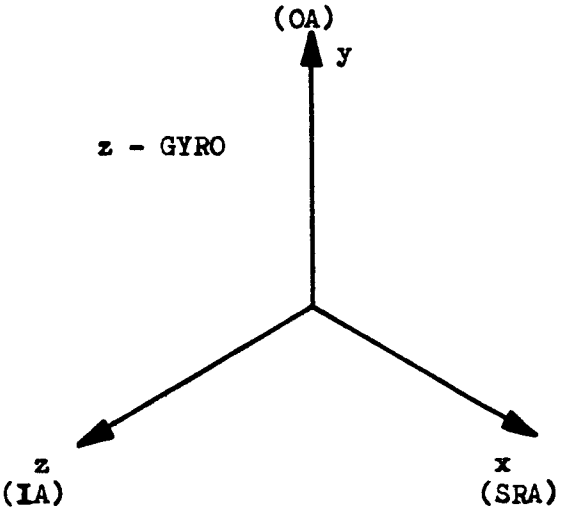

SA - SPIN AXIS

θ_o - OUTPUT

SRA - SPIN REFERENCE AXIS

OA - OUTPUT AXIS

IA - INPUT AXIS

ALIGNMENT OF RATE GYROS RELATIVE TO SPACECRAFT FRAME (x, y, z)

FIGURE 7

APPENDIX A

GYRO DRIFT CORRRUPTED EULER ANGLES

IN TERMS OF TRUE EULER ANGLES

According to NASA TR, May 1965 - Kurzhals and Grantham, the true vehicle Euler angles yield an I frame to B frame transformation matrix as follows:

$$\left[M_{IB}\right] = \left[M_{BI}\right]^{-1} = \begin{bmatrix} m_{11} & m_{21} & m_{31} \\ m_{12} & m_{22} & m_{32} \\ m_{13} & m_{23} & m_{33} \end{bmatrix}$$

$$= \begin{bmatrix} 1 & 0 & 0 \\ 0 & \cos\phi & \sin\phi \\ 0 & -\sin\phi & \cos\phi \end{bmatrix} \begin{bmatrix} \cos\theta & 0 & -\sin\theta \\ 0 & 1 & 0 \\ \sin\theta & 0 & \cos\theta \end{bmatrix} \begin{bmatrix} \cos\psi & \sin\psi & 0 \\ -\sin\psi & \cos\psi & 0 \\ 0 & 0 & 1 \end{bmatrix}$$

$$= [\phi] \; [\theta] \; [\psi] \qquad \text{(A-1)}$$

This results in (6-2) of the first Bendix preliminary report.)

Then $$\left[M_{BI}\right] = \begin{bmatrix} m_{11} & m_{12} & m_{13} \\ m_{21} & m_{22} & m_{23} \\ m_{31} & m_{32} & m_{33} \end{bmatrix}$$

$$= [-\psi] \; [-\theta] \; [-\phi] \qquad \text{(A-2)}$$

With the G frame as the drifting inertial reference frame, the indicated or drift corrupted Euler angles, ψ', θ', ϕ' specify a new matrix,

$$\left[M_{BG} \right] = \begin{bmatrix} m'_{11} & m'_{12} & m'_{13} \\ m'_{21} & m'_{22} & m'_{23} \\ m'_{31} & m'_{32} & m'_{33} \end{bmatrix}$$

$$= \left[-\psi' \right] \left[-\theta' \right] \left[-\phi' \right] \qquad \text{(A-3)}$$

The B to G transformation may be regarded as the sequence of two transformation - first a B to I (true body attitude) then an I to G (attitude of the drifting G frame relative to the non-drifting I frame). By the matrix multiplication rules,

$$\left[M_{BG} \right] = \left[M_{IG} \right] \left[M_{BI} \right] \qquad \text{(A-4)}$$

The drift matrix, $\left[M_{IG} \right]$, is assumed to be a small angle matrix. Thus, if δ_{xI}, δ_{yI}, and δ_{zI} are the I frame components of the small angle gyro drift vector

$$(\delta_G)_I,$$

the small angle drift matrix is the result of three small angle rotations about the recessive I frame (or G frame) axes,

$$M_{IG} = \begin{bmatrix} 1 & 0 & 0 \\ 0 & 1 & \delta_{xI} \\ 0 & -\delta_{sI} & 1 \end{bmatrix} \begin{bmatrix} 1 & 0 & -\delta_{yI} \\ 0 & 1 & 0 \\ \delta_{yI} & 0 & 1 \end{bmatrix} \begin{bmatrix} 1 & \delta_{zI} & 0 \\ -\delta_{zI} & 1 & 0 \\ 0 & 0 & 1 \end{bmatrix}$$

$$= \begin{bmatrix} 1 & \delta_{zI} & -\delta_{yI} \\ -\delta_{zI} & 1 & \delta_{xI} \\ \delta_{yI} & -\delta_{xI} & 1 \end{bmatrix} \qquad \text{(A-5)}$$

(In the above, small angle approximations are employed and second order terms are ignored.)

There results

$$\begin{bmatrix} m'_{11} & m'_{12} & m'_{13} \\ m'_{21} & m'_{22} & m'_{23} \\ m'_{31} & m'_{32} & m'_{33} \end{bmatrix} = \begin{bmatrix} 1 & \delta_{zI} & -\delta_{yI} \\ -\delta_{zI} & 1 & \delta_{xI} \\ \delta_{yI} & -\delta_{xI} & 1 \end{bmatrix} \begin{bmatrix} m_{11} & m_{12} & m_{13} \\ m_{21} & m_{22} & m_{23} \\ m_{31} & m_{32} & m_{33} \end{bmatrix} \tag{A-6}$$

The drift corrupted matrix elements on the left side of (A-6) are related to the drift corrupted Euler angles, $\psi' \; \theta' \; \phi'$ by equations of identical form to (6-2) of the first preliminary report. In that case

$$\left.\begin{aligned} \tan\phi' &= \frac{m'_{32}}{m'_{33}} = \frac{m_{12}\delta_{yI} - m_{22}\delta_{xI} + m_{32}}{m_{13}\delta_{yI} - m_{23}\delta_{xI} + m_{33}} \\ \tan\psi' &= \frac{m'_{21}}{m'_{11}} = \frac{-m_{11}\delta_{zI} + m_{21} + m_{31}\delta_{xI}}{m_{11} + m_{21}\delta_{zI} - m_{31}\delta_{yI}} \\ \sin\theta' &= -m'_{31} = -m_{11}\delta_{yI} + m_{21}\delta_{xI} - m_{31} \end{aligned}\right\} \tag{A-7}$$

APPENDIX B

RELATIONSHIP BETWEEN RELATIVE ANGULAR VELOCITY BETWEEN TWO COORDINATE FRAMES AND THEIR ATTITUDE MATRIX

Let the two coordinate frames be the I frame with unit axes (x_1, y_1, z_1) and the B frame with unit axes (x, y, z). Then the B to I transformation or attitude matrix is given by

$$\left[M_{BI} \right] = \begin{bmatrix} x_I \cdot x & x_I \cdot y & x_I \cdot z \\ y_I \cdot x & y_I \cdot y & y_I \cdot z \\ z_I \cdot x & z_I \cdot y & z_I \cdot z \end{bmatrix} = \begin{bmatrix} m_{11} & m_{12} & m_{13} \\ m_{21} & m_{22} & m_{23} \\ m_{31} & m_{32} & m_{33} \end{bmatrix} \quad \text{(B-1)}$$

Let $\vec{W}_{BI}$ be the angular velocity of the B frame relative to the I frame, and $\vec{W}_{IB}$, the angular velocity of the I frame relative to the B frame.

Then

$$\vec{W}_{BI} = \vec{-W}_{BI} \quad \text{(B-2)}$$

By Coriolis's theorem, the rate of change of some vector U relative to the I frame is related to the rate of change of this vector relative to the B frame by:

$$\frac{\vec{dU}}{dt_I} = \frac{\vec{dU}}{dt_B} + \vec{W}_{BI} \times \vec{U} \quad \text{(B-3)}$$

We are interested in relating the angular velocity of the B frame relative to the I frame, as resolved in the B frame, $(W_{BI})_B$, to the elements of the matrix, (M_{BI}). First, the following vectors are formed, using Coriolis's

theorem for the case of unit vectors:

$$\frac{d\vec{x}_I}{dt_B} = \vec{W}_{IB} \times \vec{x}_I$$

$$\frac{d\vec{y}_I}{dt_B} = \vec{W}_{IB} \times \vec{y}_I \qquad \text{(B-4)}$$

$$\frac{d\vec{z}_I}{dt_B} = \vec{W}_{IB} \times \vec{z}_I$$

Next, the following nine box products are formed:

$$\vec{W}_{IB} \times \vec{x}_I \cdot \vec{x} = \frac{d\vec{x}_I}{dt_B} \cdot \vec{x} = \dot{m}_{11}$$

$$\vec{W}_{IB} \times \vec{x}_I \cdot \vec{y} = \frac{d\vec{x}_I}{dt_B} \cdot \vec{y} = \dot{m}_{12}$$

$$\vec{W}_{IB} \times \vec{x}_I \cdot \vec{z} = \frac{d\vec{x}_I}{dt_B} \cdot \vec{z} = \dot{m}_{13}$$

$$\vec{W}_{IB} \times \vec{y}_I \cdot \vec{x} = \frac{d\vec{y}_I}{dt_B} \cdot \vec{x} = \dot{m}_{21}$$

$$\vec{W}_{IB} \times \vec{y}_I \cdot \vec{y} = \frac{d\vec{y}_I}{dt_B} \cdot \vec{y} = \dot{m}_{22} \qquad \text{(B-5)}$$

$$\vec{W}_{IB} \times \vec{y}_I \cdot \vec{z} = \frac{d\vec{y}_I}{dt_B} \cdot \vec{z} = \dot{m}_{23}$$

$$\vec{W}_{IB} \times \vec{z}_I \cdot \vec{x} = \frac{d\vec{z}_I}{dt_B} \cdot \vec{x} = \dot{m}_{31}$$

$$\vec{W}_{IB} \times \vec{z}_I \cdot \vec{y} = \frac{d\vec{z}_I}{dt_B} \cdot \vec{y} = \dot{m}_{32}$$

$$\vec{W}_{IB} \times \vec{z}_I \cdot \vec{z} = \frac{d\vec{z}_I}{dt_B} \cdot \vec{z} = \dot{m}_{33}$$

The last terms are obtained by noting that, for example, if x_I resolved in the B frame is

$$(\vec{x}_I)_B = \begin{matrix} \vec{x}_I \cdot \vec{x} \\ \vec{x}_I \cdot \vec{y} \\ \vec{x}_I \cdot \vec{z} \end{matrix} = \begin{matrix} m_{11} \\ m_{12} \\ m_{13} \end{matrix} , \qquad \text{(B-6a)}$$

Then

$$\left(\frac{d\vec{x}_I}{dt_B}\right)_B = \begin{matrix} \frac{d\vec{x}_I}{dt_B} \cdot \vec{x} = \dot{m}_{11} \\ \frac{d\vec{x}_I}{dt_B} \cdot \vec{y} = \dot{m}_{12} \\ \frac{d\vec{x}_I}{dt_B} \cdot \vec{z} = \dot{m}_{13} \end{matrix} \qquad \text{(B-6b)}$$

Defining the components of W_{BI} as resolved in the B frame as

$$(\vec{W}_{BI})_B = \begin{pmatrix} W_x \\ W_y \\ W_z \end{pmatrix} , \qquad \text{(B-7)}$$

We have for the box product which are the B frame components of the following three cross products,

$$(\vec{W}_{IB} \times \vec{x}_I)_B = \begin{pmatrix} W_{IB} \times \hat{x}_I \cdot \hat{x} \\ W_{IB} \times \hat{x}_I \cdot \hat{y} \\ W_{IB} \times \hat{x}_I \cdot \hat{z} \end{pmatrix} = - \begin{vmatrix} \hat{x} & \hat{y} & \hat{z} \\ W_x & W_y & W_z \\ m_{11} & m_{12} & m_{13} \end{vmatrix}$$

$$(\vec{W}_{IB} \times \vec{y}_I)_B = \text{etc.} = - \begin{vmatrix} \vec{x} & \vec{y} & \vec{z} \\ W_x & W_y & W_z \\ m_{21} & m_{22} & m_{23} \end{vmatrix} \qquad \text{(B-8)}$$

$$(\vec{W}_{IB} \times \vec{z}_I)_B \quad \text{etc.} = - \begin{vmatrix} \vec{x} & \vec{y} & \vec{z} \\ W_x & W_y & W_z \\ m_{31} & m_{32} & m_{33} \end{vmatrix}$$

Equating the right sides of (B-8) with the right sides of (B-5), the result is

$$\begin{aligned}
\dot{m}_{11} &= -W_y m_{13} + W_z m_{12} \\
\dot{m}_{12} &= -W_z m_{11} + W_x m_{13} \\
\dot{m}_{13} &= -W_x m_{12} + W_y m_{11} \\
\dot{m}_{21} &= -W_x m_{23} + W_z m_{22} \\
\dot{m}_{22} &= -W_z m_{21} + W_x m_{23} \qquad \text{(B-9)} \\
\dot{m}_{23} &= -W_x m_{22} + W_y m_{21} \\
\dot{m}_{31} &= -W_y m_{33} + W_z m_{32} \\
\dot{m}_{32} &= -W_z m_{31} + W_x m_{33} \\
m_{33} &= -W_x m_{32} + W_y m_{31}
\end{aligned}$$

The above set of equations is the basis for the strapdown gyro digital differential analyzer with W_x, W_y, and W_z as the outputs of the strapdown rate gyros, and the matrix elements as the solutions.

These elements define the attitude of the B frame (body) relative to the I frame (equivalent inertial platform). From the matrix elements, one can then determine Euler angles, if needed, of the body frame relative to the I frame, as given by (6-2) of the first Bendix preliminary report. As stated in that report, nine initial matrix elements must be specified. These are measurable by reduction of data from at least two star sightings yielding the initial attitude of the spacecraft body frame relative to the inertial reference frame. Computation must be initiated as of that instant.

The discussion here is given interms of the body frame and the inertial reference frame. Because the discussion here is mathematical, clearly the result given by (B-9) is applicable to any two coordinate frames.

APPENDIX C

TARGET TRACKING EQUATIONS

UNDER SPACECRAFT GYROCOMPASSING

Referring to Figure 1,

$$\vec{\rho} = \vec{R} + \vec{s} \tag{C-1}$$

Relative to non-rotating I frame, the velocity

$$\begin{aligned}\dot{\vec{\rho}}_I &= \dot{\vec{R}}_I + \dot{\vec{s}}_I \\ &= \vec{\Omega}_{EI} \times \vec{R} + \dot{\vec{s}}_E + \vec{\Omega}_{EI} \times \vec{s}\end{aligned} \tag{C-2}$$

where $\vec{\Omega}_{EI}$ is the angular velocity of an earth fixed frame, E, relative to the I frame. Noting that $\dot{\vec{s}}_E$ is nothing but the velocity of the craft relative to the earth,

$$\dot{\vec{s}}_E = \vec{V} = \dot{\vec{\rho}}_E \tag{C-3}$$

since the geocentric point, E, and the target, T are fixed relative to each other. From (C-2),

$$(\vec{V})_I = (\dot{\vec{\rho}}_I)_I - (\vec{\Omega}_{EI} \times \vec{\rho})_I \tag{C-4}$$

showing how $(\vec{V})_I$ is obtained from orbital data and earth angular velocity.

Denoting the spacecraft frame (x, y, z) as the B frame, by Corioles' s theorem,

$$\vec{V} = \dot{\vec{s}}_E = \dot{\vec{s}}_B + \vec{\Omega}_{BE} \times \vec{s} \tag{C-5}$$

The angular velocity of the B frame relative to the non-drifting I frame, Ω_{BE}, in turn canbbe expressed in terms of earth angular velocity as

$$\vec{\Omega}_{BE} = \vec{\Omega}_{BI} - \vec{\Omega}_{EI} \tag{C-6}$$

Resolved in the B frame,

$(\vec{\Omega}_{BI})_B$ would be measured by the three strapdown rate gyros (assuming no drift). If on the other hand, we impose the gyrocompassing constraint,

$$(\vec{\Omega}_{BI})_B = \begin{pmatrix} 0 \\ 0 \\ \Omega_z \end{pmatrix} \qquad \text{(C-7)}$$

$(\vec{\Omega}_{BI})_B$ must be identified as a command required to satisfy the target tracking or lock-on conditions, This follows from the fact that $\vec{V}$, $\vec{\Omega}_{EI}$, and s are given conditions. With the x and y components constrained to be zero, as given by (C-7), the remaining component, the spacecraft roll rate, Ω_z, is determinable from (C-5), (C-6), and (C-7). Thus all components of $(\vec{\Omega}_{BI})_B$ which satisfy Coriolis's relationship are identified as command rates required to satisfy the combination of target lock-on and gyrocompassing.

For the purpose of tracking a target outside the orbital plane, another degree of freedom (beyond that of spacecraft roll) is required. This is the gimballed rotation of a sighting telescope about the craft's x axis through the angle, A_c. This angle is also identified as a command angle which must keep the target trained by the gimballed scope. Hence another coordinate frame, the T frame (x_T, y_T, z_T) is defined with y_T as always pointing to the target. As will be seen , in order to determine the command roll rate, Ω_{cz}, and command azimuth angle A_c, so as to keep the pointing axis, y_T, on the target under the given conditions , $(V)_I$, s, and $\Omega_{cx} = 0$, $\Omega_{cy} = o$, (replacing (C-7) by the properly designated command angular velocity)

$$(\vec{\Omega}_{B_c I}) = \begin{pmatrix} 0 \\ 0 \\ \Omega_{cz} \end{pmatrix}, \qquad \text{(C-7a)}$$

the command attitude of the craft relative to the I frame must simultaneously be determined. First (C-5) is resolved in the commanded spacecraft frame:

$$(\vec{V})_{B_c} = [M_{IB_c}](\vec{V})_I = (\dot{\vec{s}}_{B_c})_{B_c} + (\Omega_{B_c E} \times s)_{B_c} \qquad \text{(C-8)}$$

$$\begin{aligned} V_{cx} &= M_{11}V_{xI} + M_{21}V_{yI} + M_{31}V_{zI} \\ V_{cy} &= M_{12}V_{xI} + M_{22}V_{yI} + M_{32}V_{zI} \\ V_{cz} &= M_{13}V_{xI} + M_{33}V_{yI} + M_{33}V_{zI} \end{aligned} \qquad \text{(C-8a)}$$

$$(s)_{B_c} = s \begin{pmatrix} 0 \\ -\cos A_c \\ \sin A_c \end{pmatrix} \qquad \text{(C-8b)}$$

$$(\Omega_{BE})_{B_c} = \begin{pmatrix} \Omega_{BEx} \\ \Omega_{BEy} \\ \Omega_{BEz} \end{pmatrix} = \begin{pmatrix} 0 \\ 0 \\ \Omega_{cz} \end{pmatrix} - \begin{pmatrix} \Omega_{EIx} \\ \Omega_{EIy} \\ \Omega_{EIz} \end{pmatrix}$$

$$= \begin{pmatrix} 0 \\ 0 \\ \Omega_{cz} \end{pmatrix} - \begin{pmatrix} M_{11}\Omega_{EIxI} + M_{21}\Omega_{EIyI} + M_{31}\Omega_{EIzI} \\ M_{12}\Omega_{EIxI} + M_{22}\Omega_{EIyI} + M_{32}\Omega_{EIzI} \\ M_{13}\Omega_{EIxI} + M_{23}\Omega_{EIyI} + M_{33}\Omega_{EIzI} \end{pmatrix} \qquad \text{(C-8c)}$$

where

$$(\Omega_{EI})_I = \begin{matrix} \Omega_{EIxI} \\ \Omega_{EIyI} \\ \Omega_{EIzI} \end{matrix} \qquad \text{(C-8d)}$$

Again by the Coriolis theorem,

$$\dot{s}_{B_c} = \dot{s}_T + \Omega_{TB_c} \times s \qquad \text{(C-9)}$$

Referring to Figure 2, the angular velocity of the T frame relative to the B_c frame is

$$\left(\vec{\Omega}_{TB_c}\right)_{B_c} = \begin{pmatrix} -\dot{A}_c \\ 0 \\ 0 \end{pmatrix} , \qquad \text{(C-9a)}$$

while

$$\left(\vec{s}_T\right)_T = \begin{pmatrix} 0 \\ -\dot{s} \\ 0 \end{pmatrix} ,$$

and

$$\left(\dot{s}_T\right)_{B_c} = \left[M_{TB_c} \right] \left(\dot{\vec{s}}_T\right)_T$$

$$= \begin{bmatrix} 1 & 0 & 0 \\ 0 & \cos A_c & +\sin A_c \\ 0 & -\sin A_c & \cos A_c \end{bmatrix} \begin{pmatrix} 0 \\ -\dot{s} \\ 0 \end{pmatrix}$$

$$= \dot{s} \begin{pmatrix} 0 \\ -\cos A_c \\ \sin A_c \end{pmatrix} \qquad \text{(C-9b)}$$

Hence,

$$\left(\dot{\vec{s}}_{B_c}\right)_{B_c} = \begin{pmatrix} 0 \\ -\dot{s}\cos A_c + s\dot{A}_c \sin A_c \\ \dot{s}\sin A_c + s\dot{A}_c \cos A_c \end{pmatrix} \qquad \text{(C-10)}$$

The unknowns that must be determined are the following: the nine command matrix elements, M_{ij}, the command roll rate Ω_{cz}, and the command azimuth of the sighting telescope, A_c.

Nine of the required eleven constraints are provided by equations of the type given by (B-9), Appendix B. Replacing m_{ij}, by M_{ij}, $W_x = 0$, $W_y = 0$, and $W_z = \Omega_{cz}$, the constraints are as follows:

$$
\begin{aligned}
M_{11}(t) &= \int_o^t \Omega_{cz}(t') M_{12}(t')\,dt' + M_{110} \\
M_{12} &= -\int_o^t \Omega_{cz} M_{11}\,dt' + M_{120} \\
M_{21} &= \int_o^t \Omega_{cz} M_{22}\,dt' + M_{210} \\
M_{22} &= -\int_o^t \Omega_{cz} M_{21}\,dt' + M_{220} \\
M_{31} &= \int_o^t \Omega_{cz} M_{32}\,dt' + M_{310} \\
M_{32} &= -\int_o^t \Omega_{cz} M_{31}\,dt' + M_{320} \\
M_{13} &= M_{130} \\
M_{23} &= M_{230} \\
M_{33} &= M_{330}
\end{aligned}
\qquad \text{(C-11)}
$$

where $M_{ijo} = M_{ij}(o)$. The simplification of (C-11) relative to (B-9) is due of course to two of three forcing functions being constrained at zero (the gyrocompassing mode).

Two additional constraints are required, and these two are selected from the three components of the B_c frame resolution of (C-8). From (C-7a) through (C-10), the x and z components of this resolution result in the following explicit formulae:

$$\Omega_{cz} = \Omega_{EIz} + \frac{V_{cx}}{s} \sec A_c + \Omega_{EIy} \tan A_c \qquad (C\text{-}12)$$

$$\dot{A}_c = \frac{1}{s} [V_{cz} \sec A_c - \dot{s} \tan A_c] - \Omega_{EIx} \qquad (C\text{-}13)$$

The last is rewritten as an integral equation which can be simulated.

$$A_c = \int_o^t \{ \frac{1}{s} [V_{cz} \sec A_c - s \tan A_c] - \Omega_{EIx} \} dt' + A_{co} \qquad (C\text{-}13a)$$

The initial command sighting azimuth for the target must be known. For practically all cases, this will be very close to zero, since otherwise the target would disappear over the horizon lateral to the orbital plane and would thus not be of interest.

In terms of inputs, the B_c components indicated in (C-12) and (C-13a) are repeated here.

$$\Omega_{EIx} = M_{11}\Omega_{EIxI} + M_{21}\Omega_{EIyI} + M_{31}\Omega_{EIzI} \qquad (C\text{-}14)$$

$$\Omega_{EIy} = M_{12}\Omega_{EIxI} + M_{22}\Omega_{EIyI} + M_{33}\Omega_{EIzI} \qquad (C\text{-}15)$$

$$\Omega_{EIz} = M_{130}\Omega_{EIxI} + M_{230}\Omega_{EIyI} + M_{330}\Omega_{EIzI} \qquad (C\text{-}16)$$

$$V_{cx} = M_{11}V_{xI} + M_{21}V_{yI} + M_{31}V_{zI} \qquad (C\text{-}17)$$

$$V_{cz} = M_{130}V_{xI} + M_{230}V_{yI} + M_{330}V_{zI} \qquad (C\text{-}18)$$

APPENDIX D

DEFINITIONS OF SOME MATRICES

1. $$[M_{BI}] = \begin{bmatrix} x_I \cdot x & x_I \cdot y & x_I \cdot z \\ y_I \cdot x & \text{etc.} & \\ z_I \cdot x & & \end{bmatrix} = \begin{bmatrix} m_{11} & m_{12} & m_{13} \\ m_{12} & \text{etc.} & \\ m_{13} & & \end{bmatrix}$$

transformation from spacecraft frame (B), (x, y, z) to non-drifting reference frame (I), (x_I, y_I, z_I).

2. $$[M_{BG}] = \begin{bmatrix} x_G \cdot x & x_G \cdot y & x_G \cdot z \\ y_G \cdot x & \text{etc.} & \\ z_G \cdot x & & \end{bmatrix} = \begin{bmatrix} m'_{11} & m'_{12} & m'_{13} \\ m'_{21} & \text{etc.} & \\ m'_{31} & & \end{bmatrix}$$

transformation from spacecraft frame (B), (x, y, z) to drifting reference frame (G), (x_G, y_G, z_G).

3. $$M_{BCI} = \begin{bmatrix} x_I \cdot x_C & x_I \cdot y_C & x_I \cdot z_C \\ y_I \cdot x_C & \text{etc.} & \\ z_I \cdot x_C & & \end{bmatrix} = \begin{bmatrix} M_{11} & M_{12} & M_{13} \\ M_{21} & \text{etc.} & \\ M_{31} & & \end{bmatrix}$$

transformation from commanded spacecraft frame (B_C), (x_C, y_C, z_C) to non-drifting reference frame (I), (x_I, y_I, z_I).

Discussion in this report involves transformations between the B, I, G and B_C frames. All these transformations are orthogonal, and hence the transpose is equal to the inverse. E.g.,

$$\left[M_{IB}\right] = \left[M_{BI}\right]^{-1} = \begin{bmatrix} m_{11} & m_{21} & m_{31} \\ m_{12} & \text{etc.} & \\ m_{13} & & \end{bmatrix}$$

Two initial condition matrices are involved here.

4. $$\left[M_{BI}(0)\right] = \begin{bmatrix} m_{110} & m_{120} & m_{130} \\ m_{210} & \text{etc.} & \\ m_{310} & & \end{bmatrix}$$

as applicable to the strapdown gyro matrix computer.

5. $$M_{B_CI}(0) = \begin{bmatrix} M_{110} & M_{120} & M_{130} \\ M_{210} & \text{etc.} & \\ M_{310} & & \end{bmatrix}$$

as applicable to the command matrix computer.

APPENDIX E

BASIS OF SPACECRAFT CONTROL ERROR SIGNALS

It is assumed that the combined effects of gyro drift and dynamic lag of the spacecraft control system are such that the B-frame (x, y, z) or spacecraft frame deviates by small angles from the commanded frame, B_c (x_c, y_c, z_c). In this case the deviation matrix (B_c to B transformation), can be formed by a seccession of small angle rotations.

$$\left[M_{B_c B}\right] = \begin{bmatrix} 1 & 0 & 0 \\ 0 & 1 & \epsilon_x \\ 0 & -\epsilon_z & 1 \end{bmatrix} \begin{bmatrix} 1 & 0 & -\epsilon_y \\ 0 & 1 & 0 \\ \epsilon_y & 0 & 1 \end{bmatrix} \begin{bmatrix} 1 & \epsilon_z & 0 \\ -\epsilon_z & 1 & 0 \\ 0 & 0 & 1 \end{bmatrix}$$

$$= \begin{bmatrix} 1 & \epsilon_z & -\epsilon_y \\ -\epsilon_z & 1 & \epsilon_x \\ \epsilon_y & -\epsilon_x & 1 \end{bmatrix} \qquad (E\text{-}1)$$

But by applying the transitive law to matrix multiplication,

$$\left[M_{B_c B}\right] = \left[M_{GB}\right] \left[M_{IG}\right] \left[M_{B_c I}\right] , \qquad (E\text{-}2)$$

That is B_c to B is equal to B_c to I, I to G, and G to B.

The matrix, $\left[M_{IG}\right]$, can be recognized as the gyro drift matrix.

Since the gyros are, by definition, blind to its own drift, this factor in the computed B_c to B transformation must be left out. Hence, the basis for a set of indicated error angles is:

$$\left[M'_{B_c B}\right] = \left[M_{GB}\right]\left[M_{B_c I}\right] \qquad \text{(E-3)}$$

$$= \begin{bmatrix} m'_{11} & m'_{21} & m'_{31} \\ m'_{12} & \text{etc.} & \\ m'_{13} & & \end{bmatrix} \begin{bmatrix} M_{11} & M_{12} & M_{13} \\ M_{21} & \text{etc.} & \\ M_{31} & & \end{bmatrix}$$

The matrix elements, m'_{ij}, can be recognized as the solutions of the strapdown gyro systems yielding craft attitude relative to a drifting reference frame, G. The matrix elements, M_{ij}, are the solutions of the command attitude matrix computer, yielding commanded craft attitude relative to the non-drifting frame. Denoting the indicated error angles as ϵ_x', ϵ_y', ϵ_z', set

$$\left[M'_{B_c B}\right] = \begin{bmatrix} 1 & \epsilon_z' & -\epsilon_y' \\ -\epsilon_z' & 1 & \epsilon_x' \\ \epsilon_y' & -\epsilon_x' & 1 \end{bmatrix} \qquad \text{(E-4)}$$

Equating the right sides of (E-3) with that of (E-4), results in

$$\begin{aligned} \epsilon_x' &= m'_{12} M_{13} + m_{22}' M_{23} + m'_{32} M_{33} \\ \epsilon_y' &= m'_{13} M_{11} + m_{23}' M_{21} + m'_{33} M_{31} \qquad \text{(E-5)} \\ \epsilon_z' &= m'_{11} M_{12} + m_{21}' M_{22} + m'_{31} M_{32} \end{aligned}$$

From the gyrocompassing constraint in the spacecraft command, it was shown in Appendix C that three command matrix elements are constants,

$$M_{13} = M_{130}$$

$$M_{23} = M_{230} \qquad \text{(E-6)}$$

$$M_{33} = M_{330}$$

From (E-2) and (E-3),

$$\left[M_{B_c B}\right] = \left[M_{GB}\right] \left[M_{IG}\right] \left[M_{BG}\right] \left[M'_{B_c B}\right] \qquad \text{(E-7)}$$

As shown in Appendix A, the drift matrix,

$$\left[M_{IG}\right] = \begin{bmatrix} 1 & \delta_{zI} & -\delta_{yI} \\ -\delta_{zI} & 1 & \delta_{xI} \\ \delta_{yI} & -\delta_{xI} & 1 \end{bmatrix} \qquad \text{(E-8)}$$

The small angle elements are the I-frame resolution of the small angle drift vector. The first three matrices, from left to right, on the right side of (E-7) may be recognized as a similarity transformation, which applied to the drift matrix results in another drift matrix with the small angle vector resolved in the B-frame. That is,

$$\left[M_{GB}\right]\left[M_{IG}\right]\left[M_{BG}\right] = \begin{bmatrix} 1 & \delta_z & -\delta_y \\ -\delta_z & 1 & \delta_x \\ \delta_y & -\delta_x & 1 \end{bmatrix} \qquad \text{(E-9)}$$

Then from (E-1), (E-4), and (E-7)

$$\begin{bmatrix} 1 & \epsilon_z & -\epsilon_y \\ -\epsilon_z & 1 & \epsilon_x \\ \epsilon_y & -\epsilon_x & 1 \end{bmatrix} = \begin{bmatrix} 1 & \delta_z & -\delta_y \\ -\delta_z & 1 & \delta_x \\ \delta_y & -\delta_x & 1 \end{bmatrix} \times \begin{bmatrix} 1 & \epsilon_z' & -\epsilon_y' \\ -\epsilon_z' & 1 & \epsilon_x' \\ \epsilon_y' & -\epsilon_x' & 1 \end{bmatrix} \qquad \text{(E-10)}$$

Ignoring second order terms,

$$\begin{aligned} \epsilon_x &= \epsilon_x' + \delta_x \\ \epsilon_y &= \epsilon_y' + \delta_y \\ \epsilon_z &= \epsilon_z' + \delta_z \end{aligned} \qquad \text{(E-11)}$$

showing that the true small angle deviations are the sum of the indicated deviations and the small drift angles, as resolved in the body frame.

III. INERTIAL MODE BY MEANS OF TWO STAR TRACKERS

1. Introduction

2. Computational requirements

   2.1 On-board Computation of Error Signals

   2.2 On-board Stored Constants

   2.3 Spacecraft Perturbation Angles in Terms of Craft Axis Rates

   2.4 Gimbal Angles of Trackers with Stars Boresighted

   2.5 Image Plane Error Signals from Gimbal Angle Errors

   2.6 Components of Spacecraft Perturbations Along Gimbal Axes

   2.7 Tracker Detector Noise Model

   2.8 Azimuth and Elevation Servo Filters and Scale Factors

APPENDICES

A. Computation of Error Signals

B. Relation Between Image Plane Error Signals and Gimbal Angle Errors

C. Components of Spacecraft Perturbations Along Gimbal Axes of Star Trackers

D. Tracker Detector Noise Model

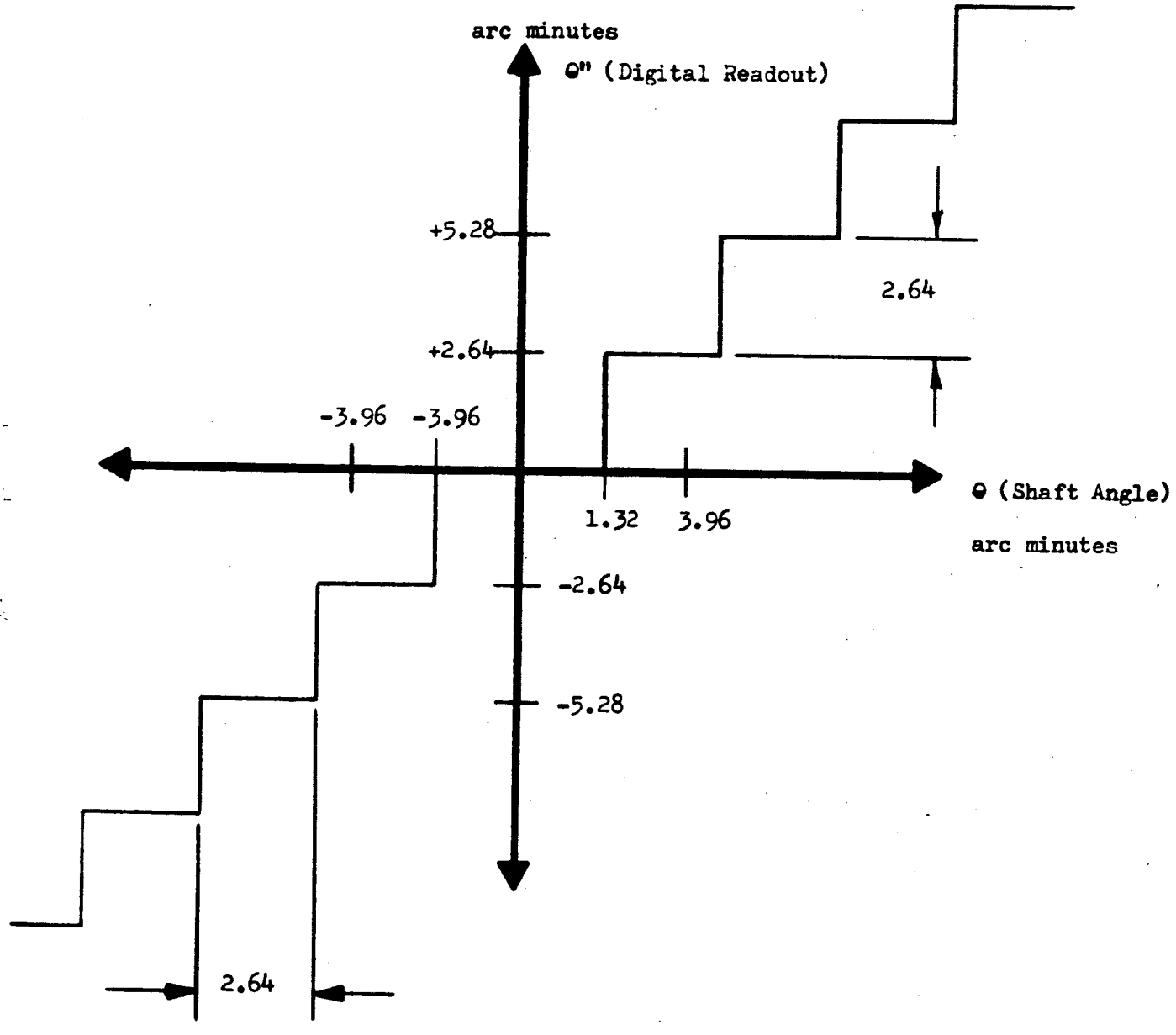

ERROR MODEL OF OPTICAL ENCODER
(BALDWIN MOD. 232)

FIGURE 9

1. Introduction

This report develops the means by which three error signals resolved in the spacecraft coordinate frame are generated from two elevation gimbal angles and one azimuth gimbal angle from two star trackers. The error signals are the body frame compononts of the crafts small angle deviation stars selected reference frame. Angular coordinates of the two stars selected as referred to the reference frame are stored in the computer. Care must be exercised in choosing the angular coordinates so as to avoid being unduly optimistic or pessimistic with regard to the geometric resolutions afforded by these angular coordinates. Because of the asymmetry of the computing method, two star lines 90 degrees apart do not necessarily yield good resolution. This problem area is discussed in Appendix A.

The two trackers are shown as mounted on opposite sides of a circular cross section of the spacecraft (see Figure 1). This mounting, with outer gimbal axes parallel is one of two choices that were considered. The other choice was for the trackers mounted 90 degrees apart on the cross section, with outer axes also 90 degrees apart. This possibility offers no clear cut advantage over the 180 degree mounting, and was thus not considered further.

The dynamics of the star trackers (Bendix Guide Star Tracker on OAO Spacecraft C) are stipulated by the servo loop shown in Figure 3.

As indicated in Section 2, although four loops (two azimuths and two elevations) strictly speaking are required for generating the three gimbal angle inputs into the error signal computer, the elimination of the second azimuth loop is amply justified. This approximates the required second azimuth gimbal angle as a means of resolving the craft's perturbation along the second tracker's inner axis (elevation), by the boresighted or error free azimuth. The resulting error is second order in servo input which should turn out to be a relatively minor input into each loop. This leads to pointing out the inputs to each loop.

First there are error signal inputs, Δy_1, Δx_1 and Δx_2 for azimuth servo 1, elevation servo 1 and elevation servo 2, respectively. These parameters represent the displacement components of the star image relative to boresight as seen in the detector's image plane. They are the parameters sensed by the detector and its electronics. In the simulation, they are computed by feeding back the servo outputs (the gimbal angles) and comparing these with computed boresight gimbal angles.

Secondly, detector noise combines with the image displacements to give corrupted image plane error signals. The detector noise for each loop, n_{y1}, n_{xi}, and n_{x2} requires an adjusted white noise generator followed by a shaping filter. The noise model indicated is appropriate for tracking a magnitude 2.5 star. The real detector noise from each axis of the image plane is independent. However,

the error signal computer couples the noises transmitted to the gimbal angles. The simulated noise for each loop, although statistically equal, must then be independent, requiring a noise generator and shaping filter for each loop. A single noise source feeding the three loops in parallel would lead to some rectification by the error signal computer, a result not representative of an operational system.

Thirdly, perturbation of the spacecraft, which is the base to which each tracker is gimballed, is a dynamic load which must be coped with by each servo. Specifically, it is the perturbation components along the outer axis of the first tracker, ϵ_x, the inner axis of the first tracker, $\vec{\epsilon} \cdot \vec{y'}_1$, and the inner axis of the second tracker, $\vec{\epsilon} \cdot \vec{y'}_2$, which are the dynamic input parameters for the three loops. (The inner axis component for the second tracker is approximated by resolving the perturbation angle vector along correct azimuth rather than gimbal azimuth.) The elevation loop differs from the azimuth loop only in respect to inertia load which is duely noted.

The three types of inputs are shown in Figure 3 as $\theta_{ST}(\Delta y_1, \Delta x_1, \Delta x_2)$ $n_V(n_{Vy1}, n_{Vx2})$, and $\theta_{BI}(\epsilon_x, \vec{\epsilon} \cdot \vec{y'}_1, \vec{\epsilon} \cdot \vec{y'}_2)$.

Finally, the tracking field of view of the Bendix Guide Star Tracker is $\pm .5$ degrees, which is adequate by several orders of magnitude in regard to the boresight errors expected in this application.

2. Computational Requirements

2.1 On-board Computation of Error Signals

$$\epsilon'_x = \frac{1}{\Delta}(\Delta_1 u_{1x} + \Delta_2 u_{1z} + \Delta_3 u_{2x}) \quad (1)$$

$$\epsilon'_y = \frac{1}{\Delta'}(s_{2yI} u_{1x} - s_{1yI} u_{2x}) \quad (2)$$

$$\epsilon'_z = \frac{1}{\Delta'}(s_{1zI} u_{2x} - s_{2zI} u_{1x}) \quad (3)$$

$$u_{1x} = \sin e'_1 - s_{1xI} \quad (4)$$

$$u_{2x} = \sin e'_2 - s_{2xI} \quad (5)$$

$$u_{1z} = \cos e'_1 \cos a'_1 - s_{1zI} \quad (6)$$

2.2 On-board Stored Constants

$$\Delta = \cos E_1^2 \sin A_1 \cos E_2 \sin(A_1 - A_2)$$

$$\Delta' = \cos E_1 \cos E_2 \sin(A_2 - A_1)$$

$$\Delta_1 = -\sin E_1 \cos E_2 \sin A_2$$

$$\Delta_2 = \cos E_1 \cos A_1 (\cos E_1 \sin A_1 - \cos E_2 \sin A_2)$$

$$\Delta_3 = \sin E_1 \cos E_2 \sin A_2$$

$$s_{1xI} = \sin E_1$$

$$s_{1yI} = -\cos E_1 \sin A_1$$

$$s_{1zI} = \cos E_1 \cos A_1$$

$$s_{2xI} = \sin E_2$$

$$s_{2yI} = -\cos E_2 \sin A_2$$

$$s_{2zI} = \cos E_2 \cos A_2$$

2.3 Space Perturbation Angles in Terms of Craft Axis Rates

$$\epsilon_x(t) = \int_o^t \Omega_x(t')\,dt' \qquad (7\text{-a})$$

$$\epsilon_y(t) = \int_o^t \Omega_y(t')\,dt' \qquad (7\text{-b})$$

$$\epsilon_z(t) = \int_o^t \Omega_z(t')\,dt' \qquad (7\text{-c})$$

2.4 Gimbal Angles of Trackers with Stars Boresighted

$$a_1 = \tan^{-1}\left(\frac{s_{1y}}{s_{1z}}\right) = \tan^{-1}\left(\frac{-\epsilon_z s_{1xI} + s_{1yI} + \epsilon_x s_{1zI}}{\epsilon_y s_{1xI} - \epsilon_x s_{1yI} + s_{1zI}}\right) \qquad (8\text{-a})$$

$$a_2 = \tan^{-1}\left(\frac{s_{2y}}{s_{2z}}\right) = \tan^{-1}\left(\frac{-\epsilon_z s_{2xI} + s_{2yI} + \epsilon_x s_{2zI}}{\epsilon_y s_{2xI} - \epsilon_x s_{2yI} + s_{2zI}}\right) \qquad (8\text{-b})$$

$$e_1 = \sin^{-1}(s_{1x}) = \sin^{-1}(s_{1xI} + \epsilon_z s_{1YI} - \epsilon_y s_{1zI}) \qquad (9\text{-a})$$

$$e_2 = \sin^{-1}(s_{2x}) = \sin^{-1}(s_{2xI} + \epsilon_z s_{2yI} - \epsilon_y s_{2zI}) \qquad (9\text{-b})$$

2.5 Image Plane Error Signals from Gimbal Angle Errors

$$\Delta y_1 = (a_1' - a_1)\cos e_1 = \Delta a_1 \cos e_1 \qquad (10\text{-a})$$

$$\Delta y_2 = (a'_2 - a_2) \cos e_2 = \Delta a_2 \cos e_2 \qquad (10\text{-b})$$

$$\Delta x_1 = e_1 - e'_1 = -\Delta e_1 \qquad (10\text{-c})$$

$$\Delta x_2 = e_2 - e'_2 = -\Delta e_2 \qquad (10\text{-d})$$

2.6 Components of Space craft Perturbations Along Gimbal Axes

ϵ_x (outer gimbal axis for both trackers)

$$\vec{\epsilon} \cdot \vec{y}'_1 = \epsilon_y \cos a'_1 + \epsilon_z \sin a'_1 \qquad (11\text{-a})$$

$$\vec{\epsilon} \cdot \vec{y}'_2 = \epsilon_y \cos a'_2 + \epsilon_z \sin a'_2 \qquad (11\text{-b})$$

(inner gimbal axis for both trackers)

Since $a_2 \approx a'_2$, the azimuth servo for the second tracker can be eliminated by replacing a'_2 by a_2 in (11-b), leading to

$$\vec{\epsilon} \cdot \vec{y}_2 \quad \epsilon_y \cos a_2 + \epsilon_z \sin a_2 \qquad (11\text{-c})$$

This simplification is dictated by the system's not requiring a'_2 as an input to the error signal computer.

2.7 Tracker Detector Noise Model

K_T (scale factor) = 2.9 mv/arc sec

N_V (white noise generator spectral power density) = 420.5 $(\text{mv})^2$/cps

$G_n(s) = \dfrac{1}{1 + .025s}$ (RC noise shaping filter)

(White noise generator and RC filter are required for each servo loop, totalling three generators and three RC filters.)

2.8 Azimuth and Elevation Servo Filters and Scale Factors

(Azimuth and Elevation Servos are the same except for inertias which are duly noted here.)

K_T = 578 volts/rad = 2.9 mv/arc sec

K_m = .754 in oz/volt

K_V = 1.00 volt/rad/sec

K_r = 0.80 volt/rad/sec

CF (Coulomb friction of gimbal bearings)

$$T_f = \begin{cases} 3.8 \text{ in oz}, & \dot{\theta}_{TB} > 0 \\ -3.8 \text{ in oz}, & \dot{\theta}_{TB} < 0 \end{cases}$$

AL (amplifier limiter

$$E = \begin{cases} e, & -20V. < e < +20V \\ 20V, & e > 20V \\ -20V, & e < -20\ V \end{cases}$$

J_A (azimuth loop inertia) = 9.33 in oz/rad/sec^2

J_E (elevation loop inertia) = 5.32 in oz/rad/sec^2

$$G_1(s) = \frac{1}{1 + .016s}$$

$$G_2(s) = 4\left(\frac{1 + 1.1s}{1 + 168s}\right)$$

$$G_3(s) = 248\,\frac{(1 + 100s)(1 + .05s)}{(1 + 5.3s)(1 + 2s)}$$

$$G_4(s) = \frac{1}{1 + .00089s}$$

$$G_5(s) = \frac{3.8}{1 + .016s}$$

2.9 Additional Definitions

$\epsilon_x, \epsilon_y, \epsilon_z$ - true error angles about vehicle axes

e'_1, a'_1, e'_2, a'_2 - indicated gimbal angles of the two trackers (azimuth and elevation)

E_1, A_1, E_2, A_2 - angular coordinates of the two stars referred to the selected inertial reference frame

$s_{1XI}, s_{1YI}, s_{1ZI}$
$s_{2XI}, s_{2YI}, s_{2ZI}$ - Components along inertial reference axes of the unit star line vectors of the two stars

Θ_{BI} - Generalized component along gimbal axis of small angular deviation of vehicle referred to onertial frame

Θ_{TI} - Generalized tracker angle about gimbal axis referred to inertial frame

Θ_{TB} - Generalized tracker angle about gimbal axis referred to vehicle frame (or indicated gimbal angle)

n_{vY1} - First tracker's injected detector noise in voltage units (Y_T - axis of T-frame)

n_{Y1} - First tracker's injected detector noise in equivalent angular units (Y_T - axis of T-frame)

ΔY_{v1} - First tracker's image plane error signal in voltage units (y_T - axis of T-frame)

ΔY_1 - First tracker's image plane error signed in equivalent angular units (Y_T-axis of T-frame)

Similarly for other parameters, axes, and second tracker.

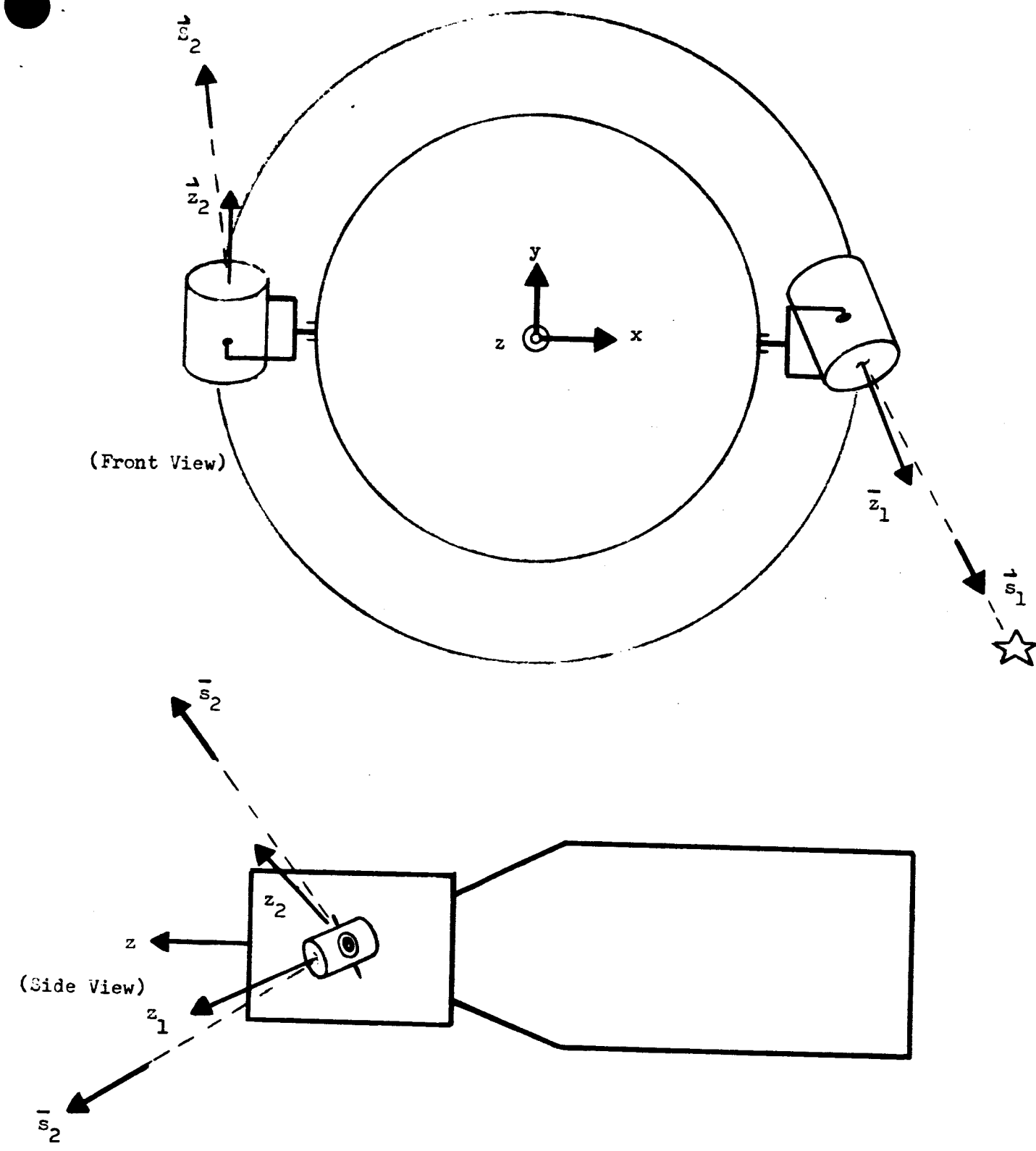

MOUNTING OF TWO GUIDE STAR TRACKERS

FIGURE 1

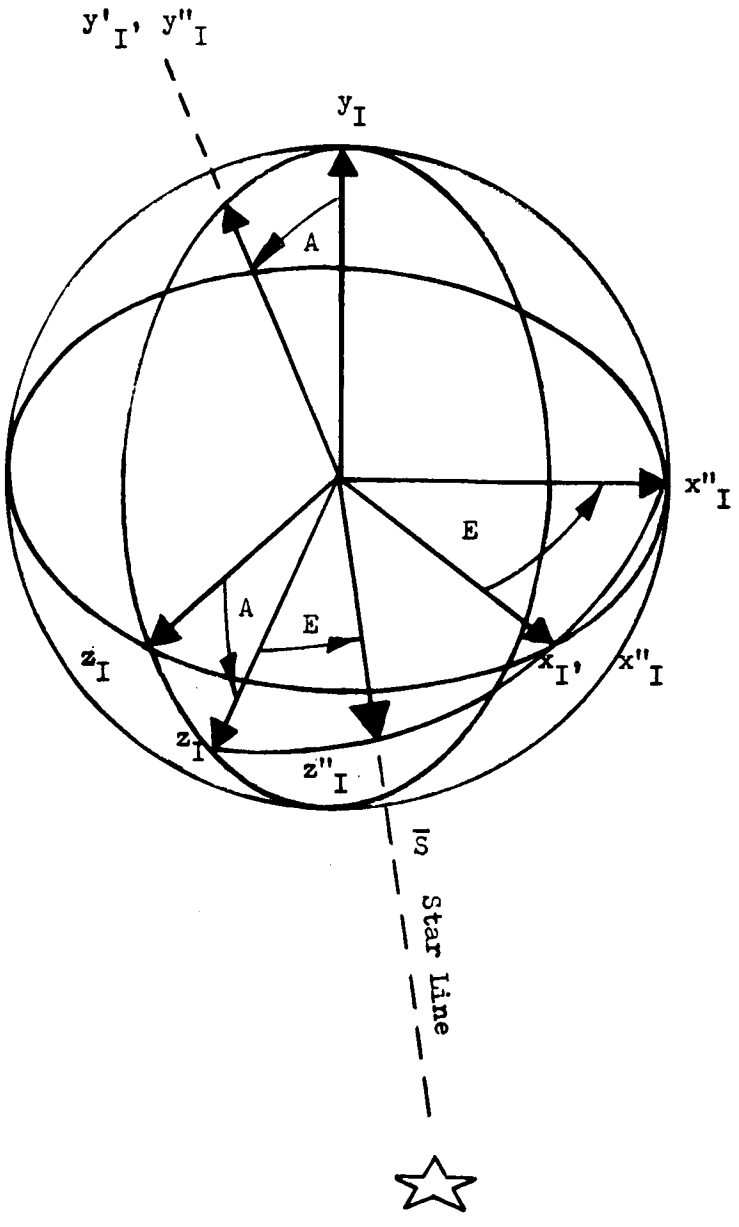

STAR LINE VECTOR

FIGURE 2

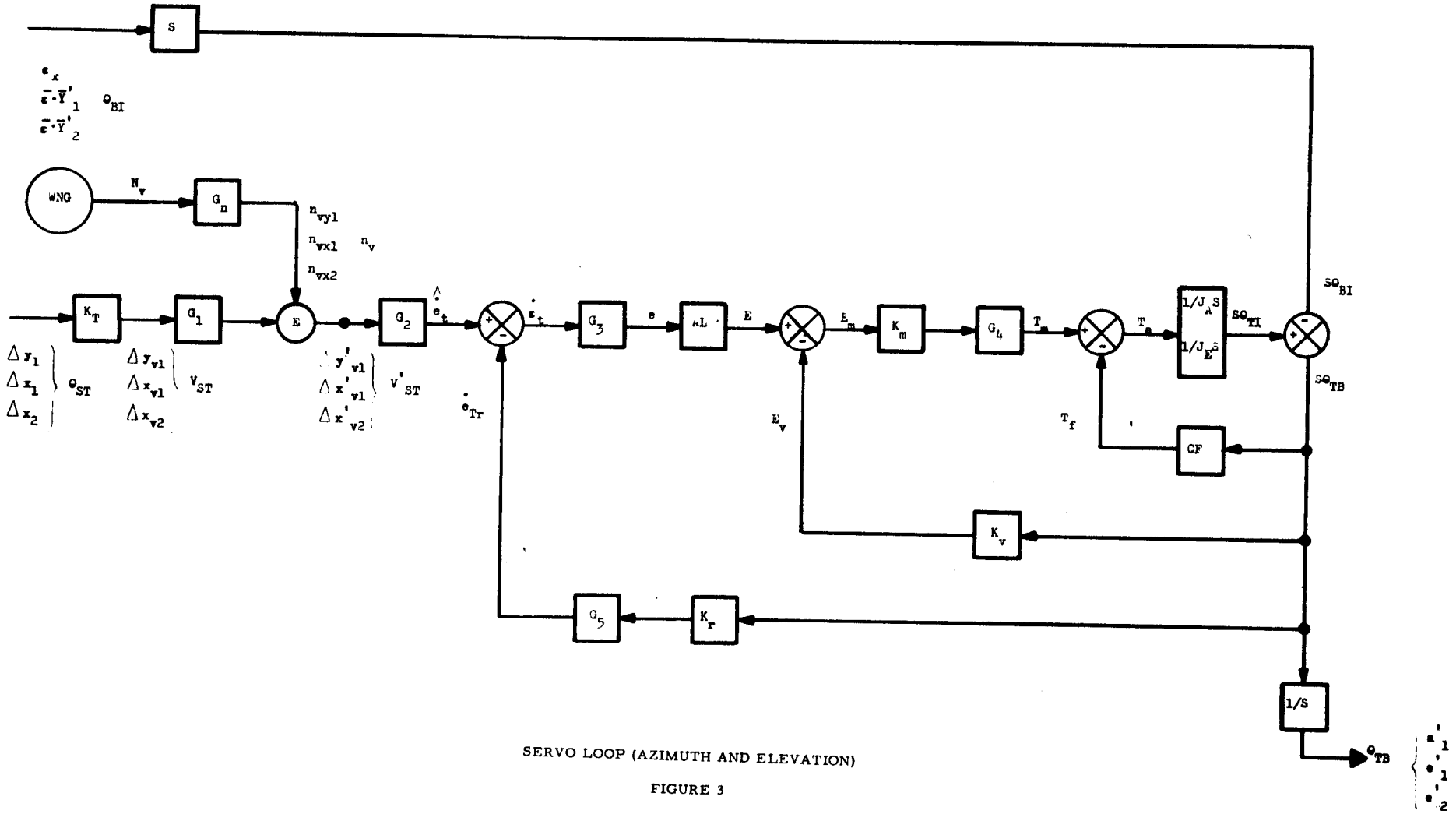

SERVO LOOP (AZIMUTH AND ELEVATION)

FIGURE 3

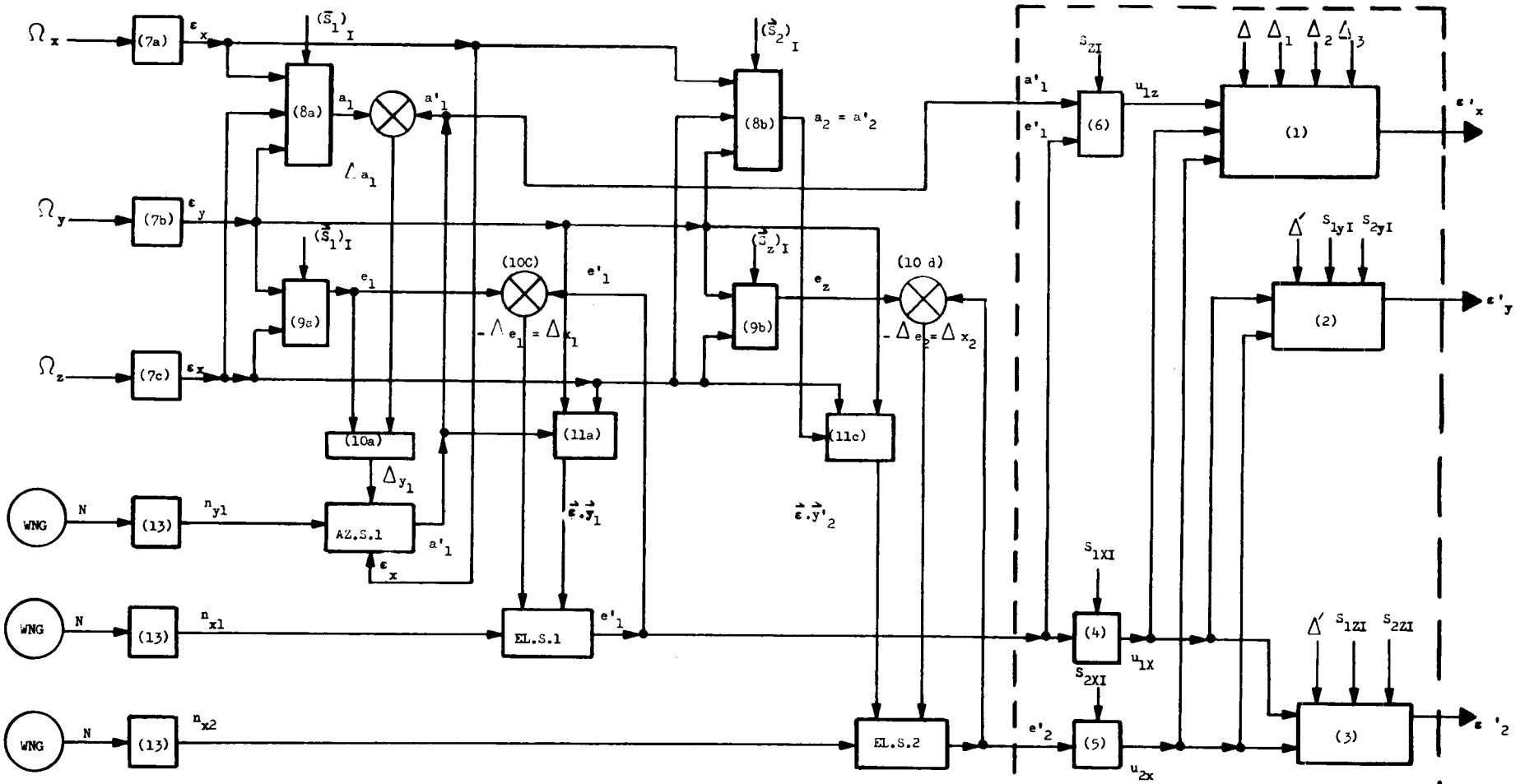

SIMULATION OF INERTIAL MODE WITH TWO STAR TRACKERS

FIGURE 4

APPENDIX A

COMPUTATION OF ERROR SIGNALS

The two selected stars and the reference frame, I, are known in advance of any measured data. With angular coordinates for the two stars, A_1, E_1 and A_2, E_2, the unit vectors, $\vec{s}_1$ and $\vec{s}_2$, which point along the star lines are first resolved in the I frame.

The azimuth, A, and elevation, E, of $\vec{s}$ are defined by Figure 1, resulting in resolutions

$$(s_1)_I = \begin{Bmatrix} s_{1xI} \\ s_{1yI} \\ s_{1zI} \end{Bmatrix} = \begin{Bmatrix} \sin E_1 \\ -\cos E_1 \sin A_1 \\ \cos E \cos A_1 \end{Bmatrix} \qquad (A\text{-}1a)$$

$$(s_2)_I = \begin{Bmatrix} s_{2xI} \\ s_{2yI} \\ s_{2zI} \end{Bmatrix} = \begin{Bmatrix} \sin E_2 \\ -\cos E_2 \sin A_2 \\ \cos E_2 \cos A_2 \end{Bmatrix} \qquad (A\text{-}1b)$$

Two matrices are now defined. The true perturbation matrix of the space-craft frame (B) relative to the reference frame (I), and the corresponding indicated perturbation of the frame (B') relative to I. These are

$$M_{IB} = \begin{Bmatrix} x.x_I & x.y_I & x.z_I \\ y.x_I & y.y_I & y.z_I \\ z.x_I & z.y_I & z.z_I \end{Bmatrix}$$

$$= \begin{Bmatrix} 1 & \epsilon_z & -\epsilon_y \\ -\epsilon_z & 1 & \epsilon_x \\ -\epsilon_y & -\epsilon_x & 1 \end{Bmatrix} \qquad \text{(A-2a)}$$

$$M_{IB'} = \begin{Bmatrix} x'.x_I & x'.y_I & x'.z_I \\ y'.x_I & y'.y_I & y'.z_I \\ z'.x_I & z'.y_I & z'.z_I \end{Bmatrix}$$

$$= \begin{Bmatrix} 1 & \epsilon'_z & -\epsilon'_y \\ -\epsilon'_z & 1 & \epsilon_x \\ \epsilon'_y & -\epsilon'_x & 1 \end{Bmatrix} \qquad \text{(A-2b)}$$

These results for small angle rotations follow the argument given in the Second Preliminary Report for equation (A-5).

The true perturbation components resolved in the B-frame are related to the B-frame components of craft angular velocity relative to the I frame, Ω, by

$$\epsilon_x(t) = \int_o^t \Omega_x(t')dt'$$

$$\epsilon_y(t) = \int_o^t \Omega_y(t')dt' \qquad (A-3)$$

$$\epsilon_z(t) = \int_o^t \Omega_z(t')dt'$$

This result, intuitively obvious, is confirmed rigorously by utilizing the results of Appendix B of the Second Preliminary Report. By identifying the direction cosine elements of (A-2a) of this report, and ignoring second order terms, one arrives at the result (A-3). Initial conditions can be set at zero, since our interest is in the RMS values of ϵ_x, ϵ_y, and ϵ_z.

The indicated angular coordinates of the two star lines are the read out gimbal angles of the two star trackers, a'_1, e'_1 and a'_2, e'_2. These are angles referred to the spacecraft frame, and differ from the true angular coordinates, a_1, e_1 and a_2, e_2, referred to this frame by the small misalignments of the two tracker optic axes relative to the star lines. Since the tracker detector error signals are noise corrupted, they are not used either in actual operation or in the simulation proposed here. The utilization of the gimbal angle data, which suffers from noise and dynamic errors, leads to the determinations of indicated spacecraft error angles. The gimbal angles, a'_1, e'_1 and a'_2, e'_2 are defined relative to the B-frame in a

manner analogous to that of the stored coordinates A_1, E_1 and A_2, E_2 relative to the I-frame. In that case, the resolutions of the star line vectors in the indicated spacecraft frame are given as

$$(\vec{s}_1)_{B'} = \begin{Bmatrix} s'_{1x} \\ s'_{1y} \\ s'_{1z} \end{Bmatrix} = \begin{Bmatrix} \sin e'_1 \\ -\cos e'_1 \sin a'_1 \\ \cos e'_1 \cos a'_1 \end{Bmatrix}$$

$$= M_{IB'}(\vec{s}_1)_I$$

$$= \begin{Bmatrix} s_{1xI} & +\epsilon'_z s_{1yI} & -\epsilon'_y s_{1zI} \\ -\epsilon'_z s_{1xI} & +s_{1yI} & +\epsilon'_x s_{1zI} \\ \epsilon'_y s_{1xI} & -\epsilon'_x s_{1yI} & +s_{1zI} \end{Bmatrix} \qquad \text{(A-4a)}$$

$$(\vec{s}_2)_{B'} = \begin{Bmatrix} s'_{2x} \\ s'_{2y} \\ s'_{2z} \end{Bmatrix} = \begin{Bmatrix} \sin e'_2 \\ -\cos e'_2 \sin a'_2 \\ \cos e'_2 \cos a'_2 \end{Bmatrix}$$

$$= M_{IB'}(\vec{s}_2)_I$$

$$= \begin{Bmatrix} s_{2xI} & +\epsilon'_z s_{2yI} & -\epsilon'_y s_{2zI} \\ -\epsilon'_z s_{2xI} & +s_{2yI} & +\epsilon'_x s_{2zI} \\ \epsilon'_y s_{2xI} & -\epsilon'_x s_{2yI} & +\epsilon_{2zI} \end{Bmatrix} \qquad \text{(A-4b)}$$

Equations (A-4) lead to six constraints in three unknowns, the indicated perturbations. Two from one vector equation and one from the second equation are to be chosen. For the purposes of this report, the choice is based on minimizing the on-board computational complexity. Therefore, the elevation angles from two trackers and the azimuth from one of the two, lead, among several choices, to the x and z component equations of (A-4a) and the x component of (A-4b).

The following three linear constraints in the unknowns are then selected as the basis for their computation:

$$
\begin{aligned}
&O\epsilon'_x - s_{1zI}\epsilon'_y + s_{1yI}\epsilon'_z = s_{1x} - s_{1xI} = u_{1x} \\
&-s_{1yI}\epsilon'_x + s_{1xI}\epsilon'_y + O\epsilon'_z = s_{1z} - s_{1zI} = u_{1z} \\
&O\epsilon'_x - s_{2zI}\epsilon'_y + s_{2yI}\epsilon'_z = s_{2x} - s_{2xI} = u_{2x}
\end{aligned}
\qquad \text{(A-5)}
$$

Explicitly, the indicated spacecraft errors are

$$
\left.
\begin{aligned}
\epsilon'_x &= \frac{1}{\Delta}(\Delta_1 u_{1x} + \Delta_2 u_{1z} + \Delta_3 u_{2x}) \\
\epsilon'_y &= \frac{1}{\Delta'}(s_{2yI} u_{1x} - s_{1yI} u_{2x}) \\
\epsilon'_z &= \frac{1}{\Delta'}(s_{1zI} u_{2x} - s_{2zI} u_{1x})
\end{aligned}
\right\}
\qquad \text{(A-6)}
$$

$$\left.\begin{aligned} u_{1x} &= \sin e'_1 - \sin E_1 \\ u_{2x} &= \sin e'_2 - \sin E_2 \\ u_{1z} &- \cos e'_1 \cos a'_1 - \cos E_1 \cos A_1 \end{aligned}\right\} \qquad (A\text{-}7)$$

The constants, Δ, Δ', Δ_1, Δ_2 and Δ_3 are given in Section 2.1. The remaining constants in (A-6) are given by (A-1a) and A-1b).

Obviously the computations, (A-6), depend on Δ and Δ' not equalling zero. Their magnitudes are a measure of the geometric resolution as provided by the two star lines. They range in magnitude from zero to unity, with the latter most desirable for suppressing the computational weighting of errors in the input data. Two star lines at right angles do not necessarily lead to Δ and Δ' equalling unity, as shown by the case $A_1 = A_2 = 0°$, $E_1 = 90°$, $E_2 = 0°$. The converse - if the magnitudes of Δ and Δ' are unity, then the star lines must be 90° apart has not been proven. The procedure adopted has been to arbitrarily choose values for the coordinate angles and test the values for Δ and Δ'. The choice, $E_1 = 0°, A_1 = 45°, E_2 = 45°, A_2 = 0°$ leads to the values $\Delta = .355, \Delta' = .500$. The star lines are 60° apart as may be found from

$$\cos \alpha = \vec{s}_1 \cdot \vec{s}_2 \qquad (A\text{-}8)$$

where α is the separation angle. This choice seems fair, there being large numbers of pairs of stars which would lead to such values for geometric weighting of errors.

APPENDIX B

RELATION BETWEEN IMAGE PLANE ERROR SIGNALS AND GIMBAL ANGLE ERRORS

Errors in a tracker's gimbal angles, a', e', will misalign the optic axis relative to the star line and the image will be displaced from the optic axis. A coordinate frame, T, with axes (x_T, y_T, z_T) is defined wherein z_T is the tracker's optic axis and the star image appears in the x_T - y_T plane. The T frame is rotated away from the spacecraft's B-frame by, first a rotation, a', about the outer gimbal axis (azimuth) assumed to coincide with the craft's x-axis, and then a rotation, e' about the inner gimbal axis (elevation) referred to as the y'-axis.

With a and e as the corresponding rotations referred to the B-frame which would take the z_T axis into exact alignment of the star line vector, $\vec{s}$, we have

$$(\vec{s})_B = \begin{Bmatrix} \sin e \\ -\cos e \sin a \\ \cos e \cos a \end{Bmatrix} \qquad (B\text{-}1)$$

Defining Δx and Δy as the coordinates of the displacement of the star image from boresight,

$$(\vec{s})_T = \begin{Bmatrix} \Delta x \\ \Delta y \\ 1 \end{Bmatrix} \qquad (B\text{-}2)$$

for small displacement error.

But

$$\vec{(s)}_T = M_{BT}\vec{(s)}_B \text{ or}$$

$$\begin{Bmatrix} \Delta x \\ \Delta y \\ 1 \end{Bmatrix} = \begin{bmatrix} \cos e' & 0 & -\sin e' \\ 0 & 1 & 0 \\ \sin e' & 0 & \cos e' \end{bmatrix} \begin{bmatrix} 1 & 0 & 0 \\ 0 & \cos a' & \sin a' \\ 0 & -\sin a' & \cos a' \end{bmatrix} \begin{pmatrix} \sin e \\ -\cos e \sin a \\ \cos e \cos a \end{pmatrix} \qquad \text{(B-3a)}$$

and to first order approximation,

$$\left.\begin{aligned} \Delta x &= e - e' = -\Delta e \\ \Delta y &= (a' - a)\cos e = \Delta a \cos e \end{aligned}\right\} \qquad \text{(B-3b)}$$

The second equation of (B-3b) shows, as is well known, the geometric attenuation with elevation of the outer loop sigmal gain. This result applies to both trackers, 1 and 2.

Allowing for detector noise, the input error signals for the two trackers' four servo loops are

$$\left.\begin{aligned} \Delta y'_1(s) &= G_1(s)\Delta y_1(s) + n(s) \\ \Delta y'_2(s) &= G_1(s)\Delta y_2(s) + n(s) \\ \Delta x'_1(s) &= G_1(s)\Delta x_2(s) + n(s) \\ \Delta x'_2(s) &= G_i(s)\Delta x_2(s) + n(s) \end{aligned}\right\} \qquad \text{(B-4)}$$

as may be noted from Figure 3.

APPENDIX C

COMPONENTS OF SPACECRAFT PERTURBATIONS ALONG GIMBAL AXES OF THE STAR TRACKER

Referring to Figure 3, we note that each servo loop has two inputs, θ_{ST}, the star line angle coordinate relative to the telescope axis (z), and the base or B-frame perturbation relative to inertial space, θ_{BI}. The latter is a dynamic load which the servo must cope with, and it is this motion that is discussed here.

This motion, three dimensionally, is the small angle perturbation vector, $\vec{\epsilon}$, which resolved in the B-frame is, as previously indicated,

$$(\vec{\epsilon})_B \begin{pmatrix} \epsilon_x \\ \epsilon_y \\ \epsilon_z \end{pmatrix} \qquad (C-1)$$

The perturbation component along the outer gimbal axes according to Figure 1, for both trackers is ϵ_x. Along the inner gimbal axes, it is $\vec{\epsilon}, \vec{y'}$, y' beigh designated as the unit vector along the elevation axis for both trackers. This axis, in general, is rotated away from the craft's y-axis by the azimuth angle, a'.

Then from

$$(\vec{\epsilon})' = \begin{pmatrix} \vec{\epsilon} \cdot \vec{x}' \\ \vec{\epsilon} \cdot \vec{y}' \\ \vec{\epsilon} \cdot \vec{z}' \end{pmatrix} = \begin{bmatrix} 1 & 0 & 0 \\ 0 & \cos a' & \sin a' \\ 0 & -\sin a' & \cos a' \end{bmatrix} \begin{pmatrix} \epsilon_x \\ \epsilon_y \\ \epsilon_z \end{pmatrix} \qquad \text{(C-2a)}$$

$$\vec{\epsilon} \cdot \vec{y}' = \epsilon_y \cos a' + \epsilon_z \sin a' \qquad \text{(C-2b)}$$

APPENDIX D

TRACKER DETECTOR NOISE MODEL

Power spectral density measurements of the Bendix tracker detector noise indicate that it is shaped like RC filter noise. That is with n(t) as the noise injected into the servo loop (see Figure 3), the spectrum is of the form

$$S_n(f) = \frac{N}{1 + 4\pi^2 T_n^2 f^2} = \frac{N}{\left|1 + 2\pi T_n j f\right|^2} \qquad \text{(D-1a)}$$

$$= \frac{S_n(0)}{\left|1 + 2\pi T_n j f\right|^2} \qquad \text{(D-1b)}$$

The tracker scale factor, K_T, converting arc seconds into millivolts is

$$K_T = 2.9 \text{ mv/arc sec} \qquad \text{(D-2)}$$

Then writing n_θ for noise in angular units, and n_V for noise in voltage units,

$$n_V = K_T n_\theta \qquad \text{(D-3)}$$

The mean square of the injected RC noise

$$\overrightarrow{n^2} = \int_0^\infty \left|G(jf)\right|^2 df = \frac{N}{4T_n} = \frac{S_n(0)}{4T_n} \qquad \text{(D-4)}$$

The white noise bandwidth, B_n, of a linear filter $G(s)$, is defined as

$$B_n = \int_0^\infty |G(jf)|^2 \, df \qquad \text{(D-5a)}$$

For an RC filter

$$G(s) = \frac{1}{1 + T_n s} \, , \qquad \text{(D-5b)}$$

$$B_n = \frac{1}{4T_n} \quad \text{as indicated in (D-4)}$$

The noise measurements showed (in angular units) that for a star of visual magnitude, $M_V = 2.5$,

$$\begin{aligned} s_{n\theta}(0) &= N_\theta = 50 \text{ arc sec}^2/\text{cps} \\ B_n &= 10 \text{ cps} \end{aligned} \qquad \text{(D-6a)}$$

Hence the time constant for the RC filter should be

$$T_n = .025 \text{ seconds} \qquad \text{(D-6b)}$$

The mean square of the injected noise in angular units is then

$$\overline{n_\theta^2} = \int_0^\infty S_{n\theta}(f) \, df = \frac{N_\theta}{4T_n} = 500 \text{ arc sec}^2 \qquad \text{(D-7a)}$$

which corresponds, in voltage units, to

$$\overline{n_V^2} = K_T^2 \overline{n_\theta^2} = 4,205.0 \text{ mv}^2 \qquad \text{(D-7b)}$$

The power density of the white noise which is the input to the RC filter in angular units

$$N_\theta = S_{n\theta}(0) = 50 \text{ arc sec}^2/\text{cps} \qquad \text{(D-8a)}$$

and in voltage units

$$N_V = S_{nV}(0) = K_T^2 S_{n\theta}(0) = 420.5 \text{ mv}^2/\text{cps} \qquad \text{(D-8b)}$$

To summarize: With a scale factor as given by (D-2), a white noise generator (WNG) attenuated to an output with a power density spectrum evaluated according to (D-8B), followed by an RC filter with transfer function,

$$G_n(s) = \frac{1}{1 + .025\,s} \qquad \text{(D-9)}$$

will adequately simulate the detector noise due to a magnitude 2.5 star.

IV. HORIZON SPECTROMETRY EXPERIMENT

1. Introduction

2. Computational Requirements

Appendices

A. Computations for Generating Error Signals from Orbital Data and Strapdown Gyro System

B. Computations for Gyro Drift Correction

C. Relation Between Image Plane Error Signals and Gimbal Angle Errors

D. Initial Conditions

E. Base Motion Dynamic Loading of the Servos

1. Introduction

The scheme discussed in detail here is aimed at holding the spacecraft with its roll axis along the ellipsoid vertical while the craft is commanded to rotate about its roll axis, enabling an experimental package to sweep the horizon.

The accuracy requirement, .01 degrees error for the normal to the horizon, precludes the use of horizon sensors, the best of which to date would track the horizon vertical with an uncertainty of about 0.2 degrees. Limiting the alternatives to fully developed and feasible instrumentation, a vertical with the required accuracy may be obtained by orbital data combined with a gyro reference coordinate frame as updated by star tracker data corrections. (See Figure 1)

The orbital data is the geocentric position vector of the craft as resolved in the selected inertial reference frame. The inertial reference frame is chosen so that one axis is parallel to the earth's rotation axis. This is not essential but in any case the earth's rotation axis must be known in the inertial reference frame. One of the geocentric components then yields geocentric latitude. Geocentric latitude is corrected by a stored correction function based on the International Ellipsoid to give geodetic latitude. From the other two geocentric components and the geodetic latitude, the direction cosines of the geodetic or ellipsoid vertical as resolved in the selected inertial frame are obtained.

A strapdown gyro system with initial conditions inserted by data from body mounted star tracker's physically establishes the selected reference frame. Intermittent transfer of tracker corrected direction cosines to the strapdown system computer's initial conditions, with integration intervals limited to those between updatings, limits the drift of the strapdown system reference frame to the drift angles of the gyros accumulated in those intervals.

With the updated direction cosines defining the attitude between vehicle and selected reference frame, the ellipsoid vertical error signals are computed as the components of the ellipsoid unit vertical along two vehicle frame axes. Differentiation of these error signals gives vertical error rates. Subtraction of the roll rate gyro output by the constant command rate (as a computer operation - not by precessing the gyro) yields the roll rate error signal, while integration yields the roll error signal. As indicated in figure 1, the roll error signals do not get the benefit of tracker corrective data since the roll angle of the vehicle is not critical.

Figure 2 shows two star trackers mounted on extension brackets to the walls of the vehicle with outer gimbal axes parallel to the roll axis. This mounting is indicated because the roll of the vehicle as stars are being tracked precludes the mounting indicated in the third Preliminary report. With the latter mounting there would be risk of gimbal lock being approached and,

concomitantly, unduly high gimbal rates. Secondly with the vehicle front end pointed to the earth, the tail, pointing to the stars, is assumed to be the location of a rocket motor.

As the vehicle rolls (for the mounting indicated) the star for each tracker will be occulted for half the roll period by the vehicle itself. Since the directions to each star must not be paralled and since data from two stars are required, the interval over which the reference frame can be established will be something less than half the roll period.

For a roll rate of 1 degree per second or a roll period of 6 minutes, data intervals limited to 1 to 3 minutes can be expected.

If the horizon experiment is to be continued over several roll periods, this implies a requirement of reacquisition and track for each tracker within its three minute "seeing window". To do this, in fact to acquire the stars in the first place, requires a separate command channel wherein the star coordinates as referred to a physically available reference frame, would be command signals. These command angles could then be transformed to vehicle referred command angles and compared with the actual tracker gimbal angles to close the loops. The implementation of this acquisition function is not indicated since it has no bearing on the accuracy of the attitude mode for this experiment.

It is quite feasible to carryout the updating function with one star tracker. Assuming the availability of an acquisition command channel, the single tracker could acquire and track, in sequence, the two selected stars as the vehicle rolls. The computational scheme would be functionally identical to the dual tracking scheme. The only modification would be of a hardware nature in that volatile storages would be required of tracker and gyro direction cosine data with appropriate synchronizations of data from these two sensors. An accuracy penalty is incurred relative to a two-tracker scheme, in that the computational scheme (identical to the two-tracker scheme) cannot detect the gyro drift accumulated in the time between storages in the two-storage sequence. With data stored from both stars, correction is available, and if the gyro drifts accumulated between sightings in the sequence is small enough so as not to seriously compromise the vertical alignment the single tracker sighting sequence technique should definitely be used.

The 18 PIRIG rate gyro can, by feasible compensation, achieve a drift rate in orbit of about 0.07 degrees per hour. Assuming an interval of 2 minutes for the sighting and data storage sequence of the two stars, a drift angle of .002 degrees for each gyro is accumulated and assuming an average angle of 45 degrees between the total drift vector and vertical, the indicated vertical would drift by $\sqrt{3} \times .002 \times \sin 45° = .0025$ degrees. This would be the degradation of the single tracker system accuracy relative to the two-tracker

system. For a goal of .01 degrees vertical error, the single-tracker scheme appears acceptable. The simulation, for purposes of error effects, is practically identical to that of the two-tracker scheme, hence results obtained for the latter should be practically the same as for the former.

With the outer axis (azimuth) parallel to the roll axis, a relatively large azimuth tracking error should be expected. Extrapolation of simulation results obtained for input ramps in the ball park of 1 degree per second into the Bendix OAO tracker, indicate that the tracking error would be about 8 minutes of arc = .13 degrees. However, because of the attitude mode called for, namely, alignment of the roll axis with the vertical, and consequently alignment of the azimuth axis with the vertical due to the mounting, the weighting by the computer of azimuth tracking errors toward indicated vertical errors will, at most, be of second order. Hence the expected large azimuth tracking error, per se, is not an argument against rolling the vehicle to sweep the horizon. More serious would be the electronic and computer complications in reacquiring the tracked stars following occultation by the vehicle roll. The suggested alternative is to mount the experimental instrumentation on an azimuth gimbal, and drive it relative to a roll stabilized vehicle (see Figure 3). The only difference between the simulation of this mode and that of the vehicle roll command mode would be-

(1) Equation (42) replaces (3).

(2) Equation (3) becomes the error rate signal for the experimental package.

(3) The azimuth or sweep (z-axis) error of the package is not available owing to the absence of a dynamic model of the experimental package azimuth loop.

The mounting as indicated for this experiment is required, while the mounting indicated for the Inertial Mode Experiment cannot be used for this experiment. Either mounting can be used for the Inertial Mode Experiment. Hence this mounting is to be regarded as superseding the previous mounting. While this would require a modification of the computations that were indicated in the Third Report, the RMS values of attitude errors found from the indicated computation are in no way invalidated, since the modification of the mounting would lead only to different components of vector equations being utilized, but not to any change in geometric resolution, on the average, in the choices of the two stars.

The requirement of four tracker data channels for this mode (two azimuths and two elevations) as against three for the inertial mode, is dictated by considerations of degeneracy in the computation as the vehicle rotates, due to orbital motion and roll, relative to inertial space.

The figures of merit of the attitude control system are the RMS values of (28) and (29), true vertical errors, and (30) true roll error for the rolled vehicle mode (para. 2.2).

2. Computational Requirements

2.1 On-board Computations of Error Signals

2.1.1 Error Signals

$$\epsilon'_x = m'_{12}\ z_{ExI} + m'_{22}\ z_{EyI} + m'_{32}\ z_{EZI} \qquad (1)$$

$$\epsilon'_y = -(m'_{11}\ z_{ExI} + m'_{21}\ z_{EyI} + m'_{31}\ z_{EzI}) \qquad (2)$$

$$\epsilon'_z = \int_o^t (W_z - \Omega_{cz})\, dt' \qquad (3)$$

2.1.2 I-frame components of ellipsoid vertical vector

$$z_{ExI} = -\sin \phi \cos \lambda \qquad (4)$$

$$z_{EyI} = -\sin \lambda \qquad (5)$$

$$z_{EzI} = -\cos \phi \cos \lambda \qquad (6)$$

2.1.3 Longitude

$$\sin \phi = \frac{w}{\sqrt{u^2 + w^2}} \tag{7}$$

$$\cos \phi = \frac{u}{\sqrt{u^2 + w^2}} \tag{8}$$

2.1.4 Geodetic or ellipsoidal latitude

$$\lambda = \lambda_R + \Delta\lambda \tag{9}$$

2.1.5 Geocentric latitude

$$\lambda_R = \sin^{-1}\left(\frac{v}{r}\right) \tag{10}$$

2.1.6 Correction of geocentric latitude

$$\Delta\lambda = .003373 \sin 2\lambda_R + .000006 \sin 4\Delta\lambda_R \tag{11}$$

(in radians)

u, v, w - (I - frame components of craft's geocentric vecotr, $\vec{r}$)

u, w - equatorial plane components

v - polar axis component

2.1.7 Tracker updated direction cosines of gyro strapdown system

$$
\begin{aligned}
m'_{11} &= \int_{t_k}^{t} (-W_y\ m'_{13} + W_z\ m'_{12})\, dt' + m_{s11}(t_k) \\
m'_{12} &= \int_{t_k}^{t} (-W_z\ m'_{11} + W_x\ m'_{13})\, dt' + m_{s12}(t_k) \\
m'_{13} &= \int_{t_k}^{t} (-W_x\ m'_{12} + W_y\ m'_{11})\, dt' + m_{s13}(t_k) \\
m'_{21} &= \int_{t_k}^{t} (-W_y\ m'_{23} + W_z\ m'_{22})\, dt' + m_{s21}(t_k) \\
m'_{22} &= \int_{t_k}^{t} (-W_z\ m'_{21} + W_x\ m'_{23})\, dt' + m_{s22}(t_k) \\
m'_{23} &= \int_{t_k}^{t} (-W_x\ m'_{22} + W_y\ m'_{21})\, dt' + m_{s23}(t_k) \\
m'_{31} &= \int_{t_k}^{t} (-W_y\ m'_{33} + W_z\ m'_{32})\, dt' + m_{s31}(t_k) \\
m'_{32} &= \int_{t_k}^{t} (-W_z\ m'_{31} + W_x\ m'_{33})\, dt' + m_{s32}(t_k) \\
m'_{33} &= \int_{t_k}^{t} (-W_x\ m'_{32} + W_y\ m'_{31})\, dt' + m_{s33}(t_k)
\end{aligned}
\qquad (12)
$$

where t_k is the time of the k th updating, and $t_k < t < t_{k+1}$

W_x, W_y, W_z - outputs of strapdown rate gyros.

2.1.8 Rate Gyro Error Models

$$W_x = \Omega_x - c_o \quad (13)$$

$$W_y = \Omega_y - c_o \quad (14)$$

$$W_z = \Omega_z - c_o \quad (15)$$

c_o (drift rate) = 0.07 degrees per hour

2.1.9 Tracker corrected direction cosines of gyro strapdown system

$$\begin{aligned}
m_{s11} &= +m'_{11} - m'_{21}\,\delta_{zI} + m'_{31}\,\delta_{yI} \\
m_{s12} &= +m'_{12} - m'_{22}\,\delta_{zI} + m'_{32}\,\delta_{yI} \\
m_{s13} &= +m'_{13} - m'_{23}\,\delta_{zI} + m'_{33}\,\delta_{yI} \\
m_{s21} &= +m'_{11}\,\delta_{zI} + m'_{21} - m'_{31}\,\delta_{xI} \\
m_{s22} &= +m'_{12}\,\delta_{zI} + m'_{22} - m'_{32}\,\delta_{xI} \\
m_{s33} &= +m'_{13}\,\delta_{zI} + m'_{23} - m'_{33}\,\delta_{xI} \\
m_{s31} &= -m'_{11}\,\delta_{yI} + m'_{21}\,\delta_{xI} + m'_{31} \\
m_{s32} &= -m'_{12}\,\delta_{yI} + m'_{22}\,\delta_{yI} + m'_{32} \\
m_{s33} &= -m'_{13}\,\delta_{yI} + m'_{23}\,\delta_{zI} + m'33
\end{aligned} \quad (16)$$

2.1.10 Gyro drift angle components

$$\delta_{xI} = \frac{1}{\Delta'} \left(s_{2xI}\, u_{1z} - s_{1xI}\, u_{2z} \right) \quad (17)$$

$$\delta_{xI} = \frac{1}{\Delta'} \left(s_{2yI}\, u_{1z} - s_{1yI}\, u_{2z} \right) \quad (18)$$

$$\delta_{zI} = \frac{1}{\Delta} \left(\Delta_1\, u_{1x} + \Delta_2\, u_{1z} + \Delta_3 u_{2z} \right) \quad (19)$$

2.1.11 Error vector components

$$u_{1x} = s_{1xG} - s_{1xI} \quad (20)$$

$$u_{1z} = s_{1zG} - s_{1zI} \quad (21)$$

$$u_{2z} = s_{2zG} - s_{2zI} \quad (22)$$

2.1.12 G-frame components of tracked star line vectors

$$s_{1xG} = m'_{11}\, s'_{1x} + m'_{12}\, s'_{1y} + m'_{13}\, s'_{1z} \quad (23)$$

$$s_{1zG} = m'_{31}\, s'_{1x} + m'_{32}\, s'_{1y} + m'_{33}\, s'_{1z} \quad (24)$$

$$s_{2zG} = m'_{31}\, s'_{2x} + m'_{32}\, s'_{2y} + m'_{33}\, s'_{2z} \quad (25)$$

2.1.13 B-frame components of tracked star line vectors

$$\begin{aligned} s'_{1x} &= -\cos e'_1 \sin a'_1 \\ s'_{1y} &= \cos e'_1 \cos a'_1 \\ s'_{1z} &= -\sin e'_1 \end{aligned} \quad (26)$$

$$s'_{2x} = -\cos e'_2 \sin a'_2$$

$$s'_{2y} = \cos e'_2 \cos a'_2 \qquad (27)$$

$$s'_{2z} = -\sin e'_2$$

e'_1 , a'_1 , e'_2 , a'_2 -gimbal angle data (elevation and azimuth) from two trackers.

2.1.14 Stored constants

$$\Delta = (\cos E_1)^2 \cos E_2 \cos A_1 \sin (A_1 - A_2)$$

$$\Delta' = \cos E_1 \cos E_2 \sin (A_1 - A_2)$$

$$\Delta_1 = -\cos E_1 \cos E_2 \sin (A_1 - A_2)$$

$$\Delta_2 = -\cos E_2 \cos A_2 \sin E_1$$

$$\Delta_3 = \cos E_1 \cos A_1 \sin E_1$$

$$s_{1xI} = -\cos E_1 \sin A_1$$

$$s_{1yI} = \cos E_1 \cos A_1$$

$$s_{1zI} = \sin E_1$$

$$s_{2xI} = -\cos E_2 \sin A_2$$

$$s_{2yI} = \cos E_2 \cos A_2$$

$$s_{2zI} = -\sin E_2$$

2.2 True Angular Perturbations Referred to Command Coordinate Frame (B_c).

2.2.1 B-frame components

$$\epsilon_x = m_{12}\ z_{ExI} + m_{22}\ z_{EyI} + m_{32}\ z_{EzI} \tag{28}$$

$$\epsilon_y = -(m_{11}\ z_{ExI} + m_{21}\ z_{EyI} + m_{31}\ z_{EzI}) \tag{29}$$

$$\epsilon_z = \int_o^t (\Omega_z - \Omega_{cz})\ dt' \tag{30}$$

2.2.2 True direction cosines

$$\left.\begin{aligned} m_{11} &= \int_o^t (-\Omega_y m_{13} + \Omega_z m_{12})\ dt' + m_{110} \\ m_{12} &= \int_o^t (-\Omega_z m_{11} + \Omega_x m_{13})\ dt' + m_{120} \\ &\ \ \vdots \\ m_{33} &= \int_o^t (-\Omega_x m_{32} + \Omega_y m_{31})\ dt' + m_{330} \end{aligned}\right\} \tag{31}$$

(These 9 equations follow the same form as for (12)

2.3 Star Tracker Error Model

2.3.1 Boresighted gimbal angles

$$a_1 = \tan^{-1}\left(\frac{-s_{1x}}{s_{1y}}\right) = -\tan^{-1}\left(\frac{m_{11}\, s_{1xI} + m_{21}\, s_{1yI} + m_{31}\, s_{1zI}}{m_{12}\, s_{1xI} + m_{22}\, s_{1yI} + m_{32}\, s_{1zI}}\right) \quad (32)$$

$$e_1 = -\sin^{-1}(s_{1z}) = -\sin^{-1}\left(m_{13}\, s_{1xI} + m_{23}\, s_{1yI} + m_{33}\, s_{1zI}\right) \quad (33)$$

$$a_2 = \tan^{-1}\left(\frac{-s_{2x}}{s_{2y}}\right) = -\tan^{-1}\left(\frac{m_{11}\, s_{2xI} + m_{21}\, s_{2yI} + m_{31}\, s_{2zI}}{m_{12}\, s_{2xI} + m_{22}\, s_{2yI} + m_{32}\, s_{2zI}}\right) \quad (34)$$

$$e_2 = -\sin^{-1}(s_{2z}) = -\sin^{-1}(m_{13}\, s_{2xI} + m_{23}\, s_{2yI} + m_{33}\, s_{2zI}) \quad (35)$$

2.3.2 Image plane error signals

$$\Delta x_1 = (a'_1 - a_1)\cos e_1 = \Delta a_1 \cos e_1 \quad (36)$$

$$\Delta y_1 = e'_1 - e_1 = \Delta e_1 \quad (37)$$

$$\Delta x_2 = (a'_2 - a_2)\cos e_2 = \Delta a_2 \cos e_2 \quad (38)$$

$$\Delta y_2 = e'_2 - e_2 = \Delta e_2 \quad (39)$$

2.3.3 Base motion loading of servos

$$\alpha_{xT} = \int_o^t (\Omega_x \cos a' + \Omega_y \sin a')\, dt' \quad (40)$$

(inner axis)

$$\alpha_z = \int_o^t \Omega_z\, dt' \quad \text{(outer axis)} \quad (41)$$

2.4 Detector Noise Model and Servo Loops

(exactly as stated in third Preliminary Report with difference that 2 azimuth and 2 elevation servos require simulation for this experiment - see figure 7 and 8)

2.5 Roll Error Signal for Roll Stabilized Vehicle (using sweep of gimballed experimental package)

$$\epsilon'_z = \int_o^t W_z \, dt' \qquad (42)$$

(replaced equation (3))

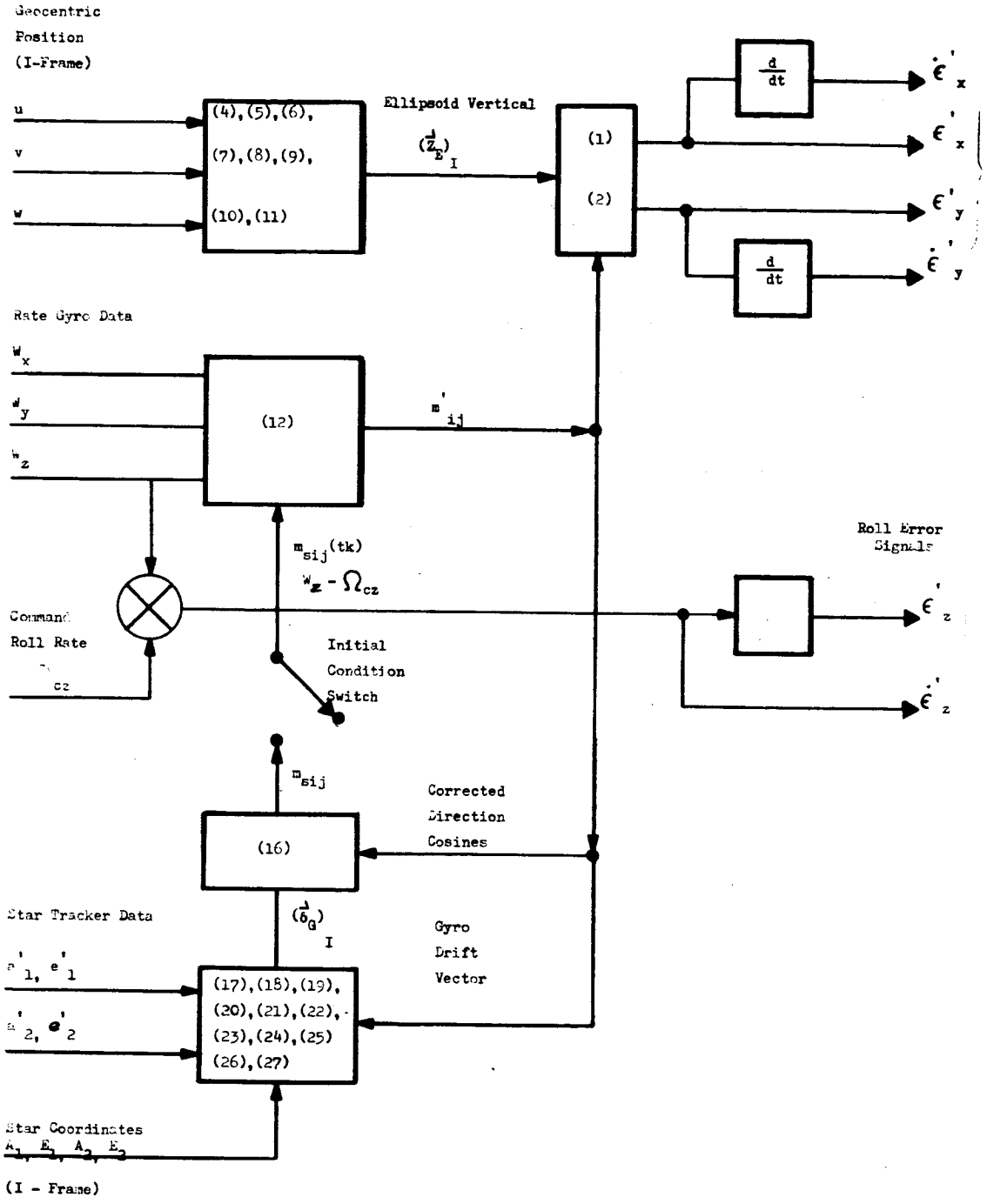

ON-BOARD SYSTEM

FIGURE 1

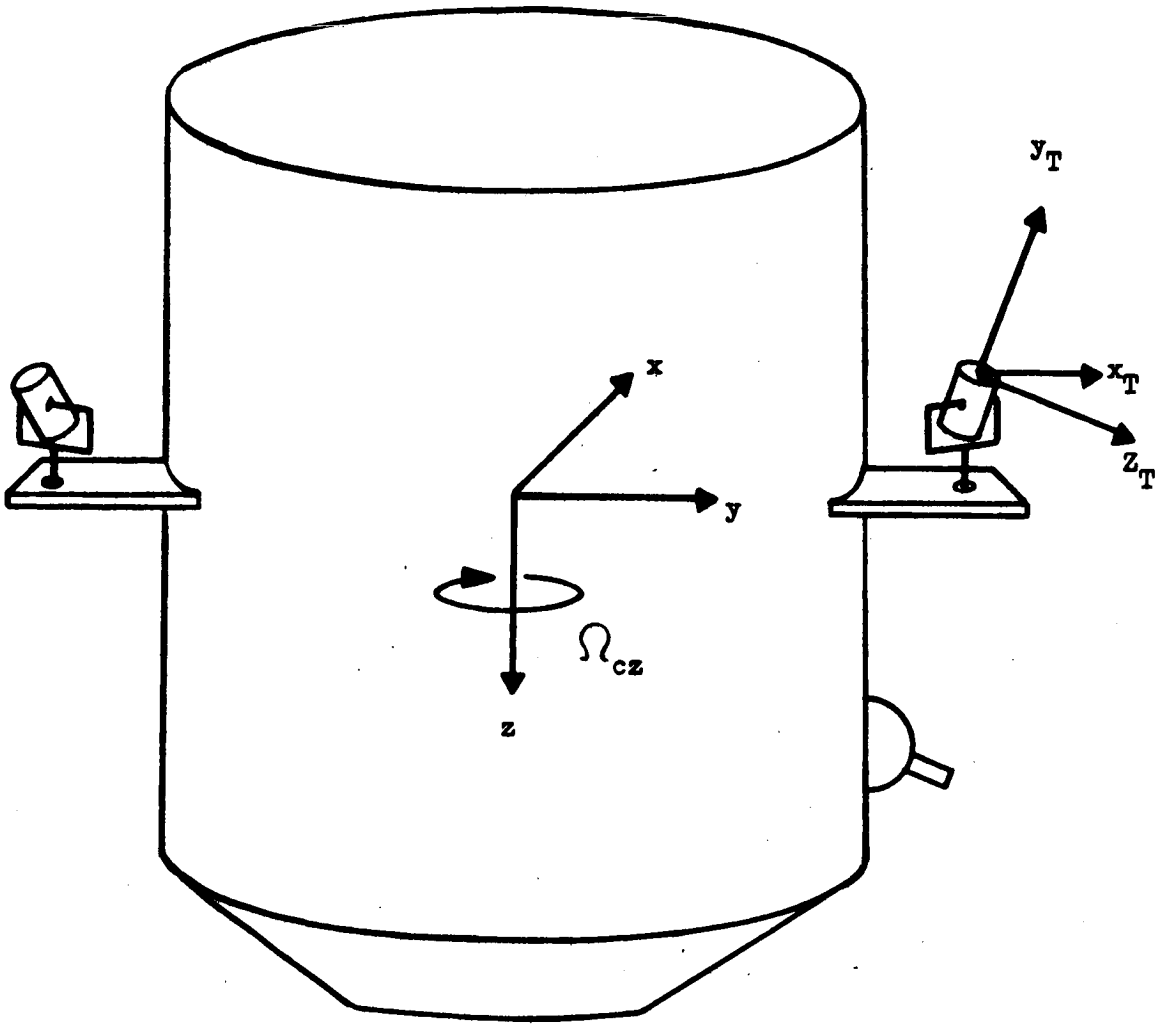

MOUNTING OF TWO GUIDE STAR TRACKERS

FIGURE 2

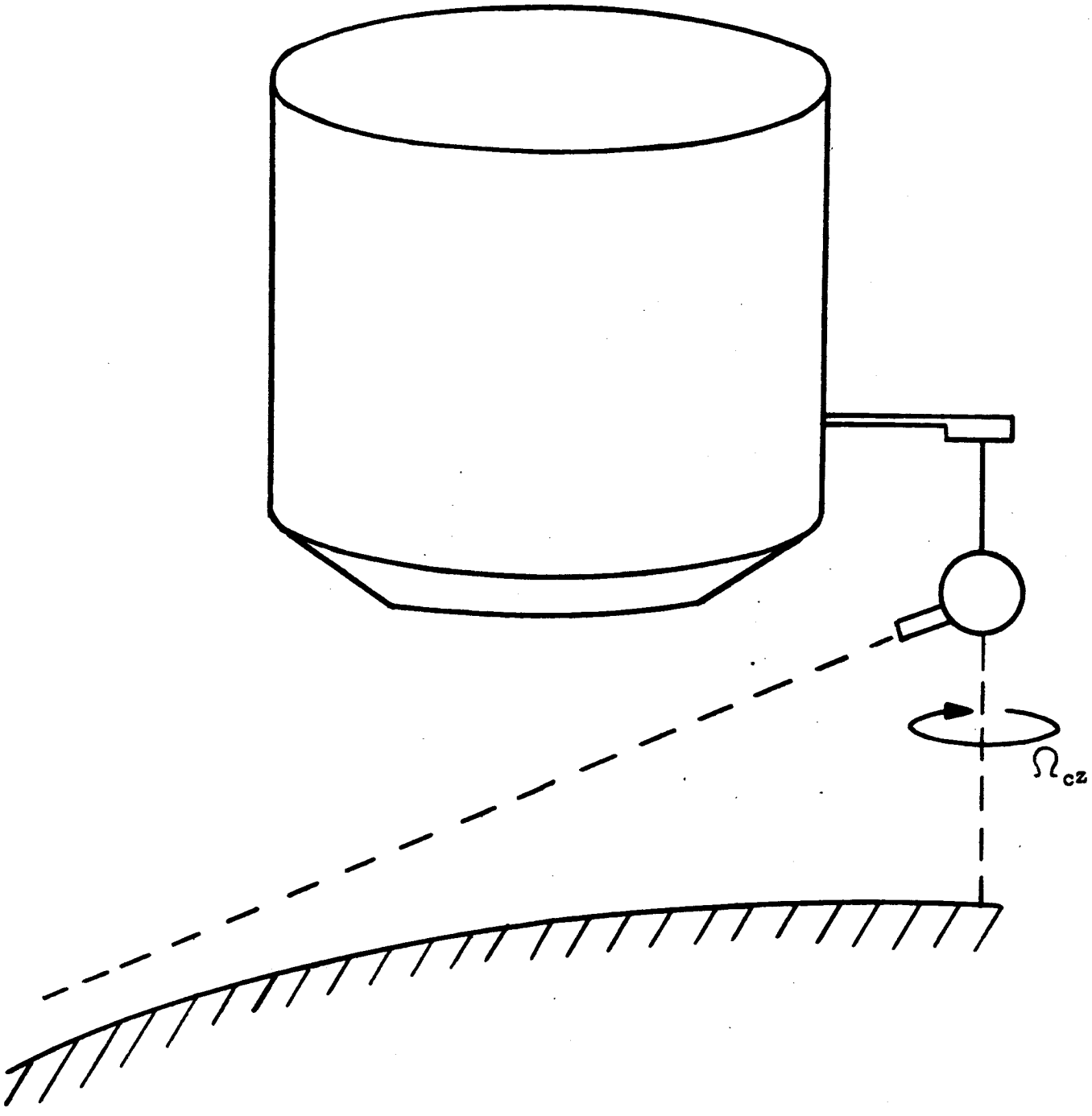

ROLL STABILIZED VEHICLE WITH HORIZON SWEEP
BY EXPERIMENTAL PACKAGE

FIGURE 3

(a)

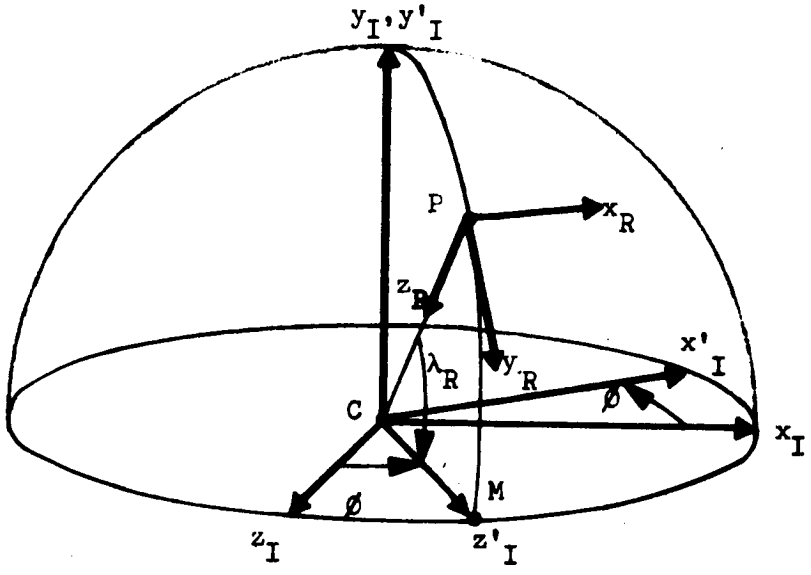

(b)

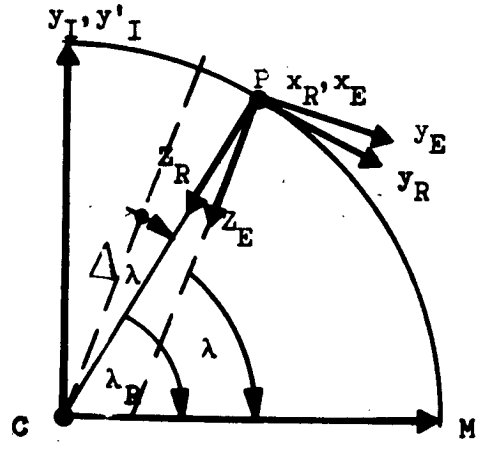

E-, R-, AND I- FRAMES, AND TWO VERTICALS

FIGURE 4

TRUE ERROR ANGLES, ERROR, AND RATE ERROR SIGNALS

FIGURE 5

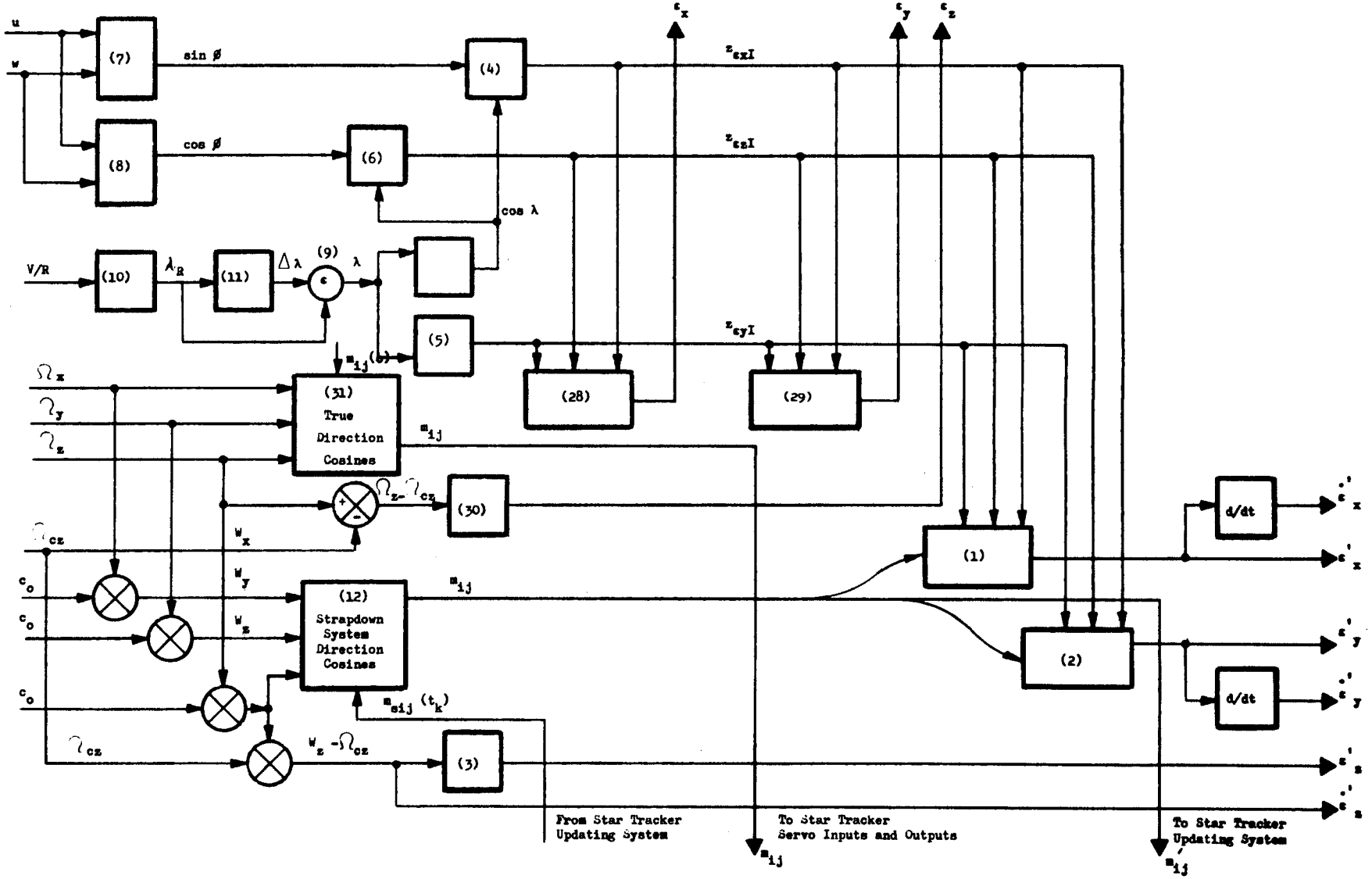

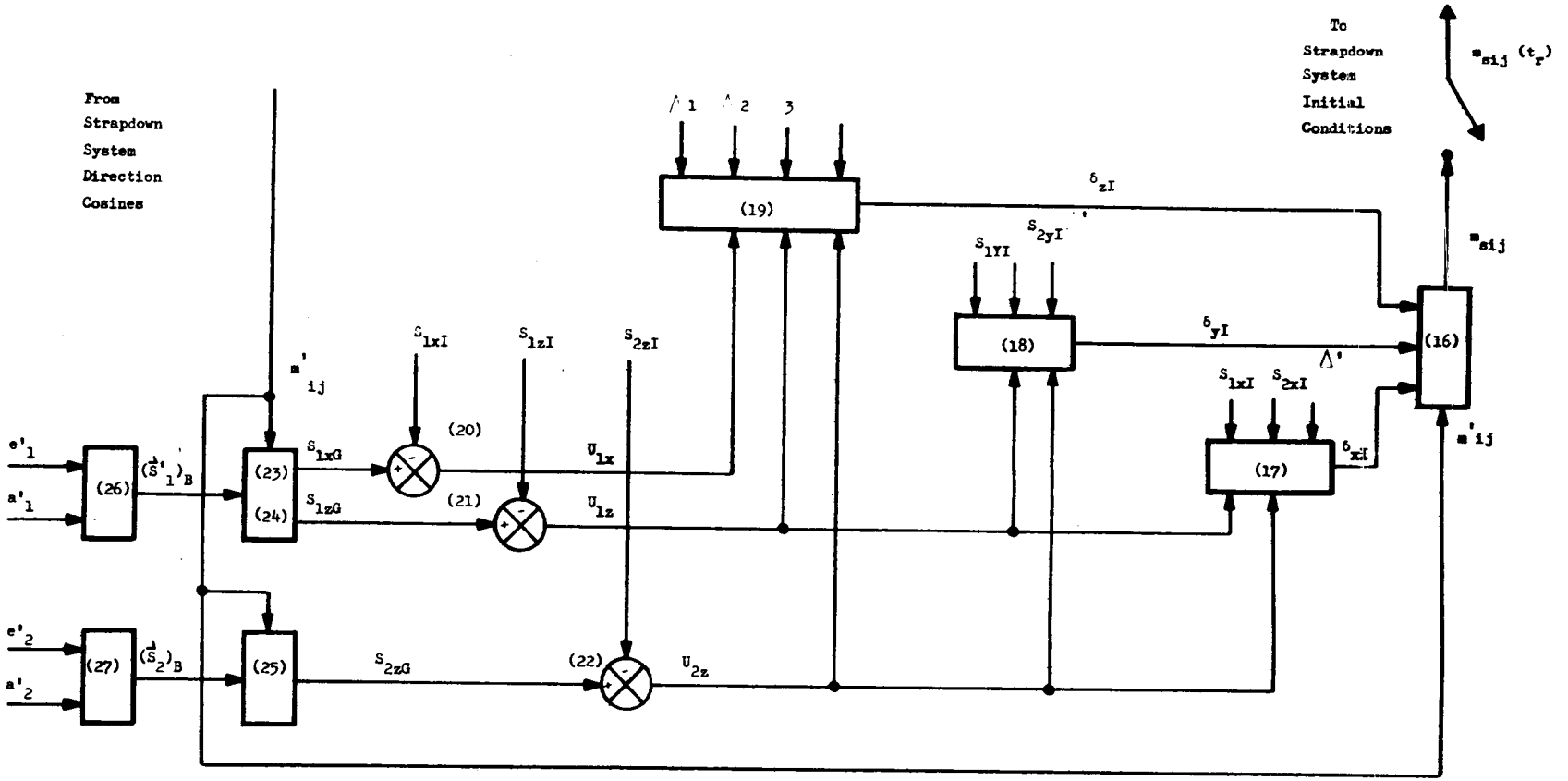

STAR TRACKER UPDATING SYSTEM

FIGURE 6

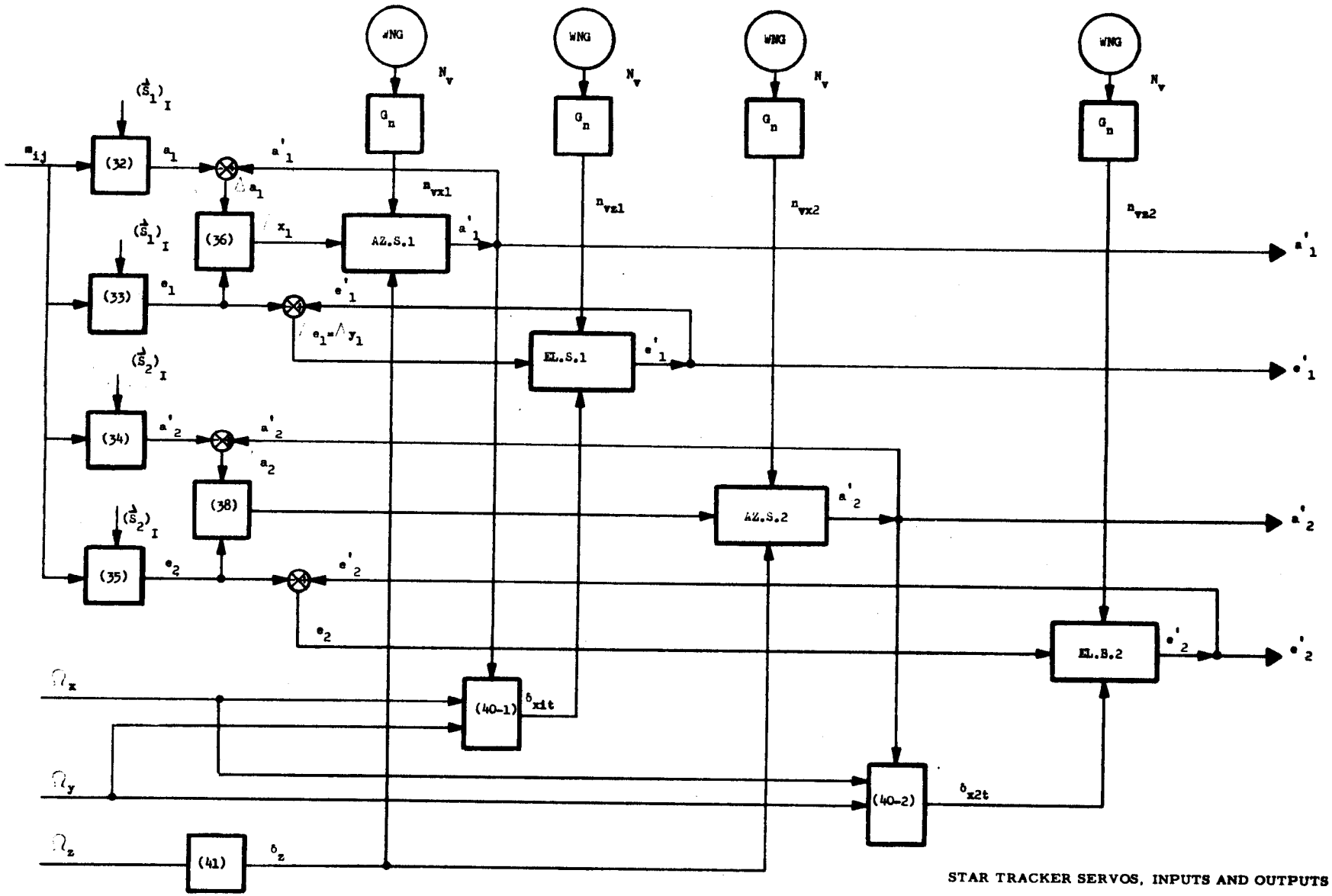

STAR TRACKER SERVOS, INPUTS AND OUTPUTS

FIGURE 7

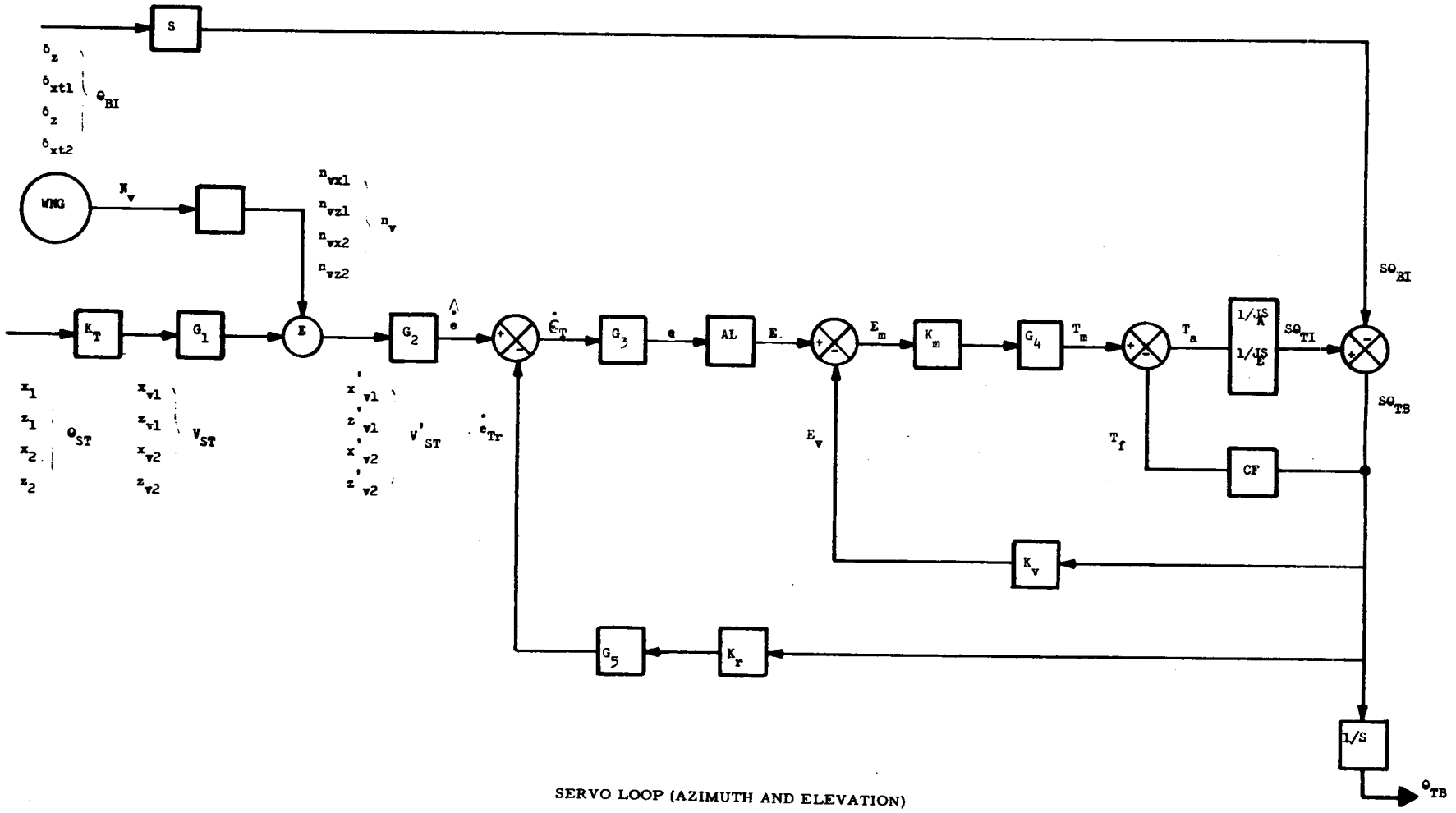

SERVO LOOP (AZIMUTH AND ELEVATION)

FIGURE 8

Appendix A

Computations for Generating Error Signals from Orbital Data and Strapdown Gyro System Data

The error signals are the components along vehicle frame axes (B) of the small angle indicated error vector $(\vec{\epsilon})_B$ of the B-frame referred to the commanded frame, B_c. This frame, (x_c, y_c, z_c) is specified in relation to the ellipsoid orbit frame, E (x_E, y_E, z_E) by alignment of its z_c-axis with the z_E=axis of the E-frame. The angular velocity of the B_c-frame relative to the E-frame is then to be the command rate, Ω_{cz}, about the common z-axis. The E-frame is related to the geocentrics orbit frame, R (x_R, y_R, z_R) by a small right hand rotation $\Delta\lambda$, about the common x-axis of the E and R frames (see figures 2-a and 2-b). With P as the position of the spacecraft, the meridian plane of the position, PCM, lies at a longitude, ϕ, relative to the z_I-axis. The longitude is a right hand rotation about y_I, while both the geocentric and geodetic latitudes, λ_c and λ, are right hand rotations about x_I. The geodetic latitude is the angle between the ellipsoid vertical and the equatorial plane.

The I-frame is indicated with its y_I-axis along the earth's axis of rotation while its x_I- and z_I- axis lie in the equatorial plane. The z_I-axis, the longitude reference, is arbitrary. In fact, the alignment of the y_I-axis with the earth rate vector is only a matter of computational convenience since the computation here must involve a latitude determination.

The geocentric unit vertical of the spacecraft is indicated as $\vec{z}_R$ while the geodetic or ellipsoid vertical is $\vec{z}_E$.

The orbital information required is the geocentric position vector of the craft resolved in the I-frame,

$$(\vec{r})_I = \begin{pmatrix} u \\ v \\ w \end{pmatrix} \qquad (A\text{-}1)$$

then

$$(\vec{z}_R)_I = -\frac{1}{r} \begin{pmatrix} u \\ v \\ w \end{pmatrix} \qquad (A\text{-}2)$$

In terms of longitude, ϕ, and geocentric latitude, x_R, the geocentric vertical is then

$$(\vec{z}_R)_I = -\begin{pmatrix} \sin \phi \ \cos \lambda_R \\ \sin \lambda_R \\ \cos \phi \ \cos \lambda_R \end{pmatrix} \qquad (A\text{-}3)$$

The ellipsoid unit vertical,

$$(\vec{z}_E)_I = \begin{matrix} - \sin\phi \cos\lambda \\ \sin\lambda \\ \cos\phi \cos\lambda \end{matrix} , \qquad (A\text{-}4)$$

with the difference between geodetic or ellipsoid lattitude and geocentric latitude,

$$\lambda = \lambda_R + \Delta\lambda \qquad (A\text{-}5a)$$

$$\Delta\lambda \text{ (radians)} = .003373 \sin 2\lambda_R + .000006 \sin 4\lambda_R \qquad (A\text{-}5b)$$

This correction is strictly correct only at the earth's surface. For altitudes limited to 200 nautical miles, it is for these purposes good enough.

From (A-2) and (A-3)

$$\lambda_R = \sin^{-}\left(\frac{v}{r}\right) \qquad (A\text{-}6a)$$

$$\cos\phi = \frac{w}{\sqrt{u^2 + w^2}} \qquad (A\text{-}6b)$$

$$\sin\phi = \frac{u}{\sqrt{u^2 + w^2}} \qquad (A\text{-}6c)$$

Equations (A-4) through (A-6c) yield the I-frame components of the unit ellipsoid vertical, $(\vec{z}_E)_I$, in terms of the components of the geocentric position vector of the craft, $(\vec{r})_I$.

Denoting the gyro indicated error signals, as ϵ'_x , ϵ'_y , ϵ'_z , the indicated error matrix is

$$M'_{B_cB} = \begin{bmatrix} 1 & \epsilon'_z & -\epsilon'_y \\ -\epsilon'_z & 1 & \epsilon'_x \\ \epsilon'_y & -\epsilon'_x & 1 \end{bmatrix} \qquad \text{(A-7a)}$$

This results from three successive small angle rotations about successive axes. The true error matrix,

$$M_{B_cB} = \begin{bmatrix} 1 & \epsilon_z & -\epsilon_y \\ -\epsilon_z & 1 & \epsilon_x \\ \epsilon_y & -\epsilon_x & 1 \end{bmatrix} \qquad \text{(A-7b)}$$

This matrix can be decomposed into three matrices,

$$M_{B_cB} = M_{B_oB} \quad M_{EB_o} \quad M_{B_cE} \quad , \qquad \text{(A-8)}$$

The roles of the B_o, B_c, and E frames are placed in evidence by resolving their relative angular velocities. The angular velocity of the vehicle frame, B, relative to the commanded frame, B_c , is the sum of the angular velocities,

$$\vec{\Omega}_{BB_c} = \vec{\Omega}_{BB_o} + \vec{\Omega}_{B_oE} + \vec{\Omega}_{EB_c} \qquad \text{(A-9)}$$

Resolving,

$$\vec{\Omega}_{BB_o}{}_{B_o} = \begin{matrix} 0 \\ 0 \\ \Omega_z \end{matrix} = \vec{\Omega}_{BB_o}{}_{B} \qquad \text{(A-10a)}$$

$$\Omega_{B_{oE}}{}_{B_o} = \begin{matrix} \dot{\epsilon}_{xo} \\ \dot{\epsilon}_{yo} \\ 0 \end{matrix} \qquad \text{(A-10b)}$$

$$\vec{\Omega}_{EB_c}{}_{E} = \begin{matrix} 0 \\ 0 \\ -\Omega_{cz} \end{matrix} = \vec{\Omega}_{EB_c}{}_{B_c} \qquad \text{(A10-c)}$$

From the preceding it may be noted that B_o is the frame which extracts only the vertical errors of the B frame. That is, it is the B-frame without the z-axis spin.

Defining,

$$\alpha_z = \int_o^t \Omega_z \, dt' \qquad \text{(A-11a)}$$

$$\beta_{cz} = \int_o^t \Omega_{cz} \, dt' = \Omega_{cz} t \qquad \text{(A-11b)}$$

$$M_{B_cB} = \begin{vmatrix} \cos\alpha_z & \sin\alpha_z & 0 \\ -\sin\alpha_z & \cos\alpha_z & 0 \\ 0 & 0 & 1 \end{vmatrix} \begin{vmatrix} 1 & 0 & -\epsilon_{yo} \\ 0 & 1 & \epsilon_{xo} \\ \epsilon_{yo} & -\epsilon_{xo} & 1 \end{vmatrix} \begin{vmatrix} \cos\alpha_{cz} & -\sin\alpha_{cz} & 0 \\ \sin\alpha_{cz} & \sin\alpha_{cz} & 0 \\ 0 & 0 & 1 \end{vmatrix} \qquad \text{(A-12)},$$

which is the expansion of (A-8).

This result may be rigorously confirmed by properly applying (B-9) of the Second Preliminary Report. As inferred, ϵ_{xo} and ϵ_{yo} are the small angle errors about the x_o - and y_o - axes between the non-spinning B_o-frame and the reference E-frame.

Neglecting second order terms in equating the right side of (A-12) with the right side of (A-7b), there results

$$\left.\begin{aligned} \epsilon_x &= \cos\alpha_z\ \epsilon_{xo} + \sin\alpha_z\ \epsilon_{yo} \\ \epsilon_y &= -\sin\alpha_z\ \epsilon_{xo} + \cos\alpha_z\ \epsilon_{yo} \\ \epsilon_z &= \alpha_z - \alpha_{cz} = \alpha_z - \Omega_{cz}t \end{aligned}\right\} \qquad (A\text{-}13)$$

By definition,

$$M_{EB_o} = \begin{matrix} x_o \cdot x_E & x_o \cdot y_E & x_o \cdot z_E \\ y_o \cdot x_E & \text{etc.} & \\ z_o \cdot x_E & & \end{matrix} \qquad (A\text{-}14)$$

Referring to the middle matrix on the right side of (A-12)

$$\begin{aligned} \epsilon_{xo} &= y_o \cdot z_E \\ \epsilon_{yo} &= -x_o \cdot z_E \end{aligned} \qquad (A\text{-}15)$$

Substituting into (A-13), and resolving $\vec{x}_o$ and $\vec{y}_o$ in the B frame using the first matrix on the right side of (A-12), one obtains

$$\epsilon_x = y \cdot z_E = z_{Ey}$$

$$\epsilon_y = -x_E \cdot z_E = -z_{Ex} \qquad \text{(A-16)}$$

$$\epsilon_z = \alpha_z - \Omega_{cz} t$$

$$(\vec{z}_E)_B = M_{IB} (\vec{z}_E)_I \qquad \text{(A-17)}$$

$$(\vec{z}_{E_I}) = - \begin{pmatrix} \dfrac{u}{\sqrt{u^2 + w^2}} \cos\left\{\sin^{-1}\left(\dfrac{v}{r}\right) + \Delta\lambda\right\} \\ \sin\left\{\sin^{-1}\dfrac{v}{r} + \Delta\lambda\right\} \\ \dfrac{w}{\sqrt{u^2 + w^2}} \cos\left\{\sin^{-1}\dfrac{v}{r} + \Delta\lambda\right\} \end{pmatrix}, \qquad \text{(A-18)}$$

as written out explicitly, using (A-4) through (A-6c).

The elements of M_{IB} are closely approximated by the gyro drifting solutions of the strapdown system, M_{GB}. Taking note that M_{IB} is the inverse of M_{BI} whose ordered array is indicated in Appendix D of the Second Preliminary Report,

$$\epsilon'_x = z'_{Ey} = m'_{12} z_{ExI} + m'_{22} z_{EyI} + m'_{32} z_{EzI} \qquad \text{(A-19)}$$

$$\epsilon'_y = -z'_{Ex} = -(m'_{11} z_{ExI} + m'_{21} z_{EyI} + m'_{31} z_{EzI})$$

$$\epsilon'_z = \int_o^t W_z \, dt' - \Omega_{cz} t$$

where m'_1 , are the elements of M_{GB}, and the indicated rate of the z-axis gyro,

$$W_z = \Omega_z - c_o \quad , \tag{A-20}$$

where c_o is the drift of the z-axis gyro.

Appendix B

Computations for Gyro Drift Correction by Star Tracker Data.

The indicated azimuth and elevation from one star tracker, a'_1 , e'_1 , and the corresponding coordinates from the second tracker, a'_2 , e'_2 , are the required data. Referring to figure 1, a' is a right hand rotation about the B-frame's z-axis with the y-axis as zero reference, while e' is a left hand rotation about the x'-axis, with y' as the zero reference. Then resolved in the B-frame the indicated star line vectors are

$$
\left(\vec{s}'_1\right)_B = \begin{pmatrix} -\cos e'_1 & \sin a'_1 \\ \cos e'_1 & \cos a'_1 \\ -\sin e'_1 & \end{pmatrix} = \begin{pmatrix} s'_{1x} \\ s'_{1y} \\ s'_{1z} \end{pmatrix}
$$

$$
\left(\vec{s}'_2\right)_B = \begin{pmatrix} -\cos e'_2 & \sin a'_2 \\ \cos e'_2 & \cos a'_2 \\ -\sin e'_2 & \end{pmatrix} = \begin{pmatrix} s'_{2x} \\ s'_{2y} \\ s'_{2z} \end{pmatrix} \qquad \text{(B-1)}
$$

The tracker's star line vectors, $\vec{s}'_1$ and $\vec{s}'_2$, differ from the boresighted vectors, $\vec{s}_1$ and $\vec{s}_2$, by the closed loop boresight errors resulting from detector noise and servo lags.

The B-frame resolutions are related to the I-frame resolutions by

$$(\vec{s}_1)_B = M_{GB}\, M_{IG}\, (\vec{s}_1)_I \qquad \text{(B-2a)}$$

$$(\vec{s}_2)_B = M_{GB}\, M_{IG}\, (\vec{s}_2)_I \qquad \text{(B-2b)}$$

In the I-frame, the resolutions of the two selected stars are known in advance of any tracking data via their coordinates A_1 , E_1 and A_2 , E_2. Defining these rotations relative to the I-frame, analogous to that resulting in (B-1),

$$(\vec{s}_1)_I = \begin{pmatrix} s_{1xI} \\ s_{1yI} \\ s_{1zI} \end{pmatrix} = \begin{pmatrix} -\cos E_1 \sin A_1 \\ \cos E_1 \cos A_1 \\ -\sin E_1 \end{pmatrix}$$

$$(\vec{s}_2)_I = \begin{pmatrix} s_{2xI} \\ s_{2yI} \\ s_{2zI} \end{pmatrix} = \begin{pmatrix} -\cos E_2 \sin A_2 \\ \cos E_2 \cos A_2 \\ -\sin E_2 \end{pmatrix} \qquad \text{(B-3)}$$

The matrix, M_{IG}, may be recognized as the gyro drift matrix,

$$M_{IG} = \begin{matrix} 1 & \delta_{zI} & -\delta_{yI} \\ -\delta_{zI} & 1 & \delta_{xI} \\ \delta_{yI} & -\delta_{xI} & 1 \end{matrix} \qquad \text{(B-4)}$$

Where the small angle gyro drift vector,

$$(\vec{\delta G})_I = \begin{matrix} \delta_{xI} \\ \delta_{yI} \\ \delta_{zI} \end{matrix} \qquad \text{(B-5)}$$

The gyro strapdown solution matrix

$$M_{GB} = \begin{matrix} m'_{11} & m'_{21} & m'_{31} \\ m'_{12} & m'_{22} & m'_{32} \\ m'_{13} & m'_{23} & m'_{33} \end{matrix} \qquad \text{(B-6)}$$

If the x- and z- components of (B-2a) and the z-component of (B-2b) are used, the three constraints suffice to determine the three components of the drift vector by means of the tracker data, e'_1, a'_1 and e'_2. Because such a determination involves a variable determinant in the denominator with no guarantee that it not go to zero, an alternative, involving the four tracking coordinates from the two stars, is employed here. Applying the inverse of M_{GB} to both sides of (B-2),

$$\vec{s}_1 \quad G = \begin{matrix} s_{1xG} \\ s_{1yG} \\ s_{iz\,G} \end{matrix} = M_{BG}\,(\vec{s}_1)_B = M_{IG}\,(\vec{s}_1)_I \quad \text{(B-7a)}$$
$$\cong M_{BG}\,(\vec{s}'_1)_B$$

$$\vec{s}_2 \quad G = \begin{matrix} s_{2xG} \\ s_{2yG} \\ s_{2zG} \end{matrix} = M_{BG}\,(\vec{s}_2)_B = M_{IG}\,(\vec{s}_2)_G \quad \text{(B-7b)}$$
$$\cong M_{BG}\,(\vec{s}'_2)_B$$

Using the $x\text{-}_G$ and $z\text{-}_G$ components of (B-7a) and the $z\text{-}_G$ components of (B-7b),

$$\left.\begin{aligned} s_{1xG} &= s_{1xI} + \delta_{zI}\, s_{1yI} - \delta_{yI}\, s_{1zI} \\ s_{1zG} &= \delta_{yI}\, s_{1xI} - \delta_{xI}\, s_{1yI} + s_{1zI} \\ s_{2zG} &= \delta_{yI}\, s_{2xI} - \delta_{xI}\, s_{2yI} + s_{2zI} \end{aligned}\right\} \qquad \text{(B-8)}$$

Solving for the drift components in (B-8),

$$\left.\begin{aligned} \delta_{xI} &= \frac{1}{\Delta'} \left(s_{2xI}\, u_{1z} - s_{1xI}\, u_{2z}\right) \\ \delta_{yI} &= \frac{1}{\Delta'} \left(s_{2yI}\, u_{1z} - s_{1yI}\, u_{2z}\right) \end{aligned}\right\} \qquad \text{(B-9)}$$

$$\delta_{zI} = \frac{1}{\Delta} \left(\Delta_1\, u_{1x} + \Delta_2\, u_{1z} + \Delta_3\, u_{2z}\right)$$

$$u_{1x} = s_{1xG} - s_{1xI}$$

$$u_{1z} = s_{1zG} - s_{1zI} \qquad \text{(B-10)}$$

$$u_{2z} = s_{2zG} - s_{2zI}$$

$$s_{1xG} = m'_{11}\, s'_{1x} + m'_{12}\, s'_{1y} + m'_{13}\, s'_{iz}$$

$$s_{1zG} = m'_{31}\, s'_{1x} + m'_{32}\, s'_{1y} + m'_{33}\, s'_{1z} \qquad \text{(B-11)}$$

$$s_{2zG} = m'_{31}\, s'_{2x} + m'_{32}\, s'_{2y} + m'_{33}\, s'_{2z}$$

The constants Δ, Δ', Δ_1, Δ_2, and Δ_3 are given in section 2.1.

The remaining constants of (B-9) are given in (B-3). The errors in the approximation indicated in (B-11) which is the expansion of the approximations in (B-7), reflecting boresight errors of the trackers, remain bounded unlike the gyro drift errors which the tracker updating system is required to correct.

As indicated in the Third Preliminary Report, Appendix A, the magnitudes of the determinants, Δ and Δ', are a measure of the geometric resolution afforded by the two star lines. For $E_1 = 0°_1 A_1 = 45°_1$ $E_2 = 45°_1 A_1 = 0°$, the star lines are 60 degrees apart, and the values of the determinants are $\Delta = .355$, and $\Delta' = .500$.

Having solved for the gyro drift angle components, the correct I to B transformation elements can be computed.

$$M_{IB} = M_{GB} M_{IG} , \qquad \text{(B-14)}$$

where M_{IG} is the drift matrix as given by (B-6). Were it not for noise and dynamic lags in the servo loops of the trackers, the computation given by (B-11), (B-12), and (B-13) would lead to the exact drift matrix. Since the computation depends on the vehicle referred indicated gimbal angles, errors are incurred in determining the gyro drift as cited and instead of (B-14), we obtain the close approximation, bounded in error,

$$M_{SB} = M_{GB} M_{SG} \cong M_{IB} , \qquad \text{(B-15)}$$

The S-frame, as determined from the star tracker data, differs from the desired I-frame as a result of the noise and dynamic lag errors in the tracking. The matrix, M_{SG}, is the tracker data version of M_{IG} as given by (B-6). Referring to (B-6) and (B-8), and denoting the elements of the matrix,

$$M_{SB} = \begin{matrix} m_{s11} & m_{s21} & m_{s31} \\ m_{s12} & & \text{etc.} \\ m_{s13} & & \end{matrix} \qquad \text{(B-16)}$$

$$
\begin{aligned}
m_{s11} &= +m'_{11} - m'_{21}\,\delta_{zI} + m'_{31}\,\delta_{yI} \\
m_{s12} &= +m'_{12} - m'_{22}\,\delta_{zI} + m'_{32}\,\delta_{yI} \\
m_{s13} &= +m'_{13} - m'_{23}\,\delta_{zI} + m'_{33}\,\delta_{yI} \\
m_{s21} &= +m'_{11}\,\delta_{zI} + m'_{21} - m'_{31}\,\delta_{xI} \\
m_{s22} &= +m'_{12}\,\delta_{zI} + m'_{22} - m'_{32}\,\delta_{xI} \\
m_{s23} &= +m'_{13}\,\delta_{zI} + m'_{23} - m'_{33}\,\delta_{xI} \\
m_{s31} &= -m'_{11}\,\delta_{yI} + m'_{21}\,\delta_{xI} + m'_{31} \\
m_{s32} &= -m'_{12}\,\delta_{yI} + m'_{22}\,\delta_{xI} + m'_{32} \\
m_{s33} &= -m'_{13}\,\delta_{yI} + m'_{23}\,\delta_{xI} + m'_{33}
\end{aligned}
\qquad \text{(B-17)}
$$

The strap down system direction cosines, m'_{ij}, drift in accordance with gyro drift. The elements corrected for gyro drift, m_{sij}, are to be used intermittently in resetting the initial conditions of the strap down gyro computer. The computer's outputs, m'_{ij}, will then suffer gyro drift effects only for the durations between resettings, or updatings. Specifically, if t_k is the instant of the k th updating, the solutions between the k th and k + 1 th updatings are:

$$m'_{11}(t) = \int_{tk}^{t} (-W_y m'_{13} + W_z m'_{12}) dt' + m_{s11}(t_k)$$

$$m'_{12}(t) = \int_{tk}^{t} (-W_z m'_{11} + W_x m'_{13}) dt' + m_{s12}(t_k)$$

$$m'_{13}(t) = \int_{tk}^{t} (-W_x m'_{12} + W_y m'_{11}) dt' + m_{s13}(t_k)$$

$$m'_{21}(t) = \int_{tk}^{t} (-W_y m'_{23} + W_z m'_{22}) dt' + m_{s21}(t_k)$$

$$m'_{22}(t) = \int_{tk}^{t} (-W_z m'_{21} + W_x m'_{23}) dt' + m_{s22}(t_k)$$

$$m'_{23}(t) = \int_{tk}^{t} (-W_x m'_{22} + W_y m'_{21}) dt' + m_{s23}(t_k)$$

$$m'_{31}(t) = \int_{tk}^{t} (-W_y m'_{33} + W_y m'_{32}) dt' + m_{s31}(t_k)$$

$$m'_{32}(t) = \int_{tk}^{t} (-W_z m'_{31} + W_x m'_{33}) dt' + m_{s32}(t_k)$$

$$m'_{33}(t) = \int_{tk}^{t} (-W_x m'_{32} + W_y m'_{31}) dt' + m_{s33}(t_k)$$

APPENDIX C

Relation Between Image Plane Error Signals and Gimbal Angle Errors

Referring to Figure 1, the image plane of the T-frame is the x_T - z_T plane with y_T along the optic axis. The rotations, a' and e', which takes the B-frame into the T-frame has been defined in Appendix A. With the T-frame boresighted to the star, the corresponding rotations are the boresight angles, a and e.

Then

$$\vec{(s)}_B = \begin{matrix} -\cos e \sin a \\ \cos e \cos a \\ -\sin e \end{matrix} \qquad \text{(C-1)}$$

$$\vec{(s)}_T = \begin{matrix} \Delta x \\ 1 \\ \Delta z \end{matrix} = (M_{BT})\vec{(s)}_B$$

$$= \begin{matrix} 1 & 0 & 0 \\ 0 & \cos e' & -\sin e' \\ 0 & \sin e' & \cos e' \end{matrix} \begin{matrix} \cos a' & \sin a' & 0 \\ -\sin a' & \cos a' & 0 \\ 0 & 0 & 1 \end{matrix} \begin{matrix} -\cos e & \sin a \\ \cos e & \cos a \\ -\sin e & \end{matrix} \qquad \text{(C-2)}$$

Using small angle approximations,

$$\Delta x = (a'-a)\cos e = \Delta a \cos e$$

$$\Delta z = e'-e = \Delta e \qquad \text{(C-3)}$$

This result is of the same nature as the result (B-3b) of the Third Preliminary Report, the difference being due to the different mountings of the trackers on the vehicle.

APPENDIX D

INITIAL CONDITIONS

The initial direction of the ellipsoid vertical

$$\vec{z}_{E(0)_I} = - \begin{matrix} \sin \phi_o & \cos \lambda_o \\ \sin \lambda_o & \\ \cos \phi_o & \cos \lambda_o \end{matrix} = - \frac{1}{ro} \begin{matrix} u_o \\ v_o \\ w_o \end{matrix} \qquad (D\text{-}1)$$

For convenience, the problem can be initiated for $\phi_o = 0$, $\lambda_o = 0$, that is, as the spacecraft crosses the equator at 0 longitude, where the longitude reference in relation to the earth, is arbitrary. Then $\lambda_c(0) = 0, \Delta\lambda_o = 0$, $u_o = 0$, $v_o = 0$ and $w_o = r_o$, which is the sum of the earth equatorial radius and the spacecraft altitude.

Initial conditions must be set into the strapdown computer before star tracker corrected direction cosines, m_{si}, (t_k), supercede them. These initial conditions are required to initiate the operation of the computer. They need only be the elements of an orthogonal matrix, and in no way, are required to resemble the elements corresponding to the initial vehicle attitude. Referring to Figure 3, it may be noted that a feedback system encloses the gyro strapdown computer, the gyro drift computer, and the updated direction cosines. The inputs to this system are the star tracker data and the star coordinates as seen in the selected reference frame. The error signals are the gyro drift

The outputs are the outputs of the strapdown computer. Hence for any initial conditions which are elements of an orthogonal matrix, after the initial condition switch is closed (closing the loop), the input data will force the strapdown computer's outputs to match the updated direction cosines with a consequent nulling of the error signals, the computed gyro drift. To put it another way, with the loop closed, the gyro drift computer cannot distinguish between gyro drift and initial misalignment of the strapdown computer's reference frame. It sees however the difference between the alignment of the computer's reference frame and the alignment required by the combination of vehicle referred star coordinates and star coordinates as seen in the required reference frame, and consequently generates error signals. The fact that the gyro drift computer updated direction cosines computers are based on linear approximations allowed by small angle misalignments, only implies that for large initial misalignment of the initial conditions, the feedback system will suffer a transient saturation, the duration of which depends on the speed of the digital computation and the amount of the misalignment. If this transient saturation is to be avoided, a suggested initial condition matrix is

$$\begin{matrix} m_{s11}(0) & m_{s12}(0) & m_{s13}(0) \\ m_{s21}(0) & m_{s22}(0) & m_{s23}(0) \\ m_{s31}(0) & m_{s32}(0) & m_{s33}(0) \end{matrix} =$$

$$= \begin{matrix} 1 & 0 & 0 \\ 0 & -1 & 0 \\ 0 & 0 & -1 \end{matrix} \qquad \text{(D-2)}$$

$$= \begin{matrix} x_I \cdot x_o & x_I \cdot y_o & x_I \cdot z_o \\ y_I \cdot x_o & \text{etc.} & \\ z_I \cdot x_o & & \end{matrix}$$

These values correspond to an exact alignment of the computer's reference frame. However, any other initial condition orthogonal matrix will eventually be aligned with the initial condition switch closed. After alignment has been attained, that is the error signals nulled, the switch is to be open corresponding to the time gyro data alone will be used in establishing the reference frame, and closed momentarily, corresponding to the availability of star tracker data. For the roll command mode, with its periodic occulations, a conservative estimate is that tracker data will be available for one minute out of the six minute roll periods. For the roll stabilized mode, tracker data will be continuously available, and should be used continuously provided tracker detector noise is no problem for the vehicle control system. Otherwise it is to be used intermittently in an updating mode, and at intervals dictated by accuracy requirements and gyro drift.

APPENDIX E

Base Motion Dynamic Loading of the Servos

Unlike the base motion loading of the inner and outer axis servos in the inertial attitude mode discussed in the third Preliminary Report, the base motions for this experiment are large angle excursions on the spacecraft transverse axes, and an ever increasing ramp with time on the roll axis. Hence, small angle approximations don't hold here, and instead, components along gimbal axes of the spacecraft's inertial angular velocity are found first. This angular velocity, which is determined as solutions of the craft's equations of motion,

$$\left(\vec{\Omega}\right)_{BI}{}_{B} = \begin{pmatrix} \Omega_x \\ \Omega_y \\ \Omega_z \end{pmatrix} , \qquad (E\text{-}1)$$

leads to $\vec{\Omega} \cdot \vec{x}_T = \Omega_x \cos a' + \Omega_y \sin a' \qquad (E\text{-}2)$

as the component along the inner gimbal axis, and

$$\vec{\Omega} \cdot \vec{z} = \Omega_z , \qquad (E\text{-}3)$$

as the component along the outer gimbal axis. Then the rotational loading of the servos for the inner and outer axis servos are respectively,

$$\alpha_{xT} = \int_o^t (\Omega_x \cos a' + \Omega_y \sin a') \, dt' \qquad (E\text{-}4)$$

$$\alpha_z = \int_o^t \Omega_z \, dt' \qquad (E\text{-}5)$$

The angle α_{xT} will be periodic (ignoring perturbations due to disturbances and variation of the azimuth angle, a') and will be the sum of two independent sine waves, a long wave corresponding to the period of the orbit and a short wave corresponding to the period of the craft's roll angle. For a roll rate of 1 degree per second, the latter period will be 6 minutes.

The angle, α_{xT} (ignoring perturbations) will be a ramp in time, resulting from the commanded roll rate of 1 degree per second.

V. MICROWAVE TRANSMISSION EXPERIMENT

1. Introduction

2. Computational Requirements

Appendices

A. True Error Angles

B. Horizon Sensor Error Model

C. Gyrocompassing Constraints and Rate Error Signals

1. Introduction

The allowance of 0.5 degrees vertical error and 0.1 degrees per second vertical rate error permits the use of an advanced horizon sensor with expectation of good margin of safety. This sensor will yield the vertical error signals (pitch and roll). Because the sensor, in orbit, would scan three or four points of the horizon depending on sun presence, as filtered through a narrow spectral passband, the sensor generates error signals relative to the ellipsoid or geodetic vertical, for all practical purposes. Errors associated with the horizon sensor are an instrument null error, horizon anomalies which are due to the information channel and not to the instrument, output noise, and geometric cross-coupling. The last two are quite negligible. The anomaly, though random, is expected to vary slowly.

There is no data on its spatial autocorrelation, and hence, the bandwidth as generated by an orbiting horizon sensor is unknown. It was, therefore, modelled as a constant bias error at its known RMS uncertainty. The instrument null error is a bias error and is the RSS of all main sources of error as provided by the manufacturer. The bias error quantity appearing in Equations (1) and (2) of 2.1.1 is the RSS of the horizon anomaly and the instrument null error.

Three strapdown rate gyros furnish rate error signals. One of these gyros (roll), in addition, provides the yaw error signal which is enabled by the yaw error coupling with the orbital rate of an assumed roll stabilized vehicle. The discussion on this gyrocompassing technique follows from the

discussion in Section A.2 of "Task Area IV, MORL System Improvement Study" Book 3, Douglas Aircraft Company.

Of the rate error signals, the pitch rate error signal needs examination as to its effect on attitude accuracy via, the simulation program for the attitude mode of this experiment. As explained in Appendix C, the avoidance of significant complication in the on-board system will lead to a small oscillation in pitch error at harmonics of the orbital frequency. The amplitudes of these harmonics depend on the relative weighting of gains for indicated pitch and pitch rate, and are thus not predictable. The pitch rate error signal is then tentatively indicated as a biasing of the pitch rate gyro output with the geocentric orbital rate, a constant for a circular orbit.

The drift rates of the gyros (18. P.I.R.I.G.) are those indicated for the horizon spectrometry experiment, and while such accuracy may not be needed for this experiment, the most demanding of the experiments must determine its accuracy.

The on-board system and the overall simulation requirement is the simplest of the four discussed in this contract.

2. Computational Requirements

2.1 On-Board System

2.1.1 Horizon Sensor (showing dynamic lag)

$$\varepsilon_x'(s) = P'(s) = \frac{1.008}{1 + .06s}\,\varepsilon_x(s) + \eta_P/s \tag{1}$$

$$\varepsilon_z'(s) = R'(s) = \frac{1.008}{1 + .06s}\,\varepsilon_z(s) + \eta_R/s \tag{2}$$

$$\eta_P = \eta_R = 6.4 \times 10^{-4} \text{ radians}$$

2.1.2 Gyrocompassing Error Signal

$$\varepsilon_y' = Y' = W_z \tag{3}$$

2.1.3 Rate Error Signals

$$\dot{\varepsilon}_x' = \dot{P}' = W_x - \bar{\omega}_c \tag{4}$$

$$\dot{\varepsilon}_y' = \dot{Y}' = W_y \tag{5}$$

$$\dot{\varepsilon}_z' = \dot{R}' = W_z \tag{6}$$

2.2 True Error Angles

$$\varepsilon_x = -m_{22} \sin \phi + m_{32} \cos \phi \tag{7}$$

$$\varepsilon_y = m_{13} \cos \lambda - m_{23} \cos \phi \sin \lambda - m_{33} \sin \phi \sin \lambda \tag{8}$$

$$\varepsilon_z = m_{11} \sin \lambda + m_{21} \cos \phi \cos \lambda + m_{31} \sin \phi \sin \lambda \tag{9}$$

$$\lambda = \lambda_R + \Delta\lambda \tag{10}$$

$$\Delta\lambda = .003373 \sin 2\lambda_R + .000006 \sin 4\lambda_R \tag{11}$$

$$\lambda_R = \sin^{-1}\left(\frac{x}{r}\right) \tag{12}$$

$$\cos \phi = \frac{y}{\sqrt{y^2 + z^2}} \tag{13}$$

$$\sin \phi = \frac{z}{\sqrt{y^2 + z^2}} \tag{14}$$

$$r = \sqrt{x^2 + y^2 + z^2} \tag{15}$$

(x, y, z - I- frame components of geocentric position and required as input profiles to the simulation, analogous to U, V, W of Fourth Preliminary Report).

m_{ij} (True Direction Cosines)-Equation (31) of Fourth Preliminary Report

2.3 Suggested Initial Conditions

for ϕ (0), λ (0) = 0,

x(0) = 0, 3(0) = 0, y(0) = r(0)

For an orbital declination of 45°,

$$\begin{bmatrix} m_{110} & m_{120} & m_{130} \\ m_{210} & m_{220} & m_{230} \\ m_{310} & m_{320} & m_{330} \end{bmatrix} = \begin{bmatrix} \frac{1}{\sqrt{2}} & 0 & \frac{1}{\sqrt{2}} \\ 0 & 1 & 0 \\ -\frac{1}{\sqrt{2}} & 0 & \frac{1}{\sqrt{2}} \end{bmatrix}$$

2.4 Additional Definitions

Y, Z - equatorial plane components

X - polar axis component

r - geocentric distance of vehicle

ϕ - longitude referred to Y_I - axis

λ_R - geocentric latitude

λ - gecdetic latitude

$\Delta\lambda$ - latitude corrective function

$\varepsilon_x = P$ - true pitch error

$\varepsilon_z = R$ - true roll error

η_p - pitch bias error (horizon scanner)

η_R - roll bias error (horizon scanner)

$\varepsilon_x' = P'$ - indicated pitch error

$\varepsilon_z' = R'$ - indicated roll error

$\varepsilon_y' = Y'$ - indicated yaw error

ω_x - pitch rate gyro output

ω_y - yaw rate gyro output

ω_z - roll rate gyro output (used also as yaw error signal)

$\bar{\omega}_c$ - circular orbit angular rate for geocentric vertical c (practically, reciprocal of orbital period)

c_o - rate gyro drift rate

$\Omega_x, \Omega_y, \Omega_z$ - vehicle frame components of vehicle frame angular velocity relative to inertial frame

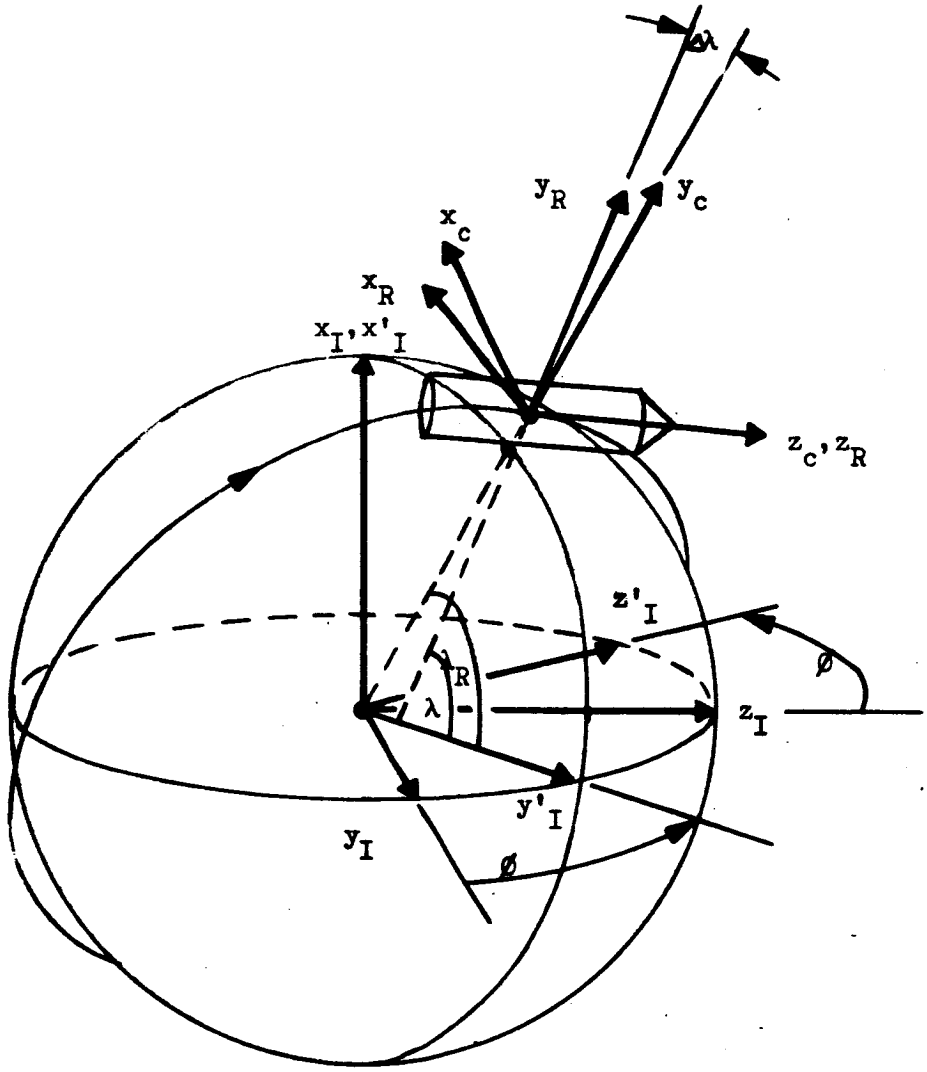

I-, R-, AND C- FRAMES

FIGURE 1

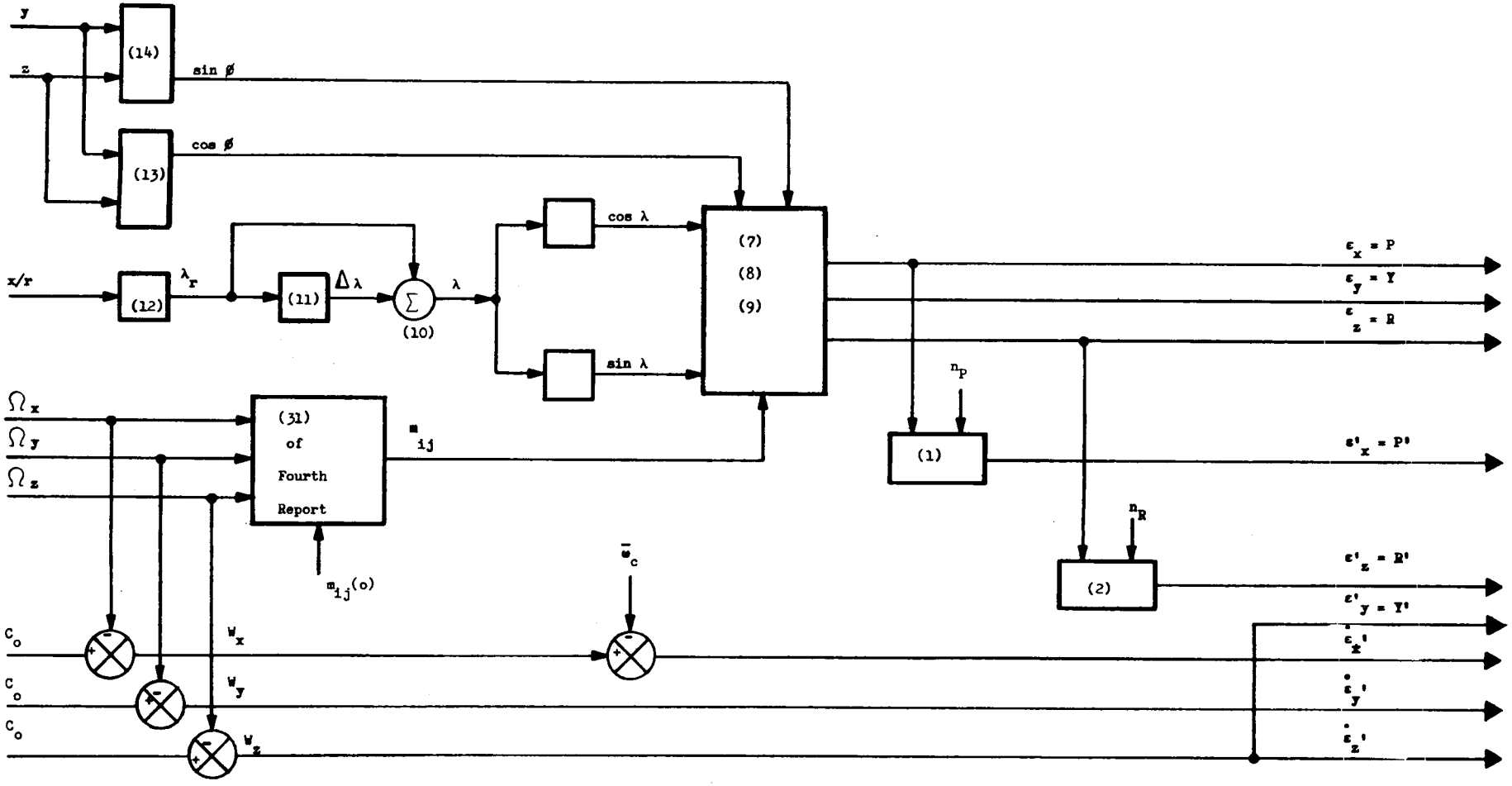

SIMULATION OF HORIZON SENSOR - GYROCOMPASS SYSTEM

FIGURE 2

APPENDIX A

True Error Angles

The command coordinate frame is designated as the B_c-frame (x_c, y_c, z_c), with y_c as the ellipsoid or geodetic vertical, x_c as the normal to the orbital plane, and z_c lying in the orbital plane (see Figure 1). For a circular orbit, z_c is parallel to the orbital velocity. The B_c-frame in this report is aligned parallel to the E-frame of the Fourth Preliminary Report, the difference being in the sense of the vertical and in the designation of axes. Note also the difference in the designation of axes for the inertial frame here as compared with that of the Fourth Report. These differences stem from adapting to the two attitude modes and the need to designate the vehicle frame (B - x, y, z) with the z-axis as the roll axis for both modes. The difference in the I-frames causes no computing complication in handling both modes, since the I-frame in this experiment is not established in the on-board system via a rate gyro fed direction cosine computer. Moreover, orbital data is not used here to establish a vertical in the on-board system. However, orbital data is required as input profiles to establish constraints required for obtaining the true angular deviations, ϵ_x, ϵ_y, ϵ_z, of the vehicle in the simulation program. With $\vec{r}$ as the geocentric vector, its components in the I-frame are

$$\left(\vec{r}\right)_I \qquad \begin{pmatrix} x \\ y \\ z \end{pmatrix} \tag{A-1a}$$

The geocentric vertical,

$$(S_R)_I \quad \begin{pmatrix} \sin \lambda_R \\ \cos \phi \cos \lambda_R \\ \sin \phi \sin \lambda_R \end{pmatrix} \qquad \text{(A-1b)}$$

Comparing (A-1a) and (A-1b) with (A-1) and (A-3) of the Fourth Preliminary Report, it may be seen that the geocentric coordinates in this report are related to those of the Fourth Report by

$$\left.\begin{aligned} x &= v \\ y &= w \\ z &= u \end{aligned}\right\} \qquad \text{(A-2)}$$

Thus, for a given orbit, the coordinate profiles determined for the previous I-frame alignment, yield very easily these profiles for the I-frame alignment given in Figure 1.

For small angular deviations, the true error matrix

$$M_{B_c B} \quad \begin{bmatrix} 1 & \varepsilon_z & -\varepsilon_y \\ -\varepsilon_z & 1 & \varepsilon_x \\ \varepsilon_y & -\varepsilon_x & 1 \end{bmatrix} \qquad \text{(A-3)}$$

$$M_{B_c B} = M_{IB}\, M_{B_c I} \tag{A-4}$$

$$M_{IB} = \begin{bmatrix} x \cdot x_I & x \cdot y_I & x \cdot z_I \\ y \cdot x_I & \text{etc.} & \\ z \cdot x_I & & \end{bmatrix} \tag{A-4a}$$

$$= \begin{bmatrix} m_{11} & m_{21} & m_{31} \\ m_{12} & \text{etc.} & \\ m_{13} & & \end{bmatrix}$$

$$M_{B_c I} \begin{bmatrix} \cos\lambda & \sin\lambda & 0 \\ -\cos\phi \sin\lambda & \cos\phi \cos\lambda & -\sin\phi \\ -\sin\phi \sin\lambda & \sin\phi \cos\lambda & \cos\phi \end{bmatrix} \tag{A-4b}$$

(As may be noted from Figure 1, the above transformation is obtained by a rotation, λ, about z_I', followed by a rotation, $-\phi$ about x_I.)

Substituting (A-4a) and (A-4b) into (A-4), and equating with the right side of (A-3), there results

$$\left.\begin{aligned} \varepsilon_x &= -m_{22} \sin\phi + m_{32} \cos\phi \\ \varepsilon_y &= m_{13} \cos\lambda - m_{23} \cos\phi \sin\lambda - m_{33} \sin\phi \sin\lambda \\ \varepsilon_z &= m_{11} \sin\lambda + m_{21} \cos\phi \cos\lambda + m_{31} \sin\phi \sin\lambda \end{aligned}\right\} \tag{A-5}$$

Again referring to Figure 1,

ε_x - true pitch error

ε_y - true yaw error

ε_z - true roll error.

Thus ε_x and ε_z are the true vertical errors, whose RMS values are figures of merit, mainly of the horizon sensor, while ε_y is the figure of merit of the gyrocompassing constraint as established mainly by the roll channel of the horizon sensor and the roll rate gyro.

From (A-1a) and (A-1b),

$$\left.\begin{aligned} \lambda_r &= \sin^{-1}\left(\frac{x}{r}\right) \\ \cos\phi &= \frac{y}{\sqrt{y^2 + z^2}} \\ \sin\phi &= \frac{z}{\sqrt{y^2 + z^2}} \end{aligned}\right\} \qquad \text{(A-6)}$$

As given in the Fourth Report, the geodetic or ellipsoid latitude, λ, as related to the geocentric latitude, λ_R, by

$$\left.\begin{aligned} \lambda &= \lambda_R + \Delta\lambda \\ \Delta\lambda &= .003373 \sin 2\lambda_R + .000006 \sin 4\lambda_R \end{aligned}\right\} \qquad \text{(A-7)}$$

With (A-6) and (A-7) substituted into (A-5), and with the true direction cosines, m_{ij}, obtained by (31) of the Fourth Report, the translational inputs, x, y, z, and the rotational inputs, Ω_x, Ω_y, and Ω_z, yield the true error angles.

APPENDIX B

Horizon Sensor Error Model

The Advanced Orbital Geophysical Observatory Horizon Sensor System made by Advanced Technology Division of American-Standard has been chosen as the horizon sensor for this experiment, on the basis of accuracy.

It is strapped to the vehicle and yields roll error, R', and pitch error, P'. It has a time constant for each channel of .06 seconds.

Its output noise per channel is .0067 degrees RMS, and distributed over a noise bandwidth from 0.0 to 0.05 cps. While this narrow band noise will probably be passed by the vehicle control system unattenuated, its RMS value is negligible compared to other error sources and can, therefore, be ignored.

The RMS instrument null error, due to all sources, at altitude for which compensation is made, is

$$\eta_I = .033 \text{ degrees}$$

The horizon uncertainty due to horizon anomalies, at about 200 n. mi. altitude, using a newly developed narrow spectral passband filter (14.0 to 15.9 microns), has an RMS value

$$\eta_H = .015 \text{ degrees}$$

The instrument null error is the nature of a bias error. The horizon anomaly error is random, but estimated to be so slowly varying as the sensor orbits over the earth, as to be practically also of a fixed bias nature.

For each of the two channels, the effective null error, n, taken as the RSS of n_I and n_H is then for roll and pitch each

$$n_P = n_R = .036 \text{ degrees} = 6.4 \times 10^{-4} \text{ radians} \qquad \text{(B-1)}$$

The RMS value of the scale factor error for both channels is .8 per cent, or .008.

Thus, for the roll and pitch channels, the indications are related to the true values as follows

$$R'(s) = \epsilon_z' = \frac{1.008}{1 + .06s} R(s) + 6.4 \times 10^{-4}/s \qquad \text{(B-2a)}$$

$$P'(s) = \epsilon_x' = \frac{1.008}{1 + .06s} P(s) + 6.4 \times 10^{-4}/s \qquad \text{(B-2b)}$$

where $R = \epsilon_z$, $P = \epsilon_x$ (B-2c)

APPENDIX C

Gyrocompassing Constraints and Rate Error Signals

The indicated error matrix,

$$M'_{B_c B} = \begin{bmatrix} 1 & \varepsilon'_z & -\varepsilon'_y \\ -\varepsilon'_z & 1 & \varepsilon'_x \\ \varepsilon'_y & -\varepsilon'_x & 1 \end{bmatrix}$$

$$= \begin{bmatrix} 1 & R' & -Y' \\ -R' & 1 & P' \\ Y' & -P' & 1 \end{bmatrix} \quad \text{(C-1)}$$

Three strapdown rate gyros can provide rate error signals. One of these, the roll rate gyro, can, in combination with the constraint of holding the indicated roll (horizon sensor) to zero, provide the yaw error signal, $\varepsilon'_y = Y'$.

In terms of true error angles and true error rates, we have for the true error angular velocity,

$$\vec{\Omega}_{BB_c} = \vec{\Omega}_{BI} - \vec{\Omega}_{B_c I} \quad \text{(C-2)}$$

(Ω_{BB_c} is, for example, the angular velocity of the B-frame relative to the B_c-frame, and is thus the true error angular velocity).

$$\left(\Omega_{BB_c}\right)_B = \begin{pmatrix} \dot{\varepsilon}_x \\ \dot{\varepsilon}_y \\ \dot{\varepsilon}_z \end{pmatrix} = \begin{pmatrix} \dot{P} \\ \dot{Y} \\ \dot{R} \end{pmatrix} \qquad \text{(C-2a)}$$

$$\left(\vec{\Omega}_{BI}\right)_B = \begin{pmatrix} \Omega_x \\ \Omega_y \\ \Omega_z \end{pmatrix} \qquad \text{(C-2b)}$$

$$\left(\vec{\Omega}_{B_cI}\right)_{B_c} = \begin{pmatrix} \omega_c \\ 0 \\ 0 \end{pmatrix} \qquad \text{(C-2c)}$$

where ω_c is the orbital angular rate of the commanded frame, B_c, relative to the I-frame.

$$\left(\vec{\Omega}_{B_cI}\right)_B = M_{B_cB} \left(\vec{\Omega}_{B_cI}\right)_{B_c} = \omega_c \begin{pmatrix} 1 \\ -R \\ Y \end{pmatrix} \qquad \text{(C-2d)}$$

Hence

$$\left(\vec{\Omega}_{BB_c}\right)_B = \begin{pmatrix} \dot{P} - \omega_c \\ \dot{Y} + R\omega_c \\ \dot{R} - Y\omega_c \end{pmatrix} = \begin{pmatrix} \dot{\varepsilon}_x \\ \dot{\varepsilon}_y \\ \dot{\varepsilon}_z \end{pmatrix} \qquad \text{(C-3)}$$

In terms of indicated rates and gyro outputs,

$$\left.\begin{aligned} \dot{P}' &= \dot{\varepsilon}'_x = W_x - \omega_c \\ \dot{Y}' &= \dot{\varepsilon}'_y = W_y + R\omega_c \\ \dot{R}' &= \dot{\varepsilon}'_z = W_z - Y\omega_c \end{aligned}\right\} \qquad \text{(C-4)}$$

where the gyro outputs

$$\left.\begin{aligned} W_x &= \Omega_x - C_o \\ W_y &= \Omega_y - C_o \\ W_z &= \Omega_z - C_o \\ C_o &= 0.07 \text{ degrees per hour} \end{aligned}\right\} \qquad \text{(C-5)}$$

If the indicated yaw and roll rates were approximately held to zero, then a yaw indication is found as follows

$$Y' \cong \frac{W_z}{\omega_c} \qquad \text{(C-6a)}$$

That is the vehicle yaw is obtained as the output of the roll rate gyro divided by the orbital angular velocity. Since $1/\omega c$ may be regarded as a

gain factor for an error signal, it may be disregarded, as the gain for the yaw channel should be fixed by accuracy and stability considerations. Hence, one may as well take the indicated yaw error as the indicated roll rate W_z.

$$Y' = W_z \tag{C-6b}$$

To show that this is not a confounding of information, if the true y- and z- axis rates as given by (C-3) were held to zero, from the z- equation

$$\omega_c = \dot{R}/Y, \tag{C-7a}$$

and substituting, in the y- equation, there results

$$\dot{Y}Y + R\dot{R} = 0 \tag{C-7b}$$

Since the roll error, R, is held to zero or thereabouts by the horizon sensor roll channel, the yaw solution of (C-7b) must be identically zero or thereabouts.

Similarly, referring to the y- and z- equations of (C-4), with the indicated error rates assumed zero, one obtains

$$Y'W_y + R'W_z = 0 \tag{C-8a}$$

But with indicated roll, R', held to zero by the horizon sensor,

$$\dot{Y}' = W_y, \tag{C-8b}$$

leading to

$$Y' \dot{Y}' = 0 \qquad \text{(C-8c)}$$

The utilization of the yaw angle coupling with the orbital rate, while constraining the roll error to near zero, is a gyrocompassing technique, and is exactly analogous to obtaining yaw on a roll stabilized earthbound vehicle through its coupling with earth rate.

With the indicated yaw given by (C-6b), the indicated yaw rate given by (C-8b), both depending on the roll and roll rate negligible, the yaw angle is assumed small, and from (C-4), the roll error rate is obtained to the approximations allowed by the vehicle control,

$$W_z = \dot{R}' \qquad \text{(C-9)}$$

To summarize results so far,

$$\left.\begin{aligned}
&\left.\begin{aligned} \varepsilon_x' &= P' \\ \varepsilon_z' &= R' \end{aligned}\right\} \text{-Horizon Sensor} \\
&\varepsilon_y' = Y' = W_z \text{ -Roll Rate Gyro} \\
&\dot{\varepsilon}_y' = \dot{Y}' = W_y \text{ -Yaw Rate Gyro} \\
&\qquad \text{(see y- equation of (C-4) with } R' \text{ negligible).} \\
&\dot{\varepsilon}_z' = \dot{R}' = W_z \text{ - Roll Rate Gyro}
\end{aligned}\right\} \qquad \text{(C-10)}$$

There remains the problem of examining the x-axis error rate signal,

$$\dot{P}' = \dot{\epsilon}_x' = W_x - \omega_c \qquad \text{(C-11)}$$

as given in (C-4). This equation implies that the orbital rate of the commanded frame must be known. If (1) the commanded frame were geocentric instead of geodetic, (2) the orbit were exactly circular, then ω_c would be a constant,

$$\overline{\omega_c} = \frac{20\pi}{90 \text{ minutes}} \text{ , or thereabouts,}$$

Owing to the commanded frame being geodetic, as constrained by the horizon sensor, then for a circular orbit,

$$\omega_c = \overline{\omega_c} + \Delta\omega_c, \qquad \text{(C-12)}$$

where $\Delta\omega_c$ would reflect the time derivative of (A-7) in Appendix A. That is, tracking the geodetic vertical, results in a small forced oscillation of the vehicle's yaw axis about the geocentric vertical at the fundamental of twice the orbital frequency and its harmonics. From (A-7), the amplitude of the fundamental is .003373 radians $\cong$ .2 degrees.

For a polar orbit, the amplitude of the oscillation would be .2 degrees, or an excursion of .4 degrees, and it would be a maximum. At the other extreme, for an equatorial orbit, the amplitude of the oscillation would be zero, since the equatorial cross section of the earth is circular. In between these extremes, the amplitude would be between 0 and .2 degrees.

While we are dealing with a rate error signal, the error signal is assumed to be linearly combined with the rate error signal. That is, the control law governing the pitch CMG gimbal rate, would be of the form

$$\dot{a}_x = K_{1x}P' + K_{2x}\dot{P}'$$

$$= K_{1x}P' + K_{2x}(W_x - \omega_c). \qquad \text{(C-13a)}$$

If the unwieldy computation necessary to obtain, $\Delta\omega_c$ in (C-12) is to be avoided, the law would become

$$\dot{a}_x \cong K_{1x}P' + K_{2x}(W_x - \bar{\omega}_c). \qquad \text{(C-13b)}$$

The true vehicle pitch, ε_x, resulting from the simplifying approximation depends on the relative weightings of the gains, k_{1x} and K_{2x}, and cannot be predicted. The simulation will reveal, however,, for various gain combinations, the amplitude of a small slow oscillation about zero due to this approximation. On a tentative basis, then, the pitch rate error signal is taken as

$$\dot{\varepsilon}_x = \dot{P}' = W_x - \bar{\omega}_c , \qquad \text{(C-14)}$$

where $\bar{\omega}_c$ is accurately adjusted to the altitude of the orbit.

VI SENSOR DATA

A. Inertial Sensors

Brief Description - Referring to Figure 1 the dotted enclosure is the dynamic model of the mechanical system. When the stabilization loop is closed by torque balancing about the gyro's output axis, the steady state voltage signal output is proportional to the input angular rate.

When the gyro is used as a stable platform sensor, the platform stabilization loop is closed by torque balancing about the gyro's input axis (Figure 2). The return torque here is provided by the platform gimbal motor. The platform gimbal angle is the output signal and can be shown to be equal in the steady state, to the vehicle rotation about the gyro input axis with respect to an inertial reference axis.

It can be stated as a rough estimate that the characteristic time of a platform loop is about an order of magnitude greater than the mechanical characteristic time of its gyro sensor. Typically, this characteristic time for a floated gyro is about 0.005 seconds. That for the platform stabilization loop would then be about 0.05 seconds.

Under the expected rotational environment of the spacecraft for the attitude modes discussed here, the platform servo error would be negligible compared to the accumulated gyro drift. The single axis platform error, that is the discrepancy between the vehicle inertial angle and the measured gimbal angle, would then be the drift of the gyro. This drift in orbit would be only the acceleration insensitive drift. For a three axis platform the drift rate would be the vector

sum of the drift rates of its three gyros.

A strapdown system equivalent drift rate would also be the vector sum of its three strapdown rate gyros. Estimates of the acceleration sensitive drift rates for the highest angular velocities show that for the 18. P.I.R.I.G.* gyro, the acceleration sensitive drift rates are negligible compared to the random drift rate. Therefore, there appears to be no accuracy advantage, for the applications discussed here, of a platform relative to a strapdown system. On the other hand, the cost, volume, and weight penalties of even three single axis platforms relative to a strapdown system, leave no doubt as to the preference for the latter.

The 18. P.I.R.I.G. is a pulse torqued gyro. For strapdown applications it would be used in its rate mode. Its output would then be a series of voltages proportional to the rotational increments incurred during clocked intervals of the spacecraft about the gyro input axes. Such outputs are exactly the inputs required for the strapdown direction cosine computer when programmed as a digital differential analyzer. In that case the nine differential equations become finite difference equations whose sampled solutions are updated by rotational increments about three axes. Because the 18 P.I.R.I.G. was designed for adaptation to a digital strapdown computer, it is recommended as the choice among the three candidates cited in what follows.

The closed loop characteristic time of the gyro depends on the gain in the feedback path as well as on its mechanical characteritic time. Only the latter

* Pulsed Inertial Rate Integrating Gyro

is provided by manufacturers. Practice has shown that for both floated and air bearing gyros, the closed loop time constant can be held to .0005 seconds with good stability margin. This value is then taken as a reasonable estimate for the three gyros.

The error model for the three gyros is the total drift rate due to acceleration insensitive sources (random), accelerations along input and spin reference axes acting on mass unbalance, and coupled accelerations acting on compliant mass unbalance. With the numerical evaluations given in the following, and with conservative estimates in the location of the gyros in the rate mode the acceleration sensitive drift rates were found to be negligible compared to the acceleration insensitive drift rates.

$$\Delta W = k_o + k_1 a_{IA} + k_2 a_{SRA} + k_3 a_{IA} a_{SRA}$$

(genral error model of drift rate)

1. 18. P.I.R.I.G. (MIT-BENDIX)

1.1 k_o = 0.3°/hr (nominal)

0.07°/hr (compensated)

k_1 = 0.3°/hr/g

k_2 = 0.3°/hr/g

k_3 = 0.015°/hr/g^2

1.2 Characteristic Time - .0005 sec.

1.3 Output Signal Range - 3 to 1,000 mv

1.4 Gyro Transfer Function - 3.3 mv./mr.

1.5 Maximum Torquing Rate - Not Reported

1.6 M.T.B.F. (operating) - 10,000 hrs.

1.7 Power (operating) - 20 watts

1.8 Weight - 11 oz.

1.9 Volume - 1.8 in. diam., 6 in. thickness

1.10 Cost - $10,000/12,000

1.11 Delivery Time - about 3 months per unit in production

2. Gneral Precision Inc. - King Series C702519025

2.1 k_o = 0.5°/hr (nominal)

k_1 = 0.15°/hr/g

k_2 = 0.15°/hr/g

k_3 = 0.01°/hr/g^2

2.2 Characteristic Time - .0005 sec

2.3 Gyro Transfer Function - 7.5 volts/deg.

2.4 Maximum Torquing Rate - 5,000 deg/hr

2.5 Power (operating) - 7.5 watts

2.6 Weight - 16 oz.

2.7 Volume - 10 cu.in.

3. Honeywell DGG334 Gas Bearing Integrating Fyro

3.1 k_o = 0.1°/hr (nominal)

k_1 = 0.2°/hr/g

$k_2 = 0.2°/hr/g$

$k_3 = 0.04°/hr/g^2$

3.2 Characteristic Time - .0005 sec.

3.3 Gyro Transfer Function - 8 volts/rad.

3.4 Maximum Torquing Rate - 430×10^3 deg/hr

3.5 MTBF (operating) - 10,000 hrs

3.6 Power (operating) - 10 watts

3.7 Weight - 22 oz.

3.8 Volume - 20 cu. in.

3.9 Cost - $9,000/$11,000 (50 units)

B. Stellar Sensors

Brief Description - The description given here applies to the photodetector used in the OAO Bendix Guide Star Tracker. There are a number of types of photodetectors in current use which have various advantages and disadvantages. These are the (1) image dissector, (2) vidicon, (3) image orthican, (4) photoconducting array, (5) photomultiplier, and (6) quadrant balance multiplier. Data from two sources were availabe: Bendix Eclipse-Pioneer's (image dissector) and North American's Autonetics Division (photoconducting array).

The image dissector consists of a photocathode surface which is scanned in some radially symmetric pattern. A star image within the scanning field of view causes a continuous photoelectric emission from the site of the image. Only when the instantaneous field of view of the scan intercepts the star image, however, are photoelectrons collected at the anode and amplified. The result is a train of pulses whose pattern in time contains information as to the direction relative to baresight of the star image. Phase demodulation of the video pulse train and low pass filtering establishes servo error signals on two axes (see Figure 3). Information sufficient in detail has not been received concerning the array of CdS photoconducting cells provided in the Autonetics tracker for adequate explanation. Design and performance data are included nevertheless.

The error model for the Bendix Star Tracker has been provided via its complete servo diagram and its input noise models. That for the Autonetics tracker is

1.2.9 Azimuth Closed Loop Response Time - 0.24 seconds

1.2.10 Digital Pick-Off Resolution - 20 arc seconds (16 bit encoder

1.3 MTBF (operating) - 12,000 hours

1.4 Fully Developed

1.5 Cost (operating equipment) - $225,000 to $250,000

1.6 Cost (minimal checkout equipment) - $100,000

1.7 Delivery time - 9 months

1.8 On-board weight - 37 lbs

1.9 Power (operating) - 17 watts

2. Space Celestial Tracker (Array of CdS photoconducting cells) - Autonetics

2.1.0 Performance Data

2.1.1 RMS Azimuth Null Error - 10 arc seconds

2.1.2 RMS Elevation Null Error - 10 arc seconds

2.1.3 RMS Error of Pick-Off - 8 arc seconds

2.1.4 Closed Loop RMS angular error due to combined effects of noise, null, and pick-off error

2.1.4.1 Elevation - 15 arc seconds

2.1.4.2 Azimuth - 15 arc seconds

2.2.0 Design Data

2.2.1 Acquisition Field of View - ±0.5 degrees

2.2.2 Tracking Field of View - ± 4.3 arc minutes

2.2.3 Detector Spectral Passband - .45 to .6 microns

2.2.4 Azimuth Closed Loop Passband - 40 cps

not complete in that only lumped values for noise and servo parameters were available. This tracker is currently under development, while the Bendix tracker is fully developed.

1. OAO Guide Star Tracker (image dissector) Bendix Eclipse-Pioneer

(Where relevant, data applies to type A_o, magnitude 2.5 star.)

1.1.0 Performance Data

1.1.1 RMS Azimuth Null Error -9 arc seconds

1.1.2 RMS Elevation Null Error - 9 arc second

1.1.3 RHS Errors of Pick-off - 6 arc seconds

1.1.4 Closed loop RMS angular error due to combined effects of noise, null, and pick-off error

1.1.4.1 Elevation - 11.5 arc seconds

1.1.4.2 Azimuth - 11.5 arc seconds

1.2.0 Design Data

1.2.1 Acquisition Field of View - ± .5 degrees

1.2.2 Tracking Field of View - ± .033 degrees

1.2.3 Detector Spectral Passbased - -.4 to .8 microus

1.2.4 Elevation Closed Loop Passband - 1.4cps

1.2.5 Azimuth Closed Loop Passband - 1.2cps

1.2.6 Elevation Gimbal Authority - ± 60 degrees

1.2.7 Azimuth Gimbal Authority - ± 60 degrees

1.2.8 Elevation Closed Loop Response Time - 0.2 seconds

2.2.5 Elevation Closed Loop Passband - 40cps

2.2.6 Azimuth Closed Loop Response Time -.020 seconds

2.2.7 Elevation Closed Loop Response Time -.020 seconds

2.2.8 Azimuth Gimbal Authority - ±40 degrees

2.2.9 Elevation Gimbal Authority - ±40 degrees

2.2.10 Digital Pick-off Resolution - 1.24 arc seconds

2.3 MTBF (Operational) - 11,100 hours

2.4 Under Development

2.5 Estimated On-board Weight - 15 lbs.

2.6 Estimated Power - 20 watts

C. Earth Sensors

Brief Description - These sensors yield pitch and roll error signals relative to a vertical defined by the apparent horizon. Deivations in the apparent horizon relative to local mean sea level are given for specific locations for the first of the two sensors described here. Local mean sea level is regarded as a segment of the geoid whose normal is the plumb line vertical. Deviations of this vertical, in turn, relative to the geodetic vertical, (normal to the international ellipsoed) are under 0.1 arc seconds. Thus, for the purposes of the accuracy requirements of the two experiments requiring control to the vertical, deviations of the earth sensors relative to the geodetic vertical is an adequate measure of accuracy. The uncertainty of the horizon and therefore the uncertainty of its vertical, depends on the spectral passband of the detector filters. For the most accurate horizon sensors, the horizon uncertainty is the dominant part of the sytem error, the instrument errors being smaller than the random error in the information channel. This latter error is dependent on the spectral passband of the optical filter used, a narrow passband (14 to 15.9 microns) having produced best results.

Two sensors are described here neither of which is inside the more stringent accuracy requirement in the statement of work (.01 degree). However, with the allowed vertical error stipulated for the microwave experiment in NASA TR-Kurzhals and Grantham (May, 1965), which is 0.5 degrees, the first one, (ATL's OGO Horizon Sensor System) is inside the requirement, while the second is

outside. The second, however, is less than half the price of the first and has a time constant 1/6 of the former.

The ATL OGO Horizon Sensor is a fixed point edge tracker in that the horizon is sampled at three (or four) distinct points in azimuth (rather than swept in azimuth as in their Gemini tracker). The distinct point sampling of the horizon permits a shorter time constant and less vunderability to the sun on the horizon (see Figure 4). A sun presence signal enables the tracker to go from its normal four-horizon-point edge tracking to a three-horizon-point track operation. Four infrared search-track units (referred to as trackers) track points on the horizon separated 90 degrees in vehicle azimuth. With the system strapped to the vehicle, the horizon edge is tracked by each tracker through (a) dithering a mirror reflecting the incoming infra-red radiation into a germanium thermistor balometer, and (b) detecting and nulling the second harmonic of the resultant pulse train. The pulse train is generated as the mirror dithers through the horizon edge, alternately seeing cold space and hot earth. A symmetric pulse train corresponds to a nulled reference axis. The second harmonic of the pulse train is linear out to about 10° and monotonic out to 25° deviation of the reference axis relative to nadir. The second harmonic error signal is used to position the reference axis of the dithered mirror which is mounted on flex pivots. Two different simple arithmetic operations combine the measured horizon angles of the trackers for three- and for four-point roll and ptich determinations. Geometric cross coupling (the influence of pitch on roll indication and roll on pitch indication) at 200 n.mi. altitude

amounts to less than .01 degrees for each axis, if pitch and roll are limited to 1 degree each. To summarize, the flex mounted mirrors (referred to as Positors) are dithered, and by using the second harmonic of the resultant pulse train as an error signal, the center of the dither oscillation is positioned so as to lock to the horizon. The center of the oscillation relative to the system vertical axis (coinciding with the vehicle yaw axis) yields the tracker's apparent horizon angle, and the data of four (or three) such angles yields pitch and roll.

The Barnes Lunar and Planetary Tracker (Reflecting System) BEC Project 4290 consist of four orthogonal heads, each scanning a 10° x 90° sector. The 90° scan is achieved by sequentially sampling 100 detectors in a linear mosaic array in each head. Scanning starts on space and proceeds linearly towared the nadir. No moving parts are utilized in the system. System final outputs consist of binary gating drive signals and counter signals that indicate which detectors in each head "see" the horizon during the scan interval. By means of digital processing of these outputs, attitude and altitude readouts can be obtained.

The scan pattern, earth sector scan, is illustrated in Figure 5. . Horizon angles are extracted from the sequentially sampled data of the elements of the array by a logic which notes the edge of the space seeing sequence for each head, these angles being noted zs x_1, x_2, y_1, and y_2. Simple arithmetic operations combine the reduced data to give pitch and roll, digitally.

1. ATL Advanced OGO Horizon Sensor System

1.1 Error Model

$$R'(s) = \frac{1.008}{1.06\ s} R(s) + \frac{6.4 \times 10^{-4}}{s} \text{ radians}$$

$$P'(s) = \frac{1.008}{1.06\ s} P(s) + \frac{6.4 \times 10^{-4}}{s} \text{ radians}$$

1.2 Performance Data

1.2.1 RMS Horizon Uncertainty - .015 degrees (at 200 n.mi.)

1.2.2 RMS Instrument Null - .033 degrees

1.2.3 Altitude range - 100 to 80,000 n.mi.

1.2.4 Maximum Tilt for Tracking - ±25° (pitch and roll)

1.2.5 Linear Tilt Range - greater than 25°

1.2.6 Time Constant - .06 seconds

1.2.7 Ambient Temperature Range - -20°F to +140°F

-35°F to +160°F (design goal)

1.3 Design Data

1.3.1 Field of View - 1.2°

1.3.2 Optical Spectral Passband - 14.0 to 15.9 microns

1.3.3 Type of Detector - Immersed Germanium Thermistor Bolometer

1.3.4 Roll and Pitch Output Signals

1.3.4.1 Analog

1.3.4.2 Scale factor - 0.4V. RMS per degree

1.3.4.3 Output Range - ± 10.0 V. RMS

1.3.4.4 Suppressed Carrier Frequency - 2.461 cps.

1.4 MTBF - greater than 167,000 hours (3 tracker operation) according to tests

1.5 Status - Production Prototype Scheduled for Completion, March, 1966

1.6 Cost - $150,000 - (single unit, estimated)

£100,000 (limited production, estimated)

1.7 Delivery Time - not reported

1.8 Weight - 12.5 lbs

1.9 Power - 12 watts

2. Barnes Lunar and Planetary Horizon Scanner (Reflecting System) BEC Project 4290

2.1 Error Model

(R,P - true roll, pitch; R_e, P_e - delayed response roll, pitch R', P' - digitally indicated roll, pitch)

$$R_e(s) = \frac{R(s)}{1 + .11s} + \frac{n_R}{s}$$

$$P_e(s) = \frac{P(s)}{1 + .11s} + \frac{n_P}{s}$$

($n_P = n_R = .0035$ radians = 0.2 degrees - estimated RSS of combined effects of horizon uncertainty and instrument bias error).

(see Figure 6 for relation between R_e and R', and P_e and P')

2.2 Performance Data

2.2.1 Altitude Range - corresponds to planetary subtense from 10° to 170°

2.2.2 Maximum Tilt - 0 to 90°

2.2.3 Linear Tilt Range - 0 to 90°

2.2.4 Time Constant - .110 seconds

2.2.5 Ambient Temp. Range - -40°C to +80°C

2.3 Design Data

2.3.1 Field of View - 4 segmented orthogonal digitalized fields, each filed covering 10° by 90° with long arc in 0.9° increments

2.3.2 Optical Spectral Passband - 14 to 35 microns

2.3.3 Type of Detector - Thermopile Mosaic Array

2.3.4 Roll and Pitch Output Signals

2.3.4.1 Digital with Resolution of 0.9 degrees

2.4 MTBF (calculated) - 170,000 hours

2.5 Status - Under Development

2.6 Cost - $50,000 in limited production

2.7 Delivery Time - 6 months

2.8 Weight - 15 lbs. (approx.)

2.9 Power - 6 watts (approx.)

D. Solar Sensors

Brief Description - These sensors are designed for strapdown to the vehicle or solar panel which is to be controlled in a solar mode. Shown in Figure 7 is a cross section of the Bendix Fine Angle Sun Sensor. The two error signals are each obtained by quadrant balancing of the photovoltaic cells (silicon) in which, for each axis, a front cell output is summed with corresponding cell from the rear structure, and bucked against the summed output of the opposing pair (one from front and from rear). Thus each error signal is generated by four cells, (two from each quad structure.) It may be noted that the lens magnifies the deviation of the sun's rays from the Z-axis, thus providing the rear quad structure with a steep gradient. The front quad structure, with an unmagnified gradient, will yield outputs limited only by its field of view. The front stucture thus provides wide acquisition field of view, while the rear structure provides fine tracking.

A wide angle sun sensor with a hemispheric field of view is shown in Figure 8. The two error signals are also generated by quadrant balancing, but here there is no attempt at producing a steep error signal gradient by means of a magnifying lens. An array of twelve cells arranged as shown ensures solar impingement on two quad pairs for any incident angle within a hemisphere, and thus the two error signals are always available.

Bandpass - 5cps

Output Signal to Noise Ratio - over 1,000

Weight - 3oz.

Cost - 4 to 5,000

Delivery Time - 3 months

2. Wide Angle Sun Sensor

Type Numbers 1771858

1818787

Bendix, Eclipse-Pioneer

2.1 Bias Error Per Axis - less than 0.1 degree

2.2 Time Constant - 20 microseconds

2.3 Acquisition and Tracking Field of View - a hemisphere

2.4 Sensitivity at Null - .02 milliamps per arc minute (for external load - 100 ohms)

2.5 Linear Range - 600 arc minutes

2.6 Output Range - 0 to 45 milliamps (100 ohm load)

2.7 Temperature Range - -40°C to 70°C

For both sun sensors, there has been no attempt to derive solar angles, the sensor being used only in conjunction with a vehicle control system that will null its error signals. The data available is thus not sufficient to relate indicated angles with true angles.

The only parameter of an error model, available is the electrical bias error for these particular models. This and other data is cited below.

1. Fine Angle Sun Sensor Type Number 1818823 Bendix, Eclipse-Pioneer

1.1 Bias Error per Axis - less than 5 arc seconds

1.2 Time Constant - 20 microseconds

1.3 Acquisition and Tracking Field of View - ± 10 degrees

1.4 Sensitivity at Null - 10 microamps per arc second (for external load - 100 ohms)

1.5 Linear Range - ± 5 arc minutes

1.6 Ouput Range - 0 to 4 milliamps

1.7 Temperature Range - -55°C to +50°C

1.8 Weight - 30oz.

1.9 Volume - 2 3/4 in. diameter by 9 inches deep

1.10 Cost - $2,200 (limited production)

1.11 Delivery Time - 4 months

(Unit requires an amplifier which has been built to order)

Amplifier Data

Gain - 10,000

1.8 Delivery Time - 5 to 8 weeks for 50

Error model is based on estimations in observing test data. Output is analog.

C. Gimbal Rate Sensors

Brief Description - The tach generator has a wound armature and a permanent magnet field. When mechanically driven it generates a DC signal proportional to the input rate with a small ripple dependent on the input rate superimposed on the DC. This generator, as used for rate feedback for the OAO guide Star Tracker servos, is direct drive.

1. Inland Motor Corporation Tach Generator (TG 2108 - "A" version)

1.1 Error Model

$$\dot{\theta}' = \dot{\theta}\,(1 + .025 \sin 1800\,\dot{\theta}t) + n$$

n = (noise in angular units)

$$n(s) = \frac{N(s)}{1 + .17s}$$

$$S_N = \frac{.11\ \text{deg}^2/\text{sec}^2}{\text{cps}}$$ - spectral power density

of input white noise generator

$n_{RMS} = .4$ deg/sec.

(factor, .025, is RMS percentage linearity error)

1.2 Linear Range -350 RPM

1.3 Scale Factor (RMS) - .8 volts/rad/sec

1.4 Power Requirement - none (permanent magnets)

1.5 Weight - 9 oz.

1.6 Volume - 2.8 in. diameter, 5/8 in. thick

1.7 Cost - $200 each for an order of 50

F. Gimbal Angle Sensors

Brief Description - Principal methods of measuring a shaft angle are by means of an inductive resolver, electrostatic resolver, and optical encoder. The first two are adaptable to digitization. The latter is necessarily digital. Because information received has been concerned practically entirely with the latter, the optical encoder is described here. This is not to imply, however, that a resolver encoder is not suitable as a digital gimbal angle tranducer.

The heart of the optical encoder is a code disc on which patterns of alternate translucent and opaque bars have been photographically deposited on a glass disc base. An n-bit encoder in which a resolution of $360°/2^n$ is attainable has n distinct tracks, of the alternating pattern, concentrically arranged. The track patterns, running from inside to outside on the disc goes from coarse to fine; or equivalently, from the most significant digits to the least significant. The pattern corresponds to a cyclic bindary (grey) code. The encoder electronics then makes "0"s and "1"s available in the millivolt rnage. An amplifier is then required to bring it up to the input level of a digital computer. Silicon photovoltaic photocells, one for each track, transduce the light transmitted by the encoded patterns. A single lamp provides the source. The full word corresponding to shaft angle, is available by parallel or sequential interrogation of all tracks by the digital computer.

Data on one gimbal angle sensor is indicated as follows:

1. Baldwin Electronics Shaft Position Encoder Model 232

   1. Number of Tracks -13
   2. Angular resolution = $360°/2^{13}$ = 2.64 arc minutes
   3. Highest Output Frequency developed at 60 RPM on least significant tracks - 2,048 cps
   4. Output level "1" - mv. ± 10%

      "0" - 4 mv. ± 10%
   5. Average internal impedance - 20K
   6. Maximum Slewing Speed - 5,000 RPM
   7. Maximum Angular Acceleration - 30,000 $\frac{\text{rads}}{\text{sec}^2}$
   8. MTBF (limited by lamp) - 12,000 hrs.
   9. Estimate on cost, delivery time, and weight of MIL SPEC version are $5,000 (including triggered amplifier between encoder and computer)
   10. Delivery time - 60 days from start, and 2 to 5 per week thereafter
   11. Weight (encoder and amplifier) -32 oz.
   12. Volume encoder - 2 1/2 in. diam. -3 inches thickness
   13. Time Constant is Word Interrogation Time - 20 μ sec. for parallel track interrogation, 13x20 = 260 μ sec. for sequential track interrogation

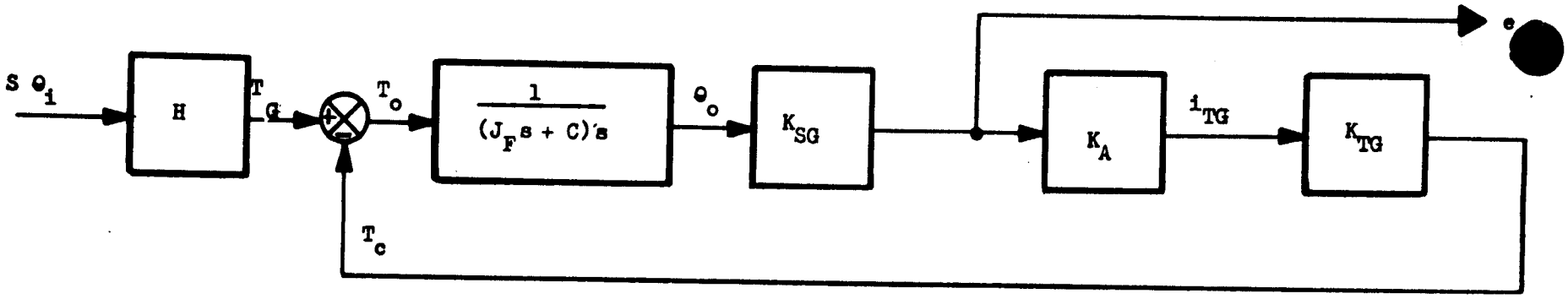

$$\frac{e_o(s)}{s\,\theta_i(s)} = \frac{K_{SG}H}{J_F s^2 + Cs + K_{SG}K_A K_{TG}}$$

θ_i - input axis displacement

θ_o - output axis displacement

T_G - gyroscopic torque

T_c - control torque

T_o - net output axis torque

J_F - float inertia about output axis

C - viscous damping coefficient

K_{SG} - signal generator gain

K_A - feedback amplifier gain

K_{TG} - torque generator gain

i_{JG} - input current to torque generator

e_o - output voltage signal

DYNAMIC MODEL OF RATE GYRO

FIGURE 1

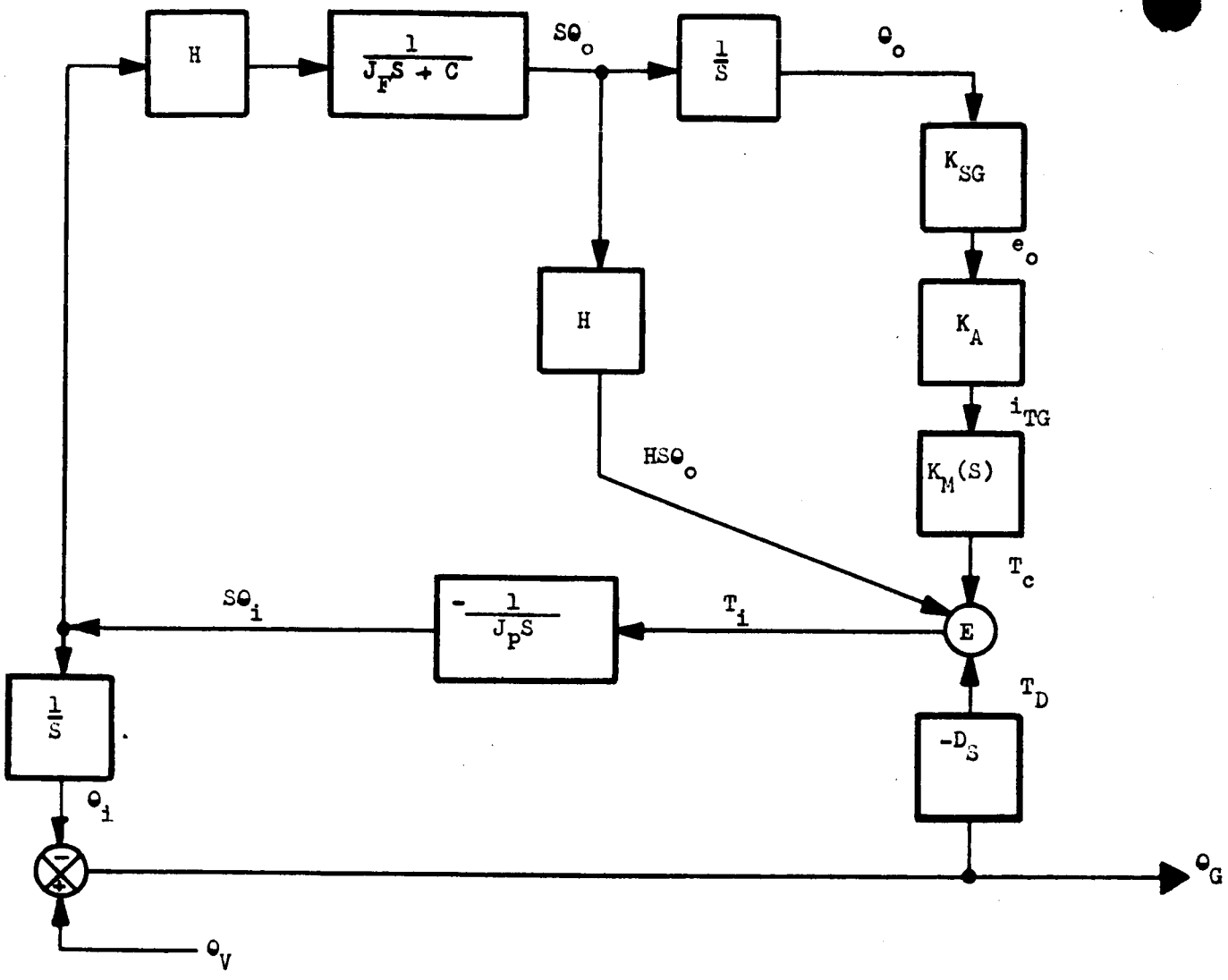

$$\frac{\Theta_G(S)}{\Theta_V(S)} = \frac{J_P J_F S^3 + J_P C S^2 + H^2 S + H K_{SG} K_A K_M(S)}{J_P J_F S^3 + (J_P C + J_F D) S^2 + (H^2 + DC) S + H K_{SG} K_A K_M(S)}$$

Θ_V - Vehicle Displacement about input axis relative to inertial frame.

Θ_G - Measured gimbal angle.

Θ_i - Platform displacement about input axis relative to inertial frame.

T_i - Net torque about input axis.

D - Viscous damping coefficient (motor back emf, bearings).

$K_M(S)$ - Gimbal motor transfer function.

J_P - Platform inertia about input axis

DYNAMIC MODEL OF PLATFORM (SINGLE AXIS)

FIGURE 2

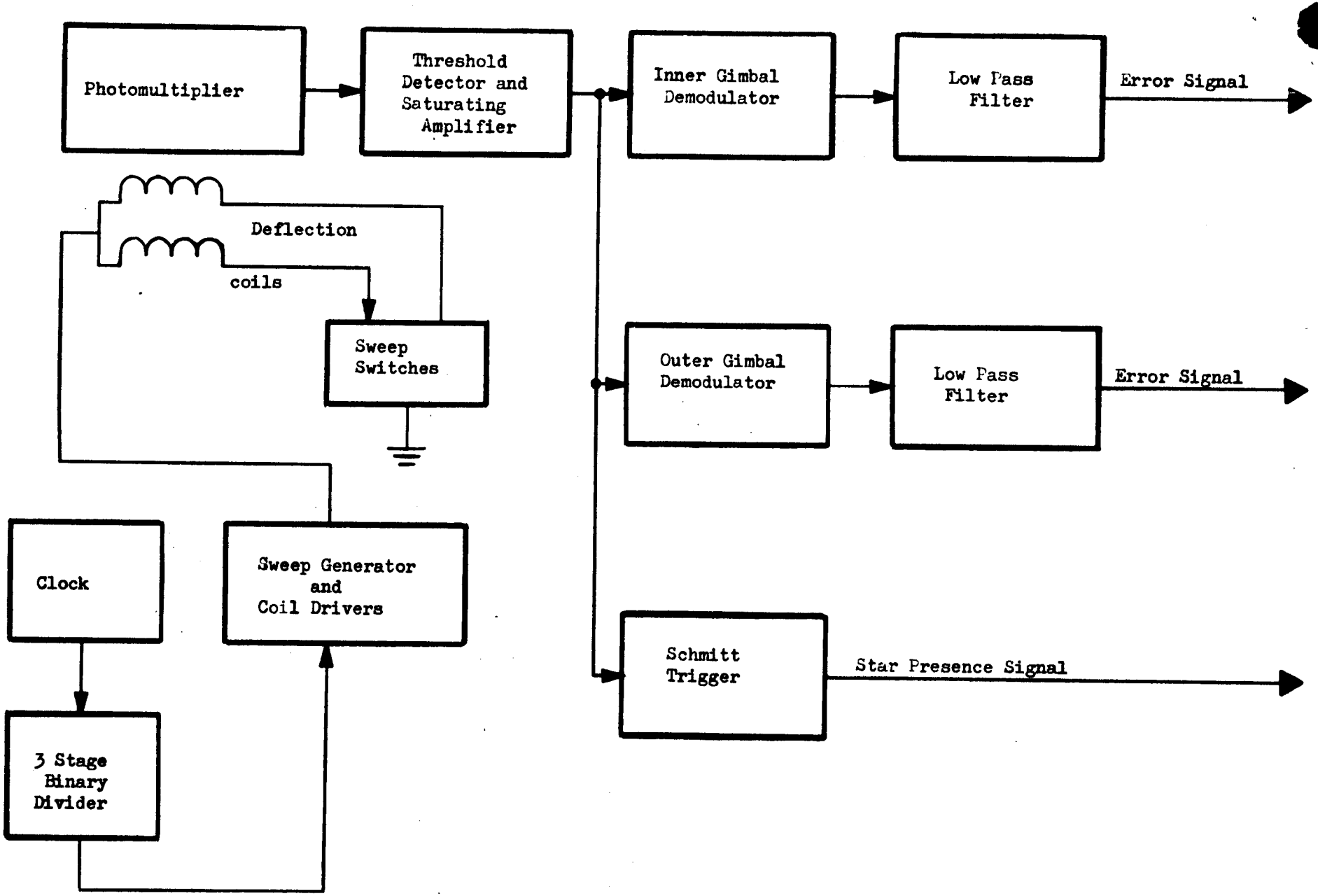

IMAGE DISSECTOR ELECTRONICS

FIGURE 3

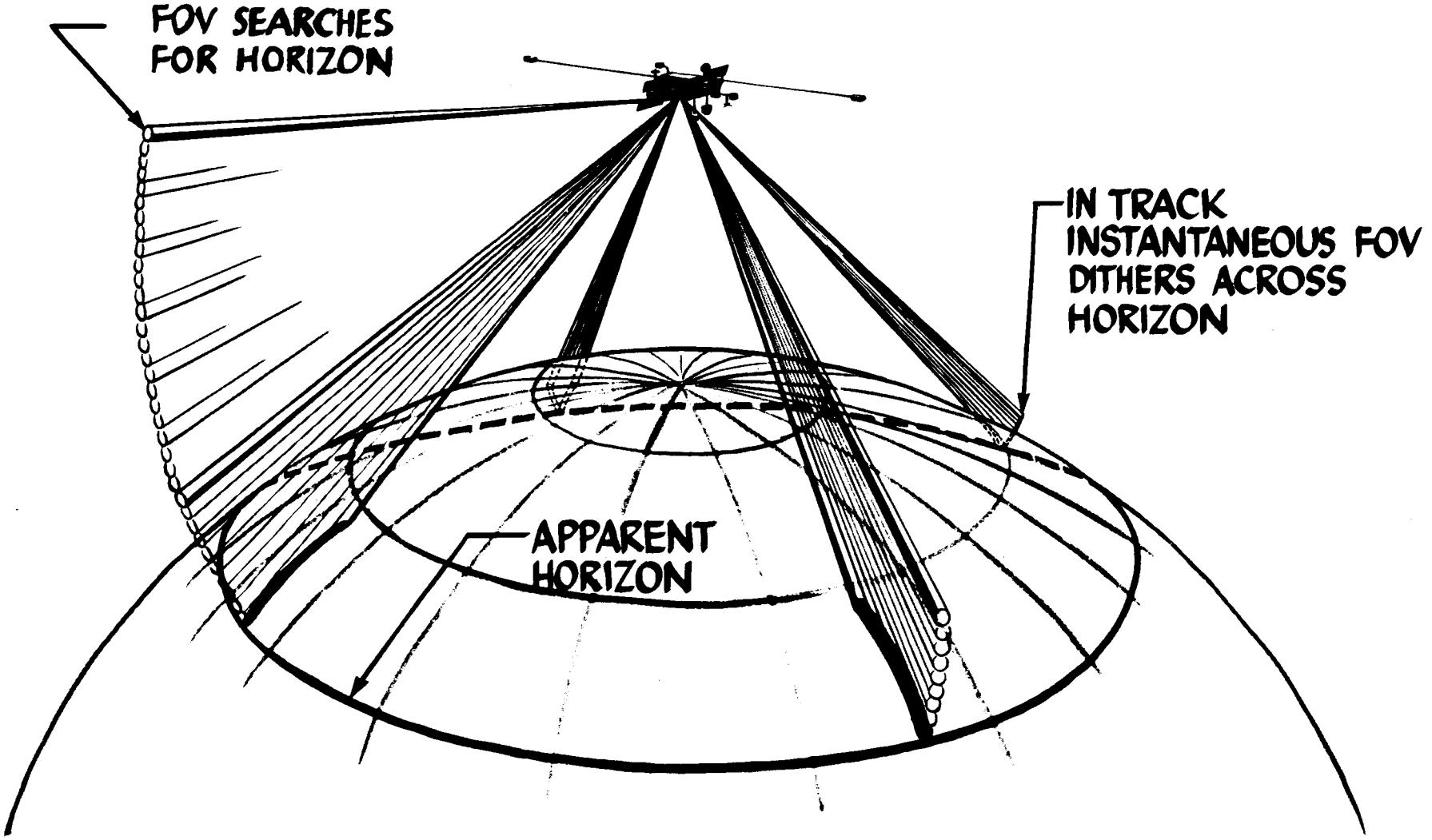

A-OGO HORIZON EDGE-TRACKING SCHEME

FIGURE 4

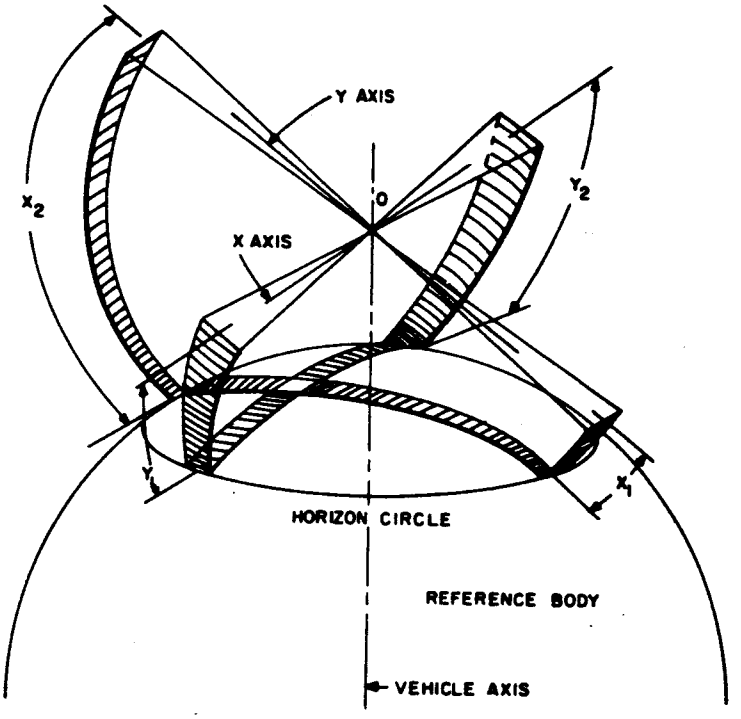

SCAN GEOMETRY

DIGITAL EARTH SECTOR SCAN (BARNES)

FIGURE 5

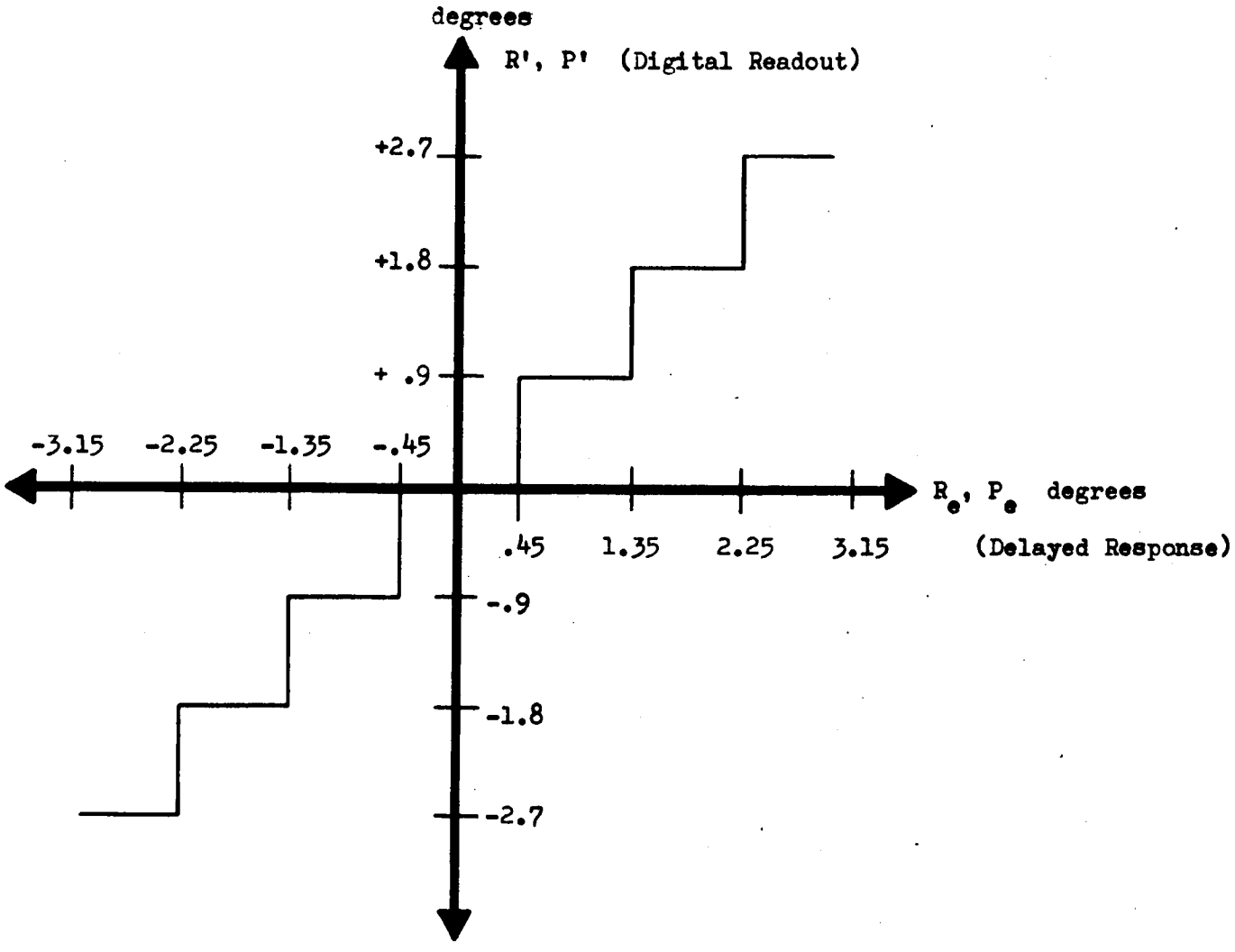

DIGITAL READOUT VS DELAYED RESPONSE
(BARNES TRACKER)

FIGURE 6

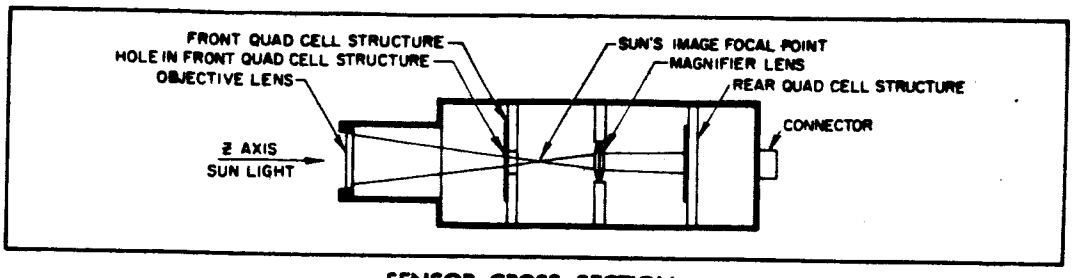

SENSOR CROSS SECTION

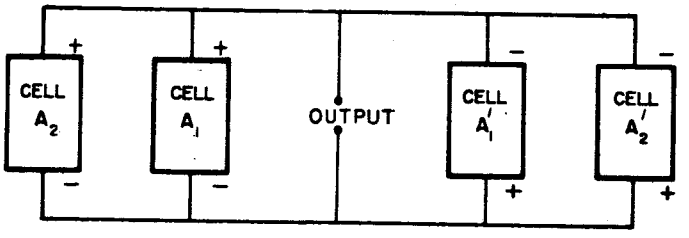

A—A′ CHANNEL

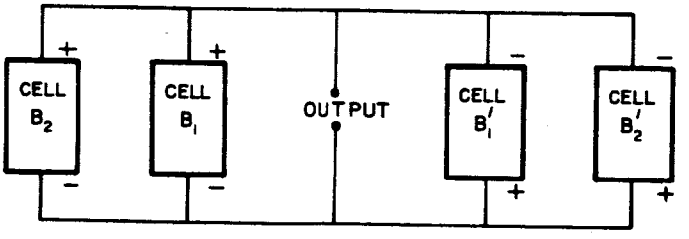

B—B′ CHANNEL

FINE ANGLE SUN SENSOR (BENDIX)
FIGURE 7

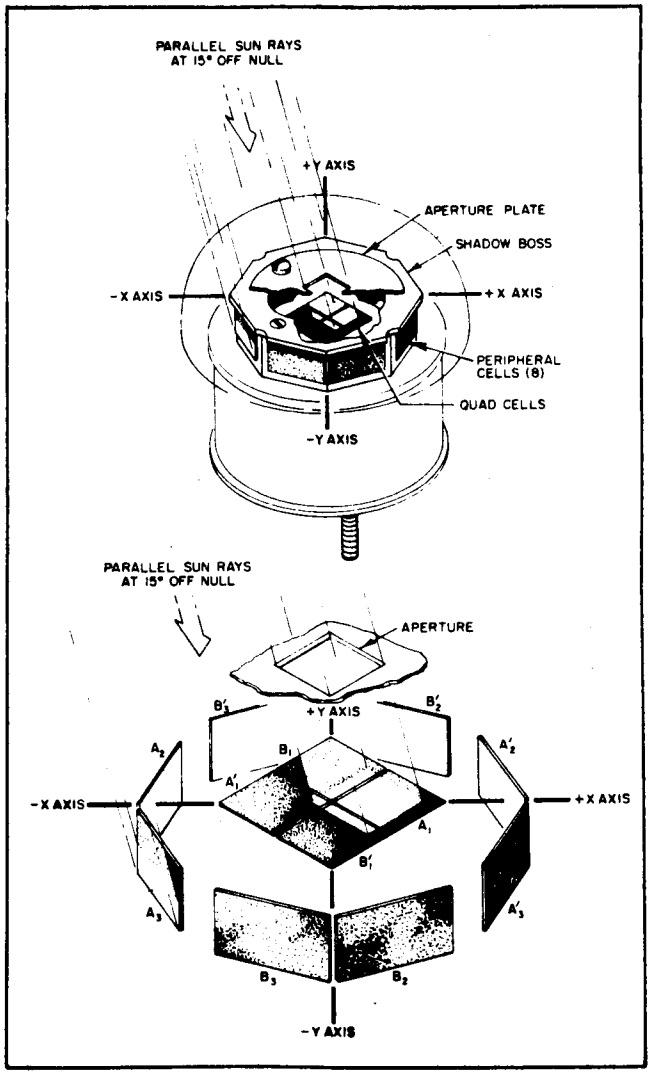

WIDE ANGLE SUN SENSOR (BENDIX)

FIGURE 8